Stock Investment Value Study

Based on Fuzzy Comprehensive Evaluation

Zongyan Xu, Zhong Liu, Feifei Zhou & Haihua Li

Military Transportation Department, Academy of Military Transportation, Tianjin 300161, China

Abstract

This paper constructs 3-level evaluation model based on index system for the listed corporations and confirm the weights by the factor analysis, then compute the investment value of listed companies in chlor-alkali industry making use of fuzzy comprehensive evaluation method and illustrate the method. The objective and reasonable basis for making investment decision is provided.

Keywords: Fuzzy comprehensive evaluation, Investing value, Mathematica

1. Introduction

Considering the characteristics that China's stock market is still in development stage and the actual situation of listed companies, and taking into account available data, we could consider the profitability of listed companies, growth and expand capacity of equity capital to reflect the investment value of listed companies.

Profitability: the earnings per share(EPS), return on equity(ROE), cash flow per share(CFPS) and total assets yield(TAY) could be set up to reflect the profitability of listed companies. EPS means the level of profitability of common stock, which is the most concerned indicators for many investors. Besides using this financial profitability to evaluate the listed companies, majority investors also use price per share of listed companies to conduct horizontal compare, by which decide to how to invest, so the indicator would best reflect the image of a listed company.

Growth indicator: the main business revenue growth rate(MBRGR), the growth rate of total assets(GROTA) and net profit growth rate(NPGR) are established to representative the growth of listed companies. From the perspective of assets, total assets of listed companies is an important indicator to measure the strength of listed companies, so, to a certain extent, the total assets growth rate means the growth of listed companies. MBRGR also plays an important role in the company's growth, indicating the focus direction of growth. Because the accumulation, development and return to investors of listed companies depends largely on the increase in net profit, NPGR is the indicator to measure the growth of listed companies.

Expand capacity of equity capital: the net assets per share(NAPS), accumulation fund per share(AFPS) and undistributed profits fund per share(UPFPS) are used to reflect the expand capacity of listed companies. For good business performance and sustainable development ability of listed companies, expand capacity of its share capital should also be strong. Now, China's listed companies has strong desire to expand, but its performance at least be able to grow with the times that it would make a sustainable power source for the development, so these three indicators were set up to reflect the expand capacity.

2. Fuzzy comprehensive evaluation model

Fuzzy comprehensive evaluation is a method that makes use of the concept of fuzzy mathematics and applies the principle of fuzzy relation composition to quantify those factors that boundaries are ambiguous and can not be quantified easily, then evaluates comprehensively according to the class situation the factors are affiliated to the evaluated object. Fuzzy comprehensive evaluation can be divided into single-level one and multi-level one.

Generally, single-level one is used to evaluate the case that there are fewer factors the evaluated object possesses .The evaluation steps is as follows. First, determine the affiliation grade each factor is to every evaluation class, then a fuzzy affiliation matrix is obtained. Second, an affiliation vector that the evaluated object is to the classes can be gotten by the composition operation of the affiliation matrix and the weight vector of each factor. Last, conclusion is obtained using different principles. In this paper, we adopted the module $M(\cdot, +)$ to calculate. The module not only take into account all factors, but also retain all the information of the single-factor evaluation.

The steps of multi-level evaluation method are as follows. First, the factor set is divided into several sub-factor sets. Second, as for the sub-factor sets, the single-level evaluation method is adopted to obtain some affiliation vectors. Third, combine the vectors to obtain a matrix, then composition operation is performed on it and its immediate higher level

weight vector. The evaluation vector can be obtained until the aforementioned three steps are used to the highest level.

3. Example analysis

Select the chlor-alkali industry, 13 companies as samples, which all indicators data of samples come from the stock channel (http://quote.stock.hexun.com). Its indicators: x_1: EPS (yuan), x_2: ROE(%), x_3: CFPS (yuan), x_4: TAY(%), x_5: MBRGR(%), x_6: GROTA(%), x_7: NPG(%), x_8: NAPS (yuan), x_9: AFPS (yuan), x_{10}: UPFPS (yuan).

3.1 Factor analysis to determine the weights

The weight of each index is decided by the questionnaire data so that the influence comes from subjective factors can be overcome to some extent. The weight is a measure of the relative importance of the factors value. Generally speaking, the traditional method to determine weight include experts estimated method, frequency statistics, and analytic hierarchy process. In order to avoid the impact of human factors, we could use factor analysis to determine weight. We would achieve weight set by running factor analysis module in mathematica.

Step1: Because of the difference of original data dimension, first of all, we adopted the standardization, and run the module standa[data_];

Step2: Program the factor analysis module fac[data_], and analysis the profitability factor using the module, then we could get the factor loading matrix as shown in Table 2.

We can see from Table 2 that EPS, ROE, CFPS, TAY return on the load factor for 0.986,0.953 0.093 0.980 separately, that is $u_1=0.986u_{11}+0.952u_{12}+0.093u_{13}+0.980u_{14}$. Factor loading matrix means the correlation between variables and factors, so the larger the load, the more closely relationship between variables and factors, that is, the greater its contribution, the greater the weight. Take normalized treatment for (0.986,0.952,0.093,0.980), we could get the 2nd-level weight set A_1=(0.327,0.316,0.032,0.325). Similarly, the weight set of growth factor has been obtained A_2=(0.368,0.522,0.110), and the weight set of expand capacity factor is A_3=(0.417,0.507,0.076).

Step3: Rurnning factor analysis module fac[data_] on the profit factor, growth factor and expand capacity factor, we got the 1st-level weight set A of comprehensive evaluation, such as Table 3 shown.

3.2 Conduct attribute function

According to the fact, judgement set V is built up. V can be expressed as poor, general and better, so the corresponding vector we can be represented with Ⅰ,Ⅱ,Ⅲ. So the stock could be divided into three grades. The higher the index value of stock, the higher the level of stock, and the lower the index value, the lower the level. According to the principles, we would take the maximum value, median value and minimum value, respectively, as the three level classification standard, as shown in Table 4.

Through refer to an abundance of documents, we selected partial large trapezoidal distribution. According to the actual situation, we could conduct three types of attribute functions as follows:

$$
\text{I}:\begin{cases} 0, & x<b \\ \dfrac{x-b}{a-b}, & b\le x<a \\ 1, & x=a \end{cases} ; \quad
\text{II}:\begin{cases} 1, & x=b \\ \dfrac{x-c}{b-c}, & c\le x<b \\ 1-\dfrac{x-b}{a-b}, & b<x\le a \end{cases} ; \quad
\text{III}:\begin{cases} 0, & x>b \\ 1-\dfrac{x-c}{b-c}, & c<x\le b \\ 1, & x=c \end{cases}
$$

Where a,b,c are the data of Table 4, and a∈max, b∈median, c∈min.

So, we could obtain the attribute: $\mu_{\text{I}}(x)$, $\mu_{\text{II}}(x)$, $\mu_{\text{III}}(x)$. Thus, we got fuzzy evaluation matrix of 2nd-level indicators. Table 5 is the fuzzy evaluation matrix of 2nd-level indicators of Jinlu Group. In the paper, we have omitted 2nd-level fuzzy evaluation matrix of all other stocks.

3.3 The 1st-level fuzzy comprehensive evaluation

Use the model $M(\cdot,+)$ to evaluate the investment value of listed companies.

Before evaluating comprehensively, the first thing should be done is to 1st-level fuzzy evaluation, which its evaluation set is $B_i = A_i \circ R_i = (b_1, b_2, b_3)$. For example, for Jinlu Group, we could obtain:

(1) profitability: from 3.1,we can see the weight A_1=(0.327,0.316,0.032,0.325), so the comprehensive evaluation for profitability as follow:

$$
B_1 = A_1 \circ R_1 = (0.327,0.316,0.032,0.325) \circ
\begin{bmatrix}
0.784 & 0.216 & 0 \\
0 & 1 & 0 \\
0.368 & 0.632 & 0 \\
0.197 & 0.803 & 0
\end{bmatrix}
= (0.332,0.668,0)
$$

(2) the growth of capability: from 3.1, we known A_2=(0.368,0.522,0.110), so the comprehensive evaluation for the growth of capability as follow:

$$B_2 = A_2 \circ R_2 = (0.368,0.522,0.110) \circ \begin{bmatrix} 0.389 & 0.611 & 0 \\ 0.151 & 0.849 & 0 \\ 0.210 & 0.790 & 0 \end{bmatrix} = (0.245,0.775,0)$$

(3) expand capability: from A_3=(0.417,0.507,0.076), we got the comprehensive evaluation for the expand capacity as follow:

$$B_3 = A_3 \circ R_3 = (0.417,0.507,0.076) \circ \begin{bmatrix} 0.325 & 0.675 & 0 \\ 0.903 & 0.097 & 0 \\ 0 & 1 & 0 \end{bmatrix} = (0.593,0.407,0)$$

Therefore, the 1st-level fuzzy comprehensive evaluation of Jinlu Group could be obtained as Table 6.

The other 12 stocks' 1st-level fuzzy comprehensive evaluation sets have the same structures as Table 6, from which we can see clearly the attribute of the stock's 1st-level indicators. In this paper, evaluate the investment value of stocks, mainly from the perspective of many different stocks to comprehensive study.

3.4 The 2nd-level fuzzy comprehensive evaluation

The 2nd-level fuzzy comprehensive evaluation matrix is $R=[B_1,B_2,B_3]^T$, that is, as shown in Table 6. Then, according to the formula $B = A \circ R = (b_1,b_2,b_3)$, we could obtain 2nd-level evaluation set, and finally evaluation results.

For example, for Jinlu Group, the comprehensive evaluation of investment value is:

$$B = A \circ R = (0.097,0.456,0.447) \circ \begin{bmatrix} 0.332 & 0.668 & 0 \\ 0.245 & 0.775 & 0 \\ 0.593 & 0.407 & 0 \end{bmatrix} = (0.253,0.747,0)$$

Based on the maximum attribute principle, Jinlu Group shares belong to the second category.

We got all 2nd-level fuzzy comprehensive evaluation results in Table 7.

From Table 7, we can see the stock could be divided into three categories:

Category 1: $\mathrm{I} = \{y_{12}, y_{13}\}$;

Category 2: $\mathrm{II} = \{y_1, y_3, y_4, y_5, y_7, y_8, y_9, y_{10}, y_{11}\}$;

Category 3: $\mathrm{III} = \{y_2, y_6\}$.

3.5 Results analysis

In analysis the various types of samples, using average of indicators:

$$\bar{x}_i = \frac{1}{n}\sum x_{ij}$$

which denote the average of the *i* indicator. Where *i* =1,2,3, and *n* denote the number of sample points.

From Table 8, we can see:

The first category clearly belongs to the low-growth, low-expansion, low performance shares. In particular, the MBRGR, GROTA, NPGR, and NAPS are relatively low, especially ROE is very low, which compared with other types have significant differences. This shows that the companies almost have no growth. Negative UPFPS shows that the category almost has no power source of sustainable development, so the category has limited investment value.

The second category stock is good return, higher growth, and better expand capacity stock. Higher NAPS and AFPS indicate better expansion capability, and useful space for development. This type of companies has good business performance, sustainable development capability, so it could be invested.

The third type stock belongs to high-yield, high-growth stocks. However, the lower NAPS and the lower AFPS indicate that its expansion capability is relatively low, and the market is relatively saturated, which means the market has entered a mature stage.

3.6 Select potential stocks ways

In addition, we can make ranks for the investment value of each category. There are two ways to select potential stocks:

(1) the largest attribute principle

According to the principle, the potential of the stock is the largest component of the comprehensive evaluation vector *B*.

(2) mathematical expectation

It could be established the expectation E(x) of stock through set up a value p_j for each component of comprehensive evaluation vector *B*. In this paper, *V* can be expressed as better, general, poor, so the corresponding p_1,p_2,p_3 value we can be represented with 0.7,0.4,0.1. Using the formula E(x)=$\sum P_j b_j$, we could get the expectation of stock. The value range between 0~1, and the greater the expectation , the greater the investment value.

Generally speaking, the first method is available to judge the investment potential of a particular stock: better, general, poor. When there are a number of shares, the second method is used to calculate expectations of these stocks, that is the investment value, which may choose the greatest investment value stock.

Select the second category shares to analysis.

From Table 7, we can see that all attribute of stocks, such as Jinlu Group *B*=(0.253,0.747,0). Adopted expectation method, we get the stock expectation: P=0.7×0.253+0.4×0.747+0.1×0=0.476.

Similarly, we could obtain expectations of all other stocks, as shown in Table 9.

From Table 9, we can see that in the second category stock, the highest fuzzy comprehensive evaluation expectation is sanyou chemical, which has profitability and good growth, and its equity has the expansion space. Its profitability, growth capacity and expand capacity, compared with last year reached 97.64(industry average of 41.41), 95.91(industry average of 40.63), 71.45(industry average of 41.41), which fully illustrate this point.

References

He dongli, & Wang nannan. (2006). Stock Value Analysis with Fuzzy Comprehensive Evaluation. *Economic theory study*. 2006, (7):27-29.

Mu Jing, & Li Quansheng. (2004). A fuzzy classified and predictive analytic model and its application to the orientation of colleges and uinversities. *Journal of Nanjing Agricultural University*(*Sciences Edition*),2004, 4(4), 75-79.

Tao Ye, & Ma Jian. (2005). Stock investment value analysis with cluster and discriminant analyses based on samples from SME board. *The Theory and Practice of Finance and Economics*,2005, 26(128), 45-48.

Tom Copeland, Tim Koller & Jack Murrin.Valuation. (2000). *Measuring and Managing the Value of Companies. John Wiley & Sons*.

Table 1. Original data

Stocks name	x_1	x_2	x_3	x_4	x_5	x_6	x_7	x_8	x_9	x_{10}
Jinlu Group	0.13	6.78	0.22	2.94	-13.23	13.59	0.69	1.95	0.12	0.68
Yinglite	0.71	26.38	2.29	2.61	38.48	211.06	17.05	2.68	0.23	1.26
Shangdong Haihua	0.42	9.18	0.50	4.05	2.60	15.81	4.07	4.33	1.62	1.38
Daqing Huake	0.14	4.01	0.31	3.48	15.95	46.06	4.24	3.50	1.91	0.34
Sino-Thai Chemical	0.93	9.27	1.67	5.23	45.23	71.02	99.85	8.77	5.54	1.84
National shares	0.51	21.25	-0.14	6.18	113.96	116.63	37.26	2.38	0.02	1.17
Haideli	0.89	25.18	0.83	9.97	20.56	67.19	30.46	3.51	0.53	1.62
Taihua share	0.13	4.87	0.51	1.89	64.55	40.44	9.81	2.66	1.05	0.50
Yaxing Chemical	0.06	1.88	0.43	0.74	11.73	-38.77	11.67	3.39	2.11	0.11
Tianli Gaoxin	0.09	2.60	0.39	0.96	15.21	109.54	23.74	3.06	1.73	0.18
Sanyou Chemical	0.55	20.12	0.52	7.50	47.47	110.12	8.55	2.95	0.69	1.06
Chlor-Alkali Chemical	0.05	1.92	0.32	0.83	35.08	-128.91	-2.76	2.51	1.52	-0.02
ST Chemical	2.68	-2026.45	-0.08	40.85	-66.39	-169.46	-33.66	-0.13	0.69	-2.01

Table 2. Profit factor loading matrix

	EPS	ROE	CFPS	TAY
load	0.986	0.952	0.093	0.980

Table 3. The weight set of evaluation index

a_1				a_2			a_3		
0.097				0.456			0.447		
a_{11}	a_{12}	a_{13}	a_{14}	a_{21}	a_{22}	a_{23}	a_{31}	a_{32}	a_{33}
0.327	0.316	0.032	0.325	0.368	0.522	0.110	0.417	0.507	0.076

Table 4. Classification standard of stock

	grade / indicator	I (max)	II (median)	III (min)
profitability	EPS	2.68	0.42	0.05
	ROE	26.38	6.78	-2026.45
	CFPS	2.29	0.43	-0.14
	TAY	40.85	3.48	0.74
growth indicator	MBRGR	113.96	20.56	-66.39
	GROTA	211.06	46.06	-169.46
	NPG	99.85	9.81	-33.66
Expand capacity of equity capital	NAPS	8.77	2.95	-0.13
	AFPS	5.54	1.05	0.02
	UPFPS	1.84	0.68	-2.01

Table 5. Jinlu Group's fuzzy evaluation matrix of 2nd-level indicators

	attribute / indicators	$\mu_I(x)$	$\mu_{II}(x)$	$\mu_{III}(x)$
profitability	EPS	0.784	0.216	0
	ROE	0	1	0
	CFPS	0.368	0.632	0
	TAY	0.197	0.803	0
growth indicator	MBRGR	0.389	0.611	0
	GROTA	0.151	0.849	0
	NPG	0.210	0.790	0
Expand capacity of equity capital	NAPS	0.325	0.675	0
	AFPS	0.903	0.097	0
	UPFPS	0	1	0

Table 6. Jinlu Group's 1st-level fuzzy comprehensive evaluation

	$\mu_I(x)$	$\mu_{II}(x)$	$\mu_{III}(x)$
profitability B_1	0.332	0.668	0
growth of capability B_2	0.245	0.775	0
expand capability B_3	0.593	0.407	0

Table 7. 2nd-level fuzzy comprehensive evaluation set

variable	Stocks name	Attribute structure			results
		Attribute for I	Attribute for II	Attribute for III	
y_1	Jinlu Group	0.253	0.747	0	II
y_2	Yinglite	0.010	0.409	0.581	III
y_3	Shangdong Haihua	0.147	0.848	0.004	II
y_4	Daqing Huake	0.055	0.945	0	II
y_5	Sino-Thai Chemical	0	0.727	0.273	II
y_6	National shares	0.003	0.407	0.590	III
y_7	Haideli	0	0.875	0.125	II
y_8	Taihua share	0.055	0.788	0.157	II
y_9	Yaxing Chemical	0.282	0.716	0.002	II
y_{10}	Tianli Gaoxin	0.078	0.725	0.197	II
y_{11}	Sanyou Chemical	0.003	0.692	0.305	II
y_{12}	Chlor-Alkali Chemical	0.4743	0.4741	0.0516	I
y_{13}	ST Chemical	0.936	0.0003	0.063	I

Table 8. The average of sample indicators

class	x_1	x_2	x_3	x_4	x_5	x_6	x_7	x_8	x_9	x_{10}
I	1.365	-1012.27	0.12	20.84	-15.655	-149.185	-18.21	1.19	1.105	-1.015
II	0.371	9.321	0.578	4.084	23.341	48.333	21.453	3.791	1.7	0.857
III	0.61	23.815	1.075	4.395	76.22	163.845	27.155	2.53	0.125	1.215

Table 9. investment value of listed companies in alkali industry

Stocks name	Sanyou Chemical	Sino-Thai Chemical	Haideli	Tianli Gaoxin	Taihua share	Daqing Huake	Shangdong Haihua	Jinlu Group	Yaxing Chemical
expectation	0.491	0.482	0.437	0.436	0.430	0.383	0.357	0.324	0.316
sort	1	2	3	4	5	6	7	8	9

Purification and Partial Characterization of Esterase

from Marine *Vibrio fischeri*

P. Ranjitha (Corresponding author)

Research Department of Microbiology, Sengunthar Arts and Science College

Tiruchengode 637 205, Tamilnadu, India

E-mail: ranjithaponn@gmail.com

E.S. Karthy

Research Department of Microbiology, Sengunthar Arts and Science College

Tiruchengode 637 205, Tamilnadu, India

A. Mohankumar

Research Department of Microbiology, Sengunthar Arts and Science College

Tiruchengode 637 205, Tamilnadu, India

Abstract

Lipolytic enzymes from marine microbes have been the focus of intense and growing research. The bioluminescence bacterium *Vibrio fischeri* was produced esterase enzyme when the medium contained specific substrate. The esterase was purified from the concentrated culture supernatant. The most active fractions were obtained using the technique of precipitation with 1N HCl. The precipitated fraction was purified by ion exchange chromatography (DEAE-Cellulose) and gel filteration chromatography (Sephadex G200). The purified active fraction exhibiting final specific activity of 300U/mg and characterized; the optimum pH was 7.5, the optimum temperature was 30°C. The enzyme was very stable at the temperature 30°C and at wide range of pH. The enzyme was monomeric protein having molecular mass of 37 KDa estimated by native PAGE assay.

Keywords: *Vibrio fischeri,* Lipolytic enzymes, Extracellular esterase

1. Introduction

Marine microorganisms which are salt tolerant, provide an interesting alternative for therapeutic purposes. Marine microorganisms have a diverse range of enzymatic activity and are capable of catalyzing various biochemical reactions with novel enzymes. Especially, halophilic microorganisms possess many hydrolytic enzymes and are capable of functioning under conditions that lead to precipitation of denaturation of most proteins. Further it is believed that sea water, which is saline in nature and chemically closer to the human blood plasma, could provide microbial products, in particular the enzymes, that could be safer having no or less toxicity or side effects when used for therapeutic applications to humans (Sabu, 2003).

The *Photobacterium (Vibrio) fischeri* group consists of rod-shaped cells with a light yellow, cell-associated pigment and a tuft of sheathed flagella (Hendrie et al., 1970). The species is restricted to the marine environment and has a specific requirement for sodium ion for growth (Reichelt and Baumann, 1973). It occurs both free living in sea water (Ruby and Nealson, 1976) and as the specific luminous symbiont of the monocentrid fish and squid.

Esterases are distinguished from lipases in that their action is generally restricted to short-chain fatty acids. Esterases catalysis of a large number of aliphatic and aromatic esters. Although the molecular and catalytic properties of this protein from mammalian sources have been well studied, only limited investigations have been made in to properties of isolated microbial esterases. Because of the potential food applications, the general economic attractiveness of extracellular enzyme is higher than the intracellular microbial industrial enzymes (Meghji et al., 1990).

Exterases have a wide range of industrial applications. The main applications are in cosmetics, paper and pulp, feed processing detergents or detergent compositions, synthesis of carbohydrate derivatives, food additives, e.g. flavor enhancer and animal feed moreover they can be used, wherever enantiopure compounds are needed and find application as research reagents in studies on plant cell wall structure. The global market for industrial enzymes is constantly growing with a rate of 5-10% per year. The numerous advantages of the new set of esterases compared to commonly used esterases present a great economical potential to a suitable industrial partner in each of the application sectors. Information of lipolytic enzymes produced by marine *Vibrio* spp is particularly limited. Therefore, the objective of this study is to focus on the esterase production of *V. fischeri* isolated from squid and on the purification and partial characterization of its esterase.

2. Experiments

2.1 Bacteria and Growth Conditions

The squids (*Sepia* sp.) were collected and cooled to about 8ºC before opening the mantle cavity along the ventrum. The following two methods were used to obtain samples of symbiotic luminescent bacteria. Light organ fluid containing bacteria was obtained from pore that leads into channels with in the organ tissue. Whole light organs were removed by dissection and homogenized in 700μl of sterile seawater (Ruby and Nagai, 1992). Material obtained in either of these ways was serially diluted in seawater complete (SWC) broth and the samples were spread on SWC (0.38M NaCl, 0.02M $MgCl_2.6H_2O$, 0.025M $MgSO_4.7H_2O$, 8mM KCl, 0.5% peptone, 0.3% yeast extract, 2% agar and 0.3% glycerol) agar plates and identified the luminous bacteria based on the work of Reichelt and Baumann (1973) and VHA (Vibrio Hareyi Agar) differential media (Harris *et al*., 1996).

2.2 Screening of Esterase Enzyme

2.2.1 ZoBell 2216E Modified Media

All strains were precultivated on the solid maintenance SWC medium. For detection of esterase activity the following basal medium (Zobell 2216E, slightly modified) was used. It contains l0g of peptone, 1g of yeast extract, 0.05g of $CaCl_2$, 15 g of bacto agar made to 1 L with aged seawater, pH was adjusted to 7.6. The media supplements with either of 1% tween 20 or 0.25% Triacylglycerol (tributyrin) were then poured into petri disches, after solidification of these media inoculated and incubated at 30ºC for 10 days. The total diameter, minus the diameter of the colony was considered to be proportional to the esterase activity rate. After 1-10 day incubation the halos, clear (on tributyrin) or turbid (on all other substrates) were measured.

2.2.2 Spirit Blue Agar

Broth culture was streaked on the spirit blue agar plates with substrate (Tween or Triacylglycerol). Then the plates were incubated at different temperature 6ºC, 17ºC, 30ºC for up to 15 days. The plates were observed after 6 hrs and every 12 hrs for the clearing of the blue or deep blue color around each streak. Esterase activities at different hours were compared by measuring the width (millimeter) of areas of cleaning or area of deep blue color around the colonies.

2.3 Physical and Chemical Conditions for Esterase Production

Different culture conditions were used to obtain the maximum levels of enzyme productivity by *V. fischeri*.

2.3.1 Incubation Temperature

Bioluminescence bacterium was grown on production medium and incubated at 24 hrs at different temperatures Viz: 10, 20, 30, 40, 50 and 60ºC respectively.

2.3.2 Different pH Values

The different buffers were prepared at different pH values (3, 5, 7 and 9). The production medium was adjusted using a standard pH meter and incubated 30ºC for 24 hrs.

2.3.3 Incubation Period

The effect of incubation period was determined by incubating the production medium at different incubation periods viz. 6, 12, 18, 24, 30, 36, 42 and 72 hrs at 30 ºC.

2.3.4 Different Carbon Sources

A defined minimal salt medium was added with carbon sources included triacylglycerol (tributyrin), tween 20, edible oil (olive, cotton seed, coconut oil) free fatty acids (oleic acid, lauric acid), glycerol and ethanol. All carbon sources were sterilized separately (ethanol by filtration) and added to a final concentration of 2% (w/v).

2.3.5 Time Course of Esterase Enzyme Production

Lipolytic enzyme of esterase production was observed from the initial time of inoculation to decline phase of the *V. fischeri*.

2.4 Purification of Esterase

2.4.1 Enzyme Production and Preparation of Cell Free Filtrate

150µl of culture was inoculated into 200ml of sea water medium with substrate and incubated at 30ºC for 3 days. The portion was centrifuged at 20,000 xg at 4ºC for 30 min. The supernatant was filtered using 0.45 µm cellulose acetate filter units. The cell free filtrate was used as the crude enzyme for the purification experiments.

2.4.2 Acid Precipitation

The crude extract was precipitated by slowly adding 1N HCl at 4ºC with stirring until pH 4.3 was attained. The precipitate containing the esterase activity was collected by centrifugation 10,000 rpm for 30 min. The pellet was dissolved in 10mM phosphate buffer and brought buffer pH 7.5 by the addition of 1N NaOH.

2.4.3 Ion Exchange Chromatography (DEAE- Cellulose)

Dissolved pellet was first applied to a column of DEAE-Cellulose, equilibrated with 20 mM phosphate buffer, pH 7.5. The proteins were eluted at a flow rate of 18 ml/h with a linear NaCl gradient (0.1 to 0.6M). The fractions containing strong esterase activity were pooled (fraction size of 3ml) and concentrate.

2.4.4 Gel Filtration Chromatography (Sephadex G200)

Esterolytic fractions collected from DEAE cellulose chromatography were redissolved in a small volume of 50mM phosphate buffer, pH 7.0, and further purified by gel filtration on Sephadex G200, equilibrated with 50mM phosphate buffer, pH 7.0, containing 0.15M NaCl. Elution with the same buffer was at the flow rate of 12ml/h, 3 ml of fractions were collected. The elution containing esterase activity was pooled and used for further characterization.

2.5 Enzyme Activity Assay

Enzyme assay used for the determination of esterase activity upon emulsified substrate and Tween solution. The final concentration of Triacylglycerol (TAG) was 10-50mM, Tween 0.8-20% (v/v). The mixture of the substrate and buffer (final volume 8ml) was adjusted to pH 8.0 by 1N NaOH and the pH was maintained for 3 min by titration with 50mM NaOH solution (blank). Then 1 ml of the esterase solution in the buffer was added and the esterolytic reaction was observed for 40 min by titration as mentioned above. Enzyme activity is expressed as U/ml and one unit (U) of activity is defined as µmols of free fatty acids liberated /min/ml by the enzyme solution under assay conditions.

2.6 Protein Mass Determination (Native PAGE)

In order to study the undenatured protein profile of esterase enzyme from *V. fischeri* in cell free broth, electrophoresis performed by the method described by Lammeli *et al*., (1970) with some modifications (Vorderwulbecke *et al*., 1992). Gel was casted by using discontinuous buffer system having 10% resolving gel and 5% stacking gel. For measurement of molecular mass of protein, commercial broad range molecular mass standard proteins were used. Protein bands were located by coomassie blue staining.

2.7 Characterization of Lipase Enzyme

2.7.1 pH Stability

Enzyme solutions at a concentration of 70mg/ml were adjusted to various pH ranging from pH 2 to 11 with either 0.1N NaOH or 0.1 N HCl and aliquots were incubated at 30ºC for 4 hrs. Then aliquot was removed and assayed for activity.

2.7.2 pH Optimum

Enzyme assays were conducted at various pH in an emulsified reaction mixture containing 0.4 ml of Tween or TAG, 4ml 50mM Tris, 0.1 ml enzyme. The pH was maintained by pH stat with 0.02 NaOH. After incubation of the reaction mixture for 40 min at 30ºC, it was titrated to pH 9. The quantity of free fatty acids released was calculated from the total quantity of base used. Control reaction mixture contained heat inactivated enzyme.

2.7.3 Temperature Stability

The solution of enzyme at the concentration of 45mg/ml was adjusted to pH 7.0 with 0.02 NaOH and aliquots were incubated at temperatures ranging from 5ºC to 65ºC for 4 hrs. Then the aliquots were assayed for activity.

2.7.4 Temperature Optimum

Enzyme activity was determined at various temperatures ranging from 5ºC to 65ºC. The reaction mixtures (except enzyme) were held at the respective temperature for 5 min before the addition of the enzyme.

2.7.5 Substrate and Enzyme Kinetics

The esterase enzyme was incubated with various concentrations of substrate and the final substrate concentration ranged from 0.5 to 10% of tween 20. Different concentrations of enzyme also studied in the concentration of 5, 10, 15 and 20 microlitres.

2.7.6 Enzyme Stability on Metal Ions and Other Chemicals

Enzymes were preincubated for 1 h at 30ºC (pH 7.0) and in 0.1M Tris-HCl buffer with various ions and other chemicals (one at a time). Assay was performed with the mixture, which did not contain $CaCl_2$ (except in test sample). The ions used were included NaCl (10mM), $BaCl_2$ (0.001M), $MgCl_2$ (0.001M), KCl (2mM), $FeSO_4$ (0.001M), $CaCl_2$ (0.001M), $SrCl_2$ (0.001M), NaF (2mM), $MnCl_2$ (2mM), CuO_2 (2mM). Other chemicals tested were ethylene diamine tetra acetic acid (0.5% EDTA), the ammonic detergent, sodium dodecyl sulphate (0.5% SDS).

2.7.7 Enzyme Stability During Storage

Enzyme solutions from 2 days culture were stored at -20, 1, 8, and 20ºC. Formaldihyde was added to a final concentration of 0.04% to prevent bacterial growth. 30 ml of a 2 days culture of esterase solution was sterilized by membrane filtration (0.22µm, Millipore corp.,). The esterase activity in the stored samples was determined periodically by the pH stat technique and expressed as percent initial activity.

3. Results and Discussion

3.1 Bacteria and Growth Condition

Vibrio fischeri encountered 100% of luminous bacteria. Total viable luminous count range was varied from 4 to 18 CFU/ml. The habitats of this squid species must receive a significant input of cells of symbiotic *V. fischeri* (Lee and Ruby, 1994). The luminous *V. fischeri* isolate was motile Gram negative rods. They produced yellow colonies on SWC agar plates. They were halophiles, unable to grow in the absence of NaCl. The colony morphology of the luminous *V. fischeri* strains tested on VHA was small (2 to 5mm) dark blue green colonies. Harris et al., (1996) reported that the VHA media displays great potential as primary isolation medium and offers significant advantages over thiosulfate-citrate- bile salts- sucrose agar.

3.2 Screening of Esterase Enzyme

In ZoBell modified media, the *V. fischeri* was showed 36 mm of halos after 10 days incubation indicates that the strain *V. fischeri* showed significant esterase activity. In fact it actively splits tween 20 than tributyrin as good substrate. Bruni et al., (1982) reported that the most strains of *Pseudomonas* sp. NCMB 1082 was split all tweens, tributyrin, but not triolein, 9 strains showed good activity on water soluble tweens, 4 on tween 85. In spirit blue agar, the width of hydrolysis areas were measured to observe the esterase activity of luminous *V. fischeri* bacteria at different temperatures. At 30ºC, the esterase activity of strain was appeared after 7 hrs with a large discoloration area or dark blue halos and the widest area observed after 1 day. At 17ºC, the activity began after 12 hrs, the size of halos increase after 3 days but the area of hydrolysis was smaller than that at 30ºC. Apparently low activity was observed at 6ºC. More or less similar mm of halos as that in ZoBell modified agar was observed in spirit blue agar with the substrate (tween, tributyrin) at 30ºC. The higher activity at 30ºC may be attributed to maximum growth of the organism and subsequently increased esterase secretion.

3.3 Physical and Chemical Conditions for Esterase Production

3.3.1 Temperature

From this study, observed that 30ºC was generally more favorable for esterase production. However, the temperature below or above the 30ºC caused a sharp decrease in enzyme yield as compared to the optimal temperature. Wood et al., (1995) found that esterolytic activity at moderate temperatures (eg. 20ºC - 30ºC) was high with structurally diverse ester substrates including aliphatic, cyclic and sugar esters.

3.3.2 pH

This test found that the best buffer was phosphate buffer at optimum pH for the production of esterase enzyme was recorded at pH 7.0. A notable decline in the enzyme productivity occurred at both higher and lower pH values. In order to favour the secretion of extracellur lipolytic enzymes the effect of temperature and carbon source has been studied by Dominguez et al., (2007). In the dynamic field of biocatalysis, several lipolytic enzymes active and stable in extreme conditions of temperature, salinity and pH have been characterized by Encarnacion et al., (2005).

3.3.3 Carbon Source

The ability of *V. fischeri* to utilizing tween 20, tributyrin as a carbon source and energy material to produce esterase. Oils were not utilized by this strain. Interestingly *V. fischeri* exhibited their maximum ability to biosynthesize esterase enzyme with in 48 hrs. The production level of esterase enzyme of *V. fischeri* depended on the substrate utilized by the cells. The specific production level of the enzyme examined was very low when ethanol serves as the sole carbon source. In contrast, with the water immiscible glycerol and triglycerides such as tributyrin, the expression of the enzyme was markedly enhanced. More over the use of sorbitan monoesters (tween 20) increased the esterase enzyme production. Different substrates were used, but the maximum esterase productivity was attained in the tween 20. The addition of fatty acids did not repress the production of the enzyme. The similar result was observed by Shabtai and Mishne (1992).

3.3.4 Incubation Period

Highest enzyme production was observed in the incubation period of 72 hrs at 30ºC.

3.3.5 Time Course for Esterase Production

Esterase from the *V. fischeri* produced maximum activity in stationary phase (Fig 1). Similarly, the maximal *Lactobacillus casei* esterase production was obtained intracellularly during the late logarithmic phase, but during the stationary phase, the esterase activity was released in the culture medium (Choi and Lee, 2001). In contrast Kakariari et al., (2000) reported that the production esterase, as assess in the intracellular extract during growth, reached maximum in the middle of the logarithmic phase and then decline rapidly.

3.4 Purification of Esterase

1N HCl precipitate of crude extract of cell free supernatant eluted in DEAE-Cellulose chromatography. The esterolytic fractions were assayed in chromogenic agar plate with the substrate of tween 20 showed yellow zone around the active fractions. The pooled material was eluted in gel filtration (Sephadox G200) chromatography. The esterase activity was represented by fractions between 28-34. Gel filtration (Sephadox G200) chromatogram shown in figure 2. This esterase had substrate specificity on tween 20, tributyrin and exhibited high activity only on the compound of sorbitan monoester. The purified esterase from gel filtration chromatography showed single peak corresponding to protein peak and exhibiting final specific activity of 300U/mg. In native PAGE electrophresis it showed single band indicates esterase from *V. fischeri* was monomeric protein.

An esterase hydrolyzing tween 80 (polyoxyethylene sorbitan monooleate) was purified from sonicated cell lysates of *Mycobacterium smegmatis* ATCC 14468 by DEAE-Cellulose, Sephadex G150, phenyl sepharose and diethyl – (2-hydroxypropyl) aminoethyl column chromatography and by subsequent preparative polyacrylamide gel electrophoresis. The esterase had narrow substrate specificity; it exhibited a high activity only on compounds having both polyoxyethylene and fatty acyl moieties such as tweens (Tomioka, 1983). Purification of the esterase was performed in three steps of anion exchange chromatography and finally by gel filteration chromatography. Separation on Sephacryl S-300 gave a symmetrical single peak (Kakariari et al., 2000). Smacchi et al., (2000) reported that the chromatography in both DEAE-cellulose and on Sepharose 6B resolved the esterase activity into one peak corresponding to the major protein peak.

3.5 Protein Mass

The esterase from *V. fischeri* was showed molecular mass of 37 KDa. Tomioka (1983) estimated that the molecular weight of esterase was to be 36,000 by sodium dodecyl sulfate polyacrylamide. The purified extracellular *Arthrobacter nicotianae* esterase showed a single band on SDS-PAGE corresponding to a molecular mass of about 32 kg mol^{-1}, suggesting that the enzyme is a monomer (Smacchi et al., 2000). Kakariari et al., (2000) obtained only one band with the crude cell free extract in SDS-PAGE, indicating a simple enzyme system, significantly different from the complex esterase system of the *P. freudenreichii* ssp *freudenreichii* strains described by Dupuis and Boyaval (1993).

3.6 Characterization of Esterase

3.6.1 pH, Temperature Optima

Vibrio fischeri esterase had an optimum pH of 7.5 on tween 20 substrate (Fig 3). In this pH the esterase enzyme was retained 100% of the optimum activity. As indicated in figure 4, the enzyme had a temperature optimum of 30ºC. At the temperatures below 25ºC, activity slowly decreased. Sixty percentage of the activity available at 37ºC. Smacchi et al., (2000) stated that the extracellular esterase of *A. nicotianae* 9458 had pH and temperature optima of 7.0 and 30ºC, respectively. Similarly crude preparations of esterases from lactic acid bacteria (Khalid and Marth, 1990) and purified esterase from *L. plantarum* (Gobbetti et al., 1997) had pH and temperature 6.5-7.0 and 30-40ºC respectively. Rhee et al., (2005) determined that the optimal pH for Est E1 esterase protein at various pH values of pH 3.0 to 9.5. The temperature range was 30 to 90ºC, at lower temperature the enzyme still showed activity.

3.6.2 pH and Temperature Stability

The enzyme was stable over a wide pH range. In pH 6 retained 60% and pH 9 retained 70% activity. At pH below 4 or above 10 the loss of enzyme activity was appreciable. Gradual loss of activity with increased temperature up to 65ºC. The temperature above 30ºC, 30% actively retained at 50ºC, 70% of the activity retained at 40 and 45ºC, 90% activity at 35ºC. Tomioka (1983) reported that tween-hydrolyzing esterase of *Mycobacterium smegmatis* was stable to heat treatment at 100ºC and to a wide range of pH.

3.6.3 Substrate and Enzyme Kinetic

The esterase activity was reached at maximum in between the concentration of 0.5 to 8 % of tween. The concentration above 8 % reduced 50 % of the enzyme activity. Macarie et al., (1999) assayed the esterase activity in the range of substrate concentration from 0.3 to 2.7 mM using pNPC6. More than 2mM inhibit the esterase activity. Bendikiene et

al., (2005) found the tween 85 was the best substrate among all the detergents studied and 10% concentration was optimal for the hydrolysis by lipolytic enzyme from *Pseudomonas mendocina* 3121-1. A linear relationship was also evident when enzyme activity was measured as a function of protein concentration. The same direct proportionality was found when crude extract were used as the source of enzyme (Oterholm et al., 1970).

3.6.4 Effect of Metal Ions, Chelators and Other Chemicals on Esterase

Figure 5 showed the results on the effect of various inhibitors on the activity of the esterase. Except NaCl, $CaCl_2$, which were showed no effect on enzyme activity. All other ions tested in the present study showed inhibition with relative degree of variation. Evidently even the low concentration of NAF and CuO_2 highly retarded the easterase activity. The inhibitory action of former was stronger than that of latter. Action of these two compounds could be attributed to their effect in creating the imbalance of ions in the reaction mixture by absorption or release, respectively. In this study the SDS was highly favored the activity of esterase (133%). The esterase enzyme activity was not inhibited by the EDTA. It produced 67% of the activity in the presence of EDTA. Similarly Moskowitz *et al.*, (1977) reported that the esterase of *Mucor miehei* was relatively unaffected by the high concentration of various salts, ethylene diamine tetraacetate (EDTA) or sulfhydryl inhibitors. Kakariari *et al.*, (2000) showed that the esterase from *P. freudenreichii* ssp *freudenreichii* did not affected by EDTA, other metal ions except Cu^{2+}, Hg^+, Fe^{2+}.

3.6.5 Enzyme Stability During Storage

Figure 6 showed the esterase activity as a function of storage time at different temperatures. Frozen storage did not affect the enzyme activity to any greater extent. These lipolytic enzymes stability suggests that the accelerated destruction of enzyme at higher temperatures.

Conclusion

The demand for industrial enzymes particularly of microbial origin is ever increasing owing to their applications in a wide variety of processes. Enzyme mediated relations are attractive alternatives to tedious and expensive chemical methods. In the above scenario enzymes such as proteases and amylases have dominated the world market owing to their hydrolytic reactions for proteins and carbohydrates. However with the realization of the biocatalytic potential of microbial lipases and esterases in the last one and a half decades, industrial fronts have shifted towards utilizing lipase, esterase enzymes for a variety of reactions of immense importance.

References

Bendikiene, V., Surinenaite, B., Bachmatova, I., Marcinkevieiene, L. & Juodka, B. (2005). The specificity of *Pseudomonas mendocina* 3121-1 lipase. Hydrolysis. Biologija.1: 27-30.

Bruni,V., Maugeri,T & Alonzo, V. (1982). Lipolytic activity of marine bacteria influence of NaCl and $MgCl_2$. Marine Biology. 67: 113-119.

Choi, Y. J. & Lee, B. H. (2001). Culture conditions for the production of esterase from *Lactobacillus casei* CL 96. Bioprocess and Biosystems Engineering. 24: 59-63.

Dominguez, A., Fucinos, P. Rua, M. L., Pastrana, L., Longo, M. A. & Sanroman, A. (2007). Stimulation of novel thermostable extracellular lipolytic enzymes in cultures of *Thermus* sp. Enzymes and Microbial Technol. 40: 187-194.

Dupuis, C. & Boyaval, P. (1993). Esterase activity of dairy *Propionbacterium*. Lait. 73: 345-356.

Gobbetti, M., Smacchi, E. & Corsetti, A. (1997). Purification and characterization of a cell surface-associated esterase from *Lactobacillus fermentum* DT41, Int. Dairy. J. F.13-21.

Encarnacion, M., Sara, M., Cristina, S. P. & Antonio. V. (2005). Lipolytic enzymes from extremophilic microorganisms. Microorganisms for industrial enzymes and Biocontrol. 9: 25-43.

Harris, L., Owens, L. & Smith, S. (1996). A selective and differential medium for *Vibrio harveyi*. Appl. Environ. Microbiol. 62(9): 3548-3550.

Hendrie, M. S., Hodgkiss, W. & Shewan, J. M. (1970). The identification, taxonomy and classification of luminous bacteria. J. Gen. Microbiol. 64: 151-169.

Kakariari, E., Georfalaki, M. D., Kalantzopoulos, G., & Tsakalidou, E. (2000). Purification and characterization of an intracellular esterase from *Propionibacterium freudenreichii* ssp *freudenreichii* ITG 14. EDP Sciences. 491-501.

Khalid, N. M. & Marth, E. H. (1990). *Lactobacilli*-their enzymes and protein ripening and spoilage of cheese: a review. J. Dairy Sci. 73: 2669-2684.

Lee, K. H. & Ruby, E. G. (1994). Effect of squid host on the abundance and distribution of symbiotic *V. fischeri* in nature. App. Environ. Microbiolog. 60: 1565-1571.

Macarie, E. A., Margo, V. A. & Baratti. J. (1999). Characterzation of a thermostable esterase activity from the moderate thermophile *Bacillus licheniformis*. Biosci. Biotechnol. Biochem. 63: 1865-1870.

Meghji, K., Ward, O. P. & Araujo, A. (1990). Production, purification and properties of extracellular carboxyl esterases from *Bacillus subtilis* NRRL 365. App. Environ. Microbiolog. 56: 3735-3740.

Moskowitz, G. J., Shen, T., Weat, R., Cassaigne, R. & Feldman, L. I. (1977). Properties of the esterase produced by *Mucormichei* to develop flavor in dairy products. J. Dairy Sci. 60: 1260-65.

Oterholm, A., Ordal. Z. J. & Witter, L. D. (1970). Purification and properties of a glycerol ester hydrolase (lipase) from *Propionibacterium shermanii*. App. Microbiol. 20: 16-22.

Reichelt, J. L. & Baumann, P. (1973). Taxonomy of the marine, luminous bacteria. Arch. Microbiol. 94: 283-330.

Rhee, J. K., Ahn, D. G., Kim, Y. G. & Oh, J. W. (2005). New thermophilic and thermostable esterase with sequence similarity to the hormone – sensitive lipase family, cloned from a metagenomic library. App. Environ. Microbiol. 71: 817-825.

Ruby, E. G. & Nagai, M. J. M. (1992). A squid that glows in the night: development of an animal bacterial animal mutualism. J. Bacteriol.174: 4865-4870.

Ruby, E. G. & Nealson, K. H. (1976). Symbiotic association of *Photobacterium fischeri* with the marine luminous fish *Monocentris japonica*: a model of symbiosis based on bacterial studies. Biol. Bull. 151: 574-586.

Sabu, A. (2003). Sources, properties and applications of microbial therapeutic enzymes. Indian J. Biotechnol. 2: 334-341.

Shabtai, Y. & Mishne, N. D. (1992). Production, purification and properties of lipase from a bacterium (*Pseudomonas aeruginosa YS-7*) capable of growing in water-restricted environments. App. Environ. Microbial. 59: 174-180.

Smacchi, E., Gobbetti, M., Rossi, J. & Fox, P. F. (2000). Purification and characterization of an extracellular esterase from *Arthrobacter nicotiancae* 9458. Lait   80: 255-265.

Tomioka, H. (1983). Purification and characterization of the Tween- hydrolyzing esterase of *Mycobacterium smegmatis*. J. Bacteriol.155: 1249-1259.

Vorderwulbecke, T., Kieslich, K. & Erdman, H. (1992). Comparison of lipases by different assays. Enzyme Microb. Technol. 14: 631-639.

Wood, A. N. P., Fernandez, L. R. & Cowan, D. A. (1995). Characterization of a novel thermostable esterase as an industrial catalyst. Biotechno. & App. Biochem. 21: 313-322.
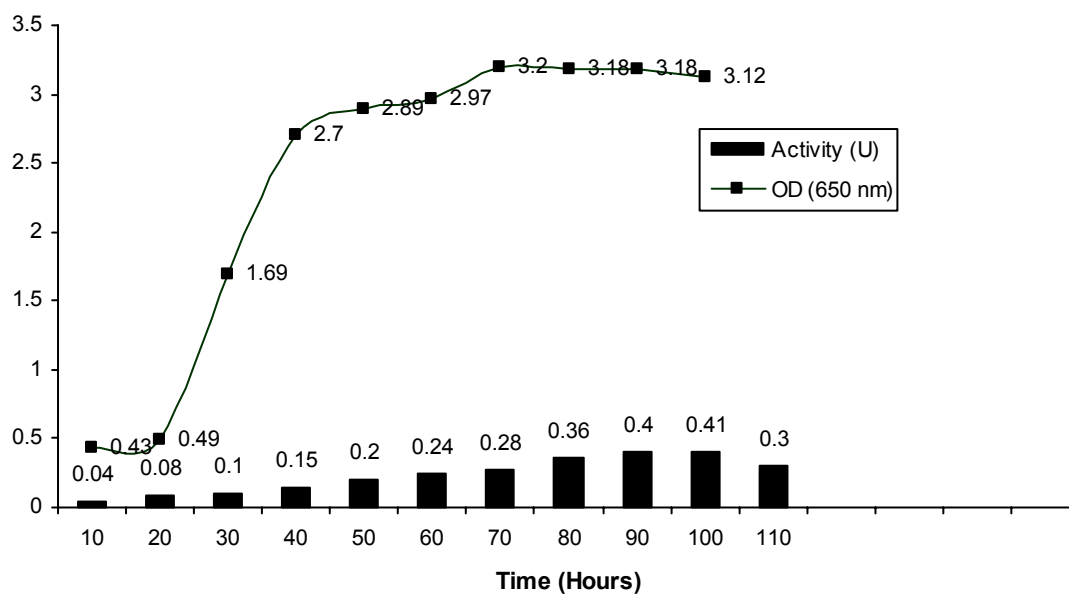
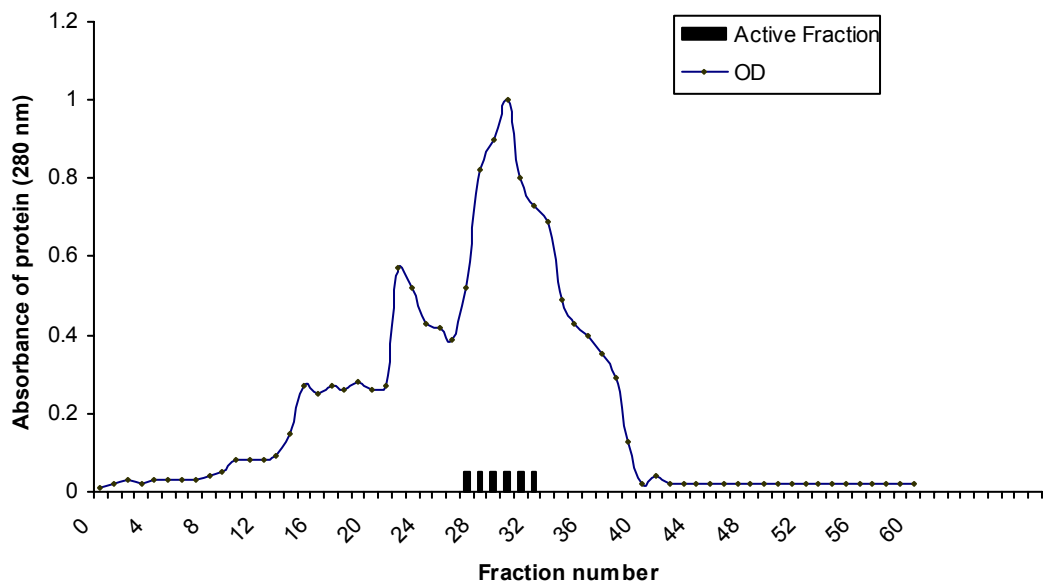Figure 1. Esterase Production during Growth of V. fischeri

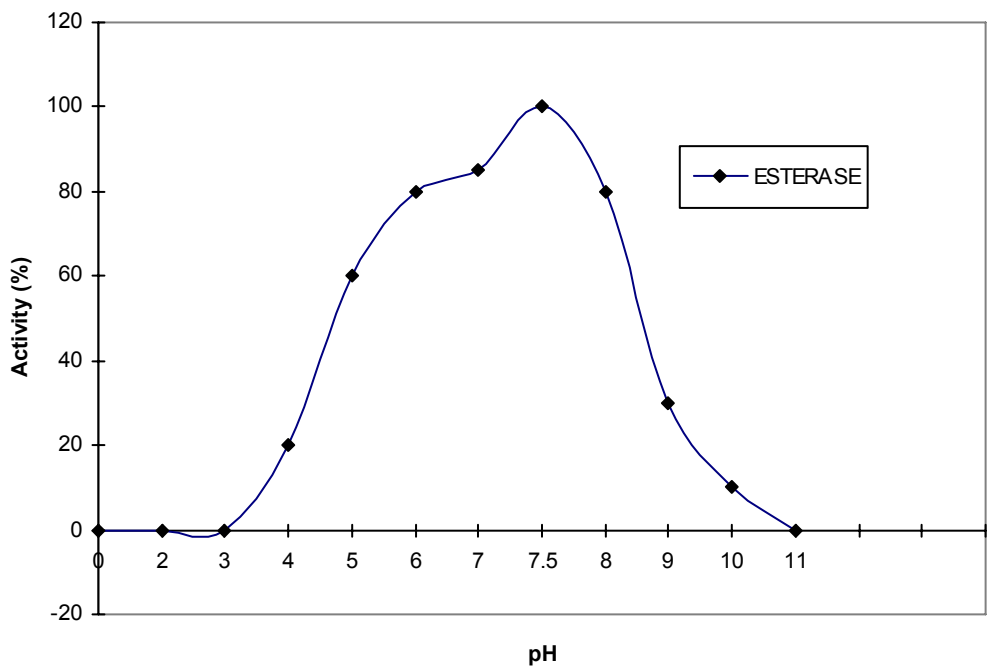Figure 2. Elution Profile of Esterase from the Sephadex G200 Column

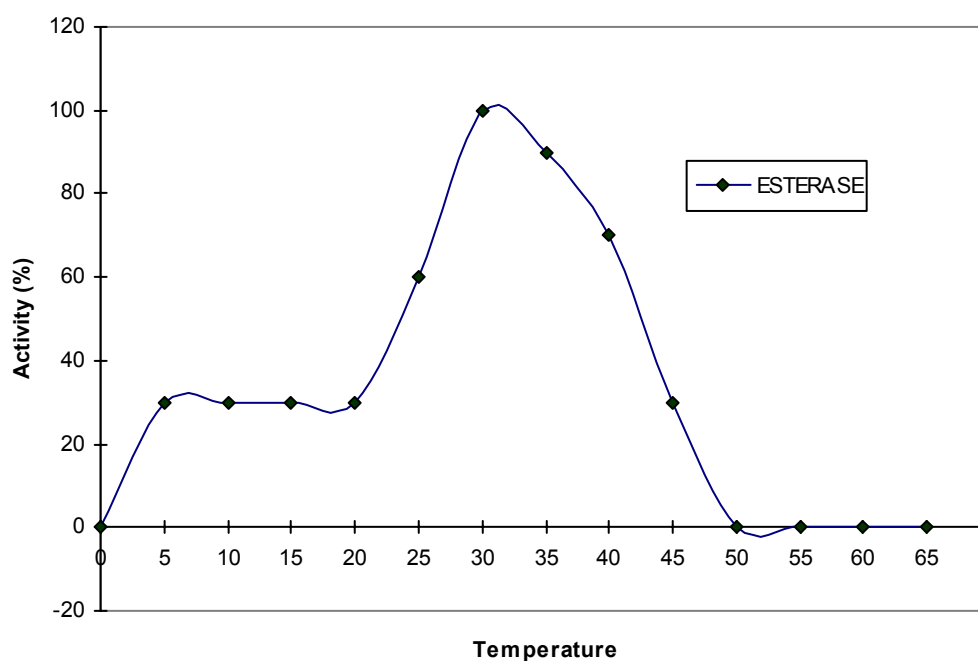Figure 3. Effect of pH on the Esterase from *V. fischeri*

Figure 4. Effect of Temperature on the Esterase from *V. fischeri*
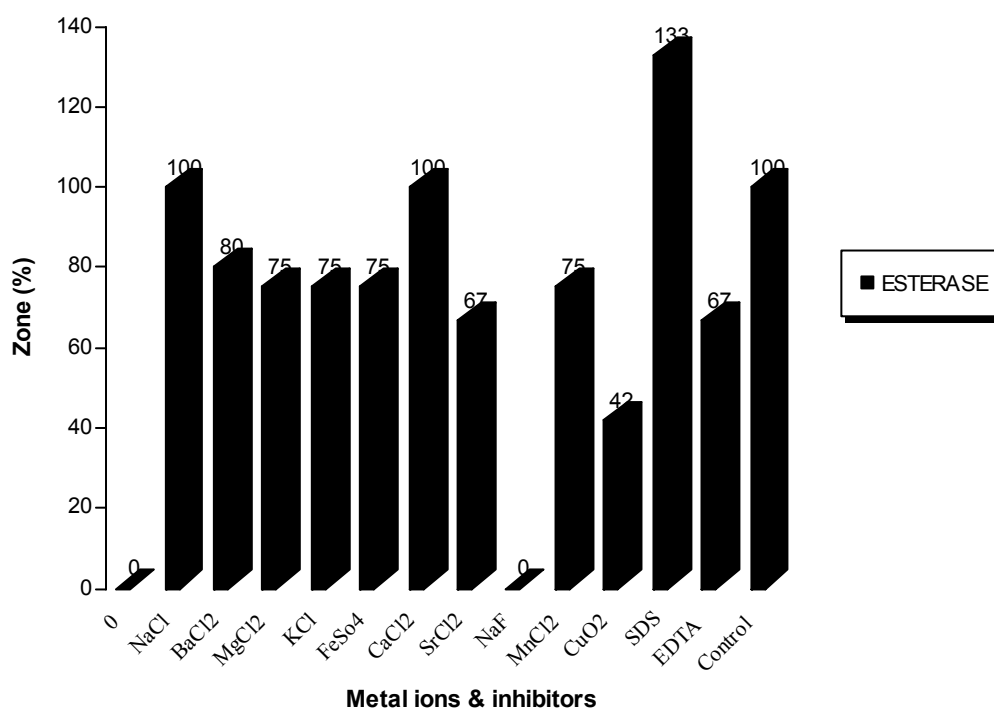

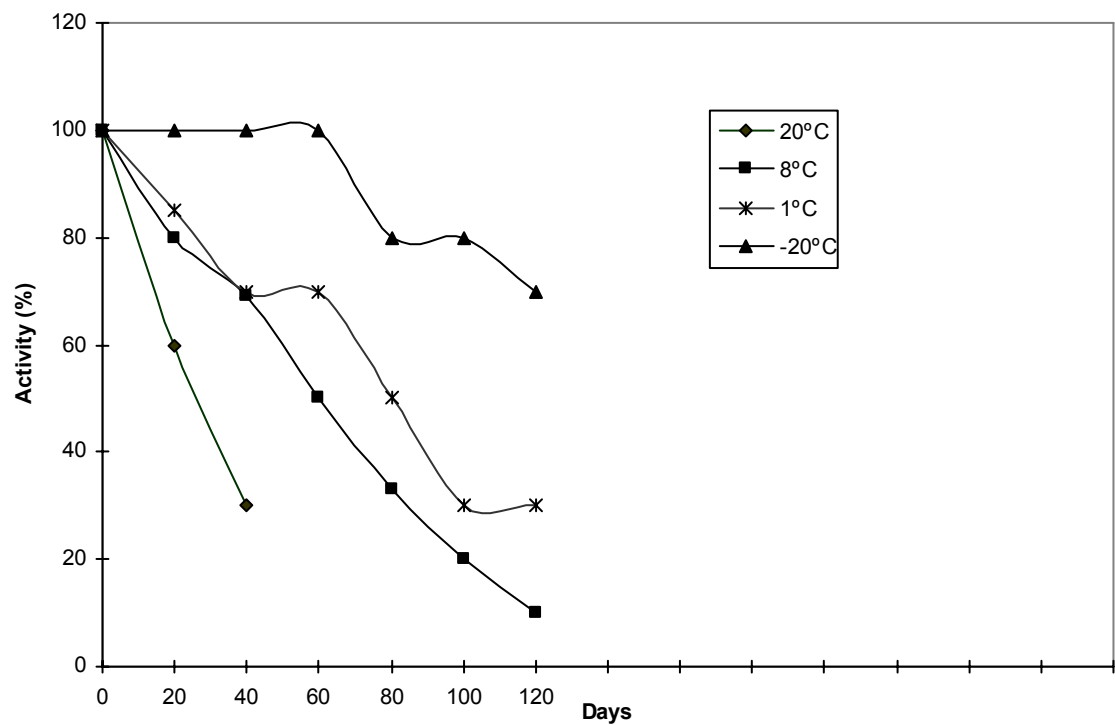
Figure 5. Effect of inhibitors on Esterase enzyme

Figure 6. Storage Stability of *V. fischeri* Esterase at Different Temperature

The Work in Process (WIP) Control

Model and Its Application Simulation

in Small-batch and Multi-varieties Production Mode

Yaochao Wang

School of Mechanical and Electronic Engineering

Tianjin Polytechnic University

Tianjin 300384, China

E-mail: wych88@hotmail.com

Abstract

This paper aimed at the phenomena of the volume of work in process (WIP) great and uneven distribution, which is caused by small batches, various breeds, the complex scheduling, and long production cycle and so on in machine manufacturing industry. The machine manufacturing industry production workshop is taken as the research object in this paper. A work in process (WIP) control model based on the limited capacity is put forward by analyzing the characteristics of multi-varieties of small-batch production, the factors of the state of workshop equipment, equipment parameters (breakdown rate and maintenance rate), delivery deadline, product process similarity and so on. Taking a gear production line of a state-owned large-scale speed reducer's factory as an example, Witness2003 is used to simulate and optimize the work in process control model of the gear production line. The case study proves that in the manufacturing of small-batch and multi-varieties production mode, WIP volume control problems can be effectively solved by the WIP control model. And the WIP control model provides an effective, workable solution for small-batch and multi-varieties production under the control of the production mode.

Keywords: Machine manufacturing industry, Small-batch and multi-varieties, Work in process (WIP), Control model, WITNESS

1. Introduction

The four target criteria of delivery time, on-time delivery, WIP, and utilization determine the objectives of production logistics. They are not only easy to measure, but are also of strategic importance for commercial success. Empirical studies show that enterprises with short delivery times grow faster and earn higher profits than their slower competitors. With the widespread efforts to reduce the WIP level throughout the value chain, on-time delivery gains importance. At present, there are some generally characteristics exists in the mechanical manufacturing industry producing such as multi-varieties, small-batch, complexity of scheduling, long production cycle and so on, it leads to the phenomena of the accumulation of WIP in the process routs, uneven WIP distribution quantity, and extension of production cycles. So how to effectively control the enterprise WIP under the guarantee product delivery deadline becomes an important restriction factor which can enhance the benefit and the competitive ability of enterprise. Currently, the approach of this phenomenon is mainly built on the basis of experience, this paper take this situation as research object, a work in process (WIP) control model based on the limited capacity is put forward, powerful basis was provided by reducing production cycle, balancing physical distribution system, optimizing control physical distribution investment as well as the transporting batch by the control factors in WIP control mode.

2. Work in Process (WIP) Control Model

2.1 Production System Model

Some suppositions are proposed before production system model: Assuming workshop human resources are sufficient, the production system is only constrained by capacity of equipment and limited products inventory. There are N processes through the bottleneck equipment production, and M available equipments in each process. Each process has a part buffer, products from out of a final process directly into the warehouse, production tasks with N processes as shown in figure 1, the production of the time structure shown in figure 2.

Supposition B_i represents buffer aggregate capacity which between i and i+1, I_i is the number of parts which in B_i, S_i is surplus spatial quantity in the B_i, so $B_i = I_i + S_i$. I_i and S_i is important attribute in WIP management. I_i decide the ability of

maintaining the regular production after machine i when machine i breakdown, S_i decide the ability of maintaining the regular production before machine i when machine i breakdown. Asuming equipment breakdown rate and repair rate obeys the exponential distribution, breakdown rate is P (t) $=1-e^{pt}$ (p- breakdown rate), repair rate is H (t) $=1-e-ht$ (h-repair rate).The production carries on in batch, production process can't be interrupt. it is only considered the system influence of equipment work, machine breaks down, the number of buffer, investment batch and movement batch and so on batch behavior and so on, under the determination production task premise.

2.2 The Determination of Queuing Order in Work Shop

A reasonable working procedure plays an important role in controlling WIP. This paper uses the group technology to determine the product the similarity factor, if similar factor $S_k-S_{k-1}<h$ (h is precision), parts which components k and k-1 as a part family, P_j (j<=k) is part family. Queuing order determined by heuristic algorithm.

2.3 The Construction of WIP Control Model

The optimal state in working procedure is smallest WIP, and stable continuously production. The objective function is $S_i(t)=B_i-I_i(t)$ $0<B_i<R$, $I_i>0$, L_i is the distance between machine i and WIP zone; The V_m is the speed of movement; S_k is similar factor of part k; P_j is part family; V_i is work time of machine i, P_i is investment batch of product i, P_{0i} is turnover batch of product i; T is the production cycle. The maintenance time of machine j which appears the breakdown in working procedure i is t (t<T): $t = \int_0^T tdH(t) = \int_0^T td(1-e-h(t)) = \frac{1}{h}(1-e^{hT}) - le^{-hT}$ (1), Their consecutive breakdown time of machine j is u(u<T): $u = \int_0^T tdP(t) = = \int_0^T td(1-e^{p(t)}) = \frac{1}{p}(1-e^{-pT}) - le^{-pT}$ (2), Before Machine j is restoring, the breakdown probability of other machines is:

$$F_2(t)' = 1-(1-F_j(t)(1-F_1(t))(1-F_2(t))\cdots(1-F_{n*m}(t)) = 1-e^{-\sum_{k=1}^{m*n}f_k t} \quad (3)$$

Before Machine j is restoring, the normal work probability of other machines is:

$$F_2(t)' = F_j(t)(1-F_1(t))(1-F_2(t))\cdots(1-F_{n*m}(t)) = e^{-\sum_{k=1}^{j-1}f_k t-\sum_{k=j+1}^{m}f_k t} - e^{-\sum_{k=1}^{m}f_k t} \quad (4)$$

$$= e^{-\sum_{k=1}^{j-1}f_k t-\sum_{k=j+1}^{m}f_k t}(1-f_j t)$$

Transporting time: $T_{Bi} = V_m * L_i$; the speed of parts enter machine: $v_1 = P/(t+t_{si})$;the speed of Components output buffer: $v_2 = P_0/T_{Bi}$; v_3 is the difference between the input and output: $v_3 = v_1 - v_2$;and the number of parts in buffer is: $v_3 \times (T-T_i)$;the number of parts which the machine is processing is: $v_0 \times (t+t_{si})$; NO. of parts in WIP = NO. of parts in transporting + NO. of parts in buffer + NO. of parts which is processing: $I_i(t) = v_i \times T_{Bi} + (P/(t+t_{si}) - P_0/T_{Bi}) + v_0 \times (t+t_{si})$ (5);

If the paper seeks to minimize the volume of WIP, at the same time the surplus of WIP must be maximum: $\max \sum F_i(t) = \sum B_i - \min \sum I_i(t)$.

3. An Example

Taking a gear production line of a state-owned large-scale speed reducer's factory as an example, there are 256 kinds of gear in this gear production line, the production batch reach from 1 to 300, and the production mode tends to small-batch and multi-varieties production. The complex scheduling is caused by above characteristics, the equipments are old, and abilities of product are limited, so the phenomenon of WIP accumulation becomes more and more serious. At present, percent 3 productions can't be delivery on time.

Take the cyclical gear from 2 to 8 whose ratio between 11 and 87 from March 2007 production plan as an example, the product processes main routs are: drilling, boring machine, gear milling, dill chamfering, coarsely flat surface grinding, accurate flat surface grinding, grind bearing hole, grinding, cyclical, and so on. According to the urgency of product delivery time, production of this product can be divided into three categories: abnormal emergency, the general emergency, forecast invest. The paper use group technology which take the parts in production process don't need to be replaced with clamping fixture but only need to be adjusted with precision products as a part family. according to the N\1 schedule problem ,this paper use SPT(shortest processing time), And according to the N\M(M>3) schedule problem ,this paper use PALMER algorithm. WITNESS2003 is used to simulate the gear production, simulation interface shown in Figure 3, according to the above WIP control model, an objective function wipfun() is establish in the simulation model.

This paper uses annealing algorithm to optimize the objective function, when the objective functions in the smallest the

value of the various variables shown in Table 1. Optimize value re-put into the model, average WIP, and the variety of production cycle is go before and after the optimization, comparing situation as shown in Table 2: Products in the average of WIP volume reduce 0.1-27 units and production cycle shortened 3 -300 hours can be found in chat through the optimization.

4. Conclusions

This paper presented a WIP control model for small-batch and multi-varieties production mode. The control model is mainly decided by the following nine factors: investment batch, delivers the batch, movement speed between working procedure, movement speed between working procedure,   maintenance rate of machine, breakdown rate of machine, setup time, the capacity size of WIP, workshop scheduling. In addition, the application simulation experiments provided some insight into the impact of sequencing rules on WIP, throughput and production cycle. As a future study, a distributed learning method will be developed to improve coordination among controllers in the Machine manufacturing industry. One of the possible scenarios to be studied is to adjust the sequencing decisions of the controller to reduce set-ups or accelerate batch operations at the succeeding product steps. In short, if management can learn to minimize the level of WIP inventory effectively, it can increase throughput and reduce lead-time requirements.

References

Cheng, Qiurong, Ma, Shihua. (2006). Production and operation management. China machine press, 2 p287-p311(In Chinese)

H.L.Dding, K.W.Yu and H.P. (2003). Wiendahl. Decentralized WIP-oriented manufacturing control (DEWIP). *Production Planning & Control*, 14(1), 42-54

Luo, Shoucheng. (1999). Application of seclude in workshop management. *Mathematical Theory and Application*, 24(3)(In Chinese)

Spearman & Woodruff. (1990). CONWIP: a pull alternative to kanban. *International Journal of Production Research,*

Zhang, Jie, Wang, Yu. (2002). Optimal of WIP inventory research. *Journal of Huazhong Science and Technology University*, 35(1):48-51(In Chinese)

Table 1. The Optimize of Output Batch And Input Batch

Part	p_i	p_{0i}	Part	p_i	p_{0i}	Part	p_i	p_{0i}	Part	p_i	p_{0i}
P223	30	15	443	200	100	P587	30	30	P747	30	30
P311	25	25	459	200	100	P59	50	50	P759	30	30
P325	50	50	487	100	50	P611	30	30	P771	20	10
P329	50	50	49	60	30	P643	40	20	P811	30	10
P417	50	30	511	50	50	P66	20	10	P817	40	20
P423	25	20	517	50	50	P711	20	20	P823	20	20
P425	15	15	523	40	20	P725	20	10	P829	30	15
P435	25	25	525	20	20	P735	30	20	P847	20	10
P859	30	10	887	30	10						

Table 2. Average WIP (AvgWIP) and Average Production Cycle (AvgTime) before and after Optimization

Name	B opt Avg-WIP	A opt Avg-Time	B opt Avg-WIP	A opt Avg-Time	Name	B opt Avg-WIP	A opt Avg-Time	B opt Avg-WIP	A opt Avg-Time
p223	1.97	78.72	1.54	75.33	p725	2.51	150.43	2.64	194.08
p311	9.23	221.55	7.76	228.24	p735	25.53	1021.29	22.24	1089.73
p325	13.2	316.86	10.11	297.09	p743	25.73	1029.3	23.86	1169.18
p329	16.12	386.77	15.15	445.45	p747	27.72	1108.77	25.75	1261.52
p417	79.44	1124.9	93.74	1167.8	p759	28.16	1126.5	27.73	1358.71
p423	24.53	588.73	41.24	1212.3	p771	15.89	953.25	18.12	1332.08
p425	2.68	107.16	4.57	224.05	p811	11.33	453.12	8.36	409.5
p435	38.2	916.71	43.85	1289.3	p817	26.74	802.2	16.87	620.08
p443	125.26	751.54	135.7	997.72	p823	4.02	241.03	9.07	666.42
p459	179.39	1076.3	193.4	1421.5	p829	15.93	637.33	16.58	812.23
p487	96.45	1157.3	95.97	1410.8	p847	5.85	350.71	11.78	865.68
p49	40.05	961.26	49.92	1467.5	p859	20.66	826.59	20.75	1016.59
p517	14.21	340.99	13.02	382.65	p523	11.86	355.74	14.01	514.96
p525	2.05	122.89	8.12	596.86	p587	10.9	436.11	12.12	594.07
p711	14.47	868.11	18.73	1376.5	p59	26.72	641.38	35.73	1050.37
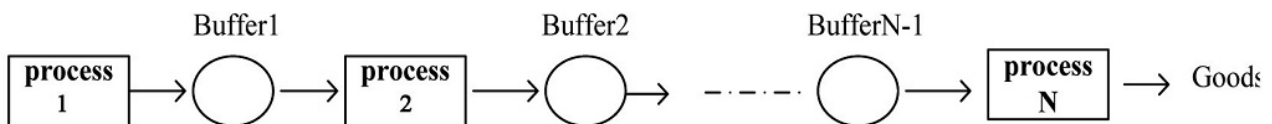
Figure 1. Production Tasks with N Processes
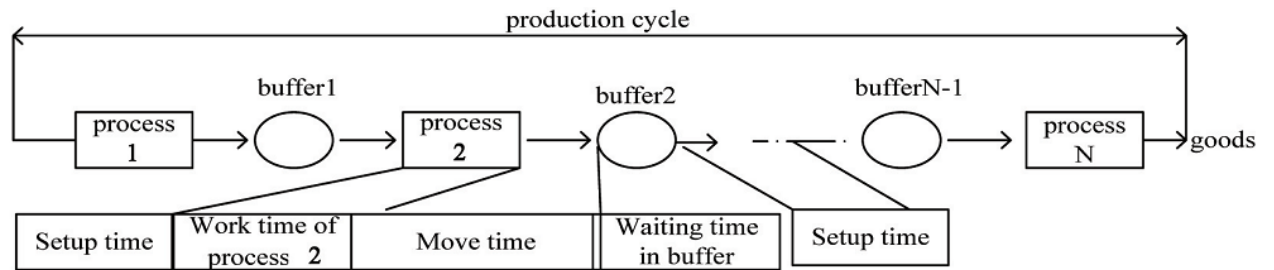
Figure 2. The Production of The Time Structure
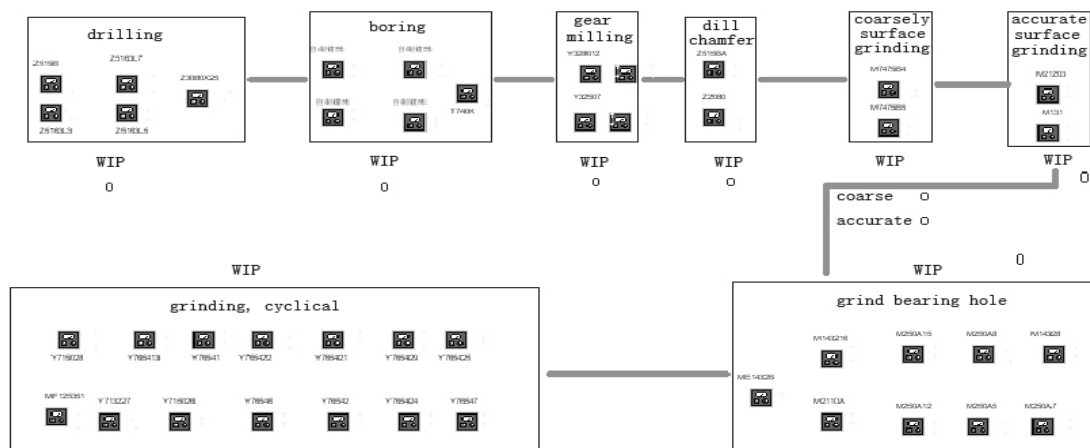
Figure 3. The Simulation Interface of Gear Production Line

Mixing Process of Binary Polymer Particles in Different Type of Mixers

S.M.Tasirin, S.K.Kamarudin & A.M.A. Hweage

Department of Chemical and Process Engineering, Universiti Kebangsaan Malaysia

43600 Bangi, Selangor, Malaysia

Tel: 60-3-8921-6422   E-mail: ctie@vlsi.eng.ukm.my

Abstract

The main objective of this paper is to investigate the mixing process of free flowing polymers binary mixtures at different densities and colors in two different mixers, namely the bubbling fluidized bed and V-mixer. The mixing of solids was studied by analyzing the variation of the proportions of the marked particles with time and position in the bed or in the mixer. The variation of mixture composition based on the samples was incorporated into Lacey mixing index which describes the degree of mixing of the particles at particular time. The performance and the mixing behavior in these two mixers were also presented. Results showed that gas velocity and bed depth were important parameters influencing solids mixing in a bubbling fluidized bed. While the rotation speeds and filled up levels were proved as important parameters in influencing the solids mixing in V-mixer. From the results, complete mixings were attained at a bed depth of 17 cm and gas velocity of 1.38Umf in the fluidized bed and 40 % filled up level and 40 rpm in the V-mixer. From the energy consumption point of view, it was found that the fluidized bed mixer offers the most efficient and economical process compared to V-mixer.

Keywords: Particle, Mixer, Fluidized Bed, V-mixer

1. Introduction

A successful mixer must do at least two things; firstly, it must create differential velocities in the moving solid, which will produce mixing, Secondly, it must leave no dead, non-moving regions, as these regions cannot mix. Solids mixing are an important process in manufacturing many industrial products like pharmaceutical, chemical, petrochemical, foodstuffs, plastics, metallurgical, fertilizers, grain etc. but until now it is still one of the least well understood. Most of the solid mixing still based on the successful method for liquid mixing although it is proved unsuitable for the mixing of particulate solids. The fact that particles of different physical properties may tend to segregate has received considerable attention in the past few years but its implications have not been widely realized.

Thus the objectives of the study is to determine the optimum operating condition in order to obtain a final mixture of specified compositions of polymer A and B, namely, 3:1, respectively followed by investigating the mixing performance in V-mixer and fluidized bed. Finally, this study will determine the best type of mixer to be used in order to obtain the most efficient and economical mixing system.

2. Theoretical Background

For any manufacturing process that involves mixing of solid particles, the level of in homogeneity must be considered when determining the quality of the final product. It is even more difficult to obtain a homogeneous mixture when the particles are at different in size or in density (Stein et al. 2000).

Mixing index is directly proportional to the standard deviation: the smaller it is, the better the mixing will be. Considering number of samples, each containing particles, the estimated mixture composition value is given by Eq. (1) (Lacey 1954):

$$\bar{y} = \frac{1}{N} \sum_{i=1}^{N} y_i \tag{1}$$

Where the mixture composition, y_i is ith value of the proportion of one component in the samples.

We can use the standard deviation of the composition for the samples taken from the mixture as a measure of the quality of the mixture. Thus a low standard deviation indicates a narrow spread in composition of samples and therefore a good mixing is attained. The sample variance is given by Eq. (2).

$$S^2 = \frac{1}{(N-1)} \sum_{i=1}^{N} (y_i - \bar{y}) \tag{2}$$

The value of standard deviation, S is calculated using equation (2) is only an estimation of the actual value of the standard deviation of the mixture, σ. The actual value of the standard deviation of a random binary mixture (in this case of a perfectly random system, lower limit), the variance σ_R is as given by Eq. (3) (Lacey 1954; Lacey 1943; Fan et al. 1990):

$$\sigma_R{}^2 = \left[\frac{P(1-P)}{n} \right] \tag{3}$$

Due to that, the experimental values "S^2" can be compared to $\sigma_0{}^2$ and $\sigma_R{}^2$ as defined as Lacey Index, M, for binary mixtures of identical particles as following:

$$M = \frac{\sigma_0{}^2 - \sigma^2}{\sigma_0{}^2 - \sigma_R{}^2} \tag{4}$$

Where σ_2 is the variance of the mixture between fully random and completely segregated mixtures, $\sigma_0{}^2$ = is upper limit (completely segregated) of mixture variance, $\sigma_R{}^2$ = is lower limit (randomly mixed) of mixture variance and M is the Lacey mixing index. A Lacey mixing index of zero would re-present complete segregation and a value of unity would represent a completely random mixture. Particle values of this mixing index are found in the range of 0.75 to 1.0 (Rhodes 1998).

3. Results and Discussion

3.1 Particle Characterization

Two types of polymer particles considered in this study, namely polymer A (white) and B (black). Table 1 lists the physical properties of polymers used.

3.2 Fluidized Bed

Figure 1 shows the experimental set-up for fluidized bed. The system consists of a Perspex cylinder, 143 mm in diameter and 1000 mm length. A pressure probe connected to a water manometer measured the pressure drop across the bed. A transparent scale was attached on the bed wall to provide direct bed expansion measurement. The gas inlet system comprises of variable speed motor, a flow and gas distributor as proposed by Geldart (Geldart 1973). The total number of orifice was calculated to be 217 orifices. Compressed air at range from 0.4 to 0.6 MPa a supplied from a central blower was used for fluidizing the air.

An experiment was started by charging a known weight of particles into the bed to give a predetermined settled bed depth as shown in Table 2. The bed depth used was chosen such that slugging won't occur in the bed. The critical bed depth, H_{msc} to onset slugging bed was calculated from equation (5).

$$\left[\frac{H_{msc}}{D} \right] \leq \frac{1.90}{(\rho_P \, \bar{d}_p)^{0.3}} \tag{5}$$

In every case it was ensured that the polymer A (white) was at a fraction of 75% by volume (i.e. 71.3% by weight) while polymer B (black) 25% by volume (i.e 28.7% by weight) of the total weight fed into the column. Polymer A (white) was poured first into the bed, followed by the polymer B (black). This was to ensure that the two types of particle are fully segregated at the beginning of any experimental test. Compressed air at range from 0.4 to 0.6 MPa was then supplied into the bed to fluidize the particles mixture. The air was supplied to give a gas velocity above the minimum fluidization velocity, Umf. The fluidization air was passed from a main compressor at ambient temperature and relative humidity ± 50%. Side-sampling thief method was used for sampling.

3.3 V-Mixer

Figure 2 shows the schematic diagram of the V-mixer used in this study. The assembly is mounted on bearings and rotated by a variable speed electric motor. The identical cylindrical shells and access cover are produced in clear acrylic to permit viewing of the process. Each shell has an internal diameter of 8 cm and joined at an angle of 87°. The volume of the V-mixer is 1800 cm3. It was measured by measuring the volume of water necessary to fill up the whole containment. The access cover is secured by two thumb screws.

The experimental work was started by loading a certain weight of segregated feed materials consisting of a 75% by volume white polymer (A) and 25% by volume black polymer (B). The total weight of solids was varied to give different filled percentages in the V-mixer. In the beginning of each run, particles mixture was completely segregated. The V-mixer was turn rotated at a predetermined rotation speed for certain duration of time. Table 3 lists the

parameters used in this case.

4. Results and Discussion

4.1 Mixing Particles in Fluidized Bed Reactor

Figure 3 shows an illustrative example of the mixing process for polymer particles in bed depth of 17 cm. The superficial gas velocity was 1.38Umf. The bed was first allowed to operate for 5s in order to attain the steady state operation. The time was set to zero at this moment, after making sure that the black and white colored particles are completely segregated at t=0s. As mixing continous, this completely segregated state gradually gives way to one another in which the particles of different colors are partially mixed. A mixing equilibrium can be noted after about 6s of mixing**.**

Figure 3 and Figures 4(a) and (b) show the bubbling fluidized bed, the bubble motion drives the solids motion. Bubbles carry particles upward in their wakes and drift. Continuously, this upward flow of solids due to bubbles was balanced by a downward flow which occurs at place where there are no bubbles. Particles move upward in the central part of the bed, and downwards beside the wall. This up-and-down movement is mean mechanism of vertical polymers (convective) mixing. Lateral mixing occurs mainly at the top of the bed where bubble burst; as illustrated in Figure 4. Near the distributor, particles completed their old cycles and are carried away by bubbles to start new cycles.

Figure 5 shows images taken at different bed depths for each mixture. Resulting images reveal a completely homogenous comparison for mixing at 1.38Umf for 17 cm bed depth. Nevertheless, this mixture was spouted, as in Figure 6. Spouting is a condition which may occur when a single hole is used to admit the gas rather than a porous plate or multi-hole distributor (Chandnani & Epstein 1986) or for group D and the larger group B particles. Nevertheless the phenomenon was observed only in the 17 cm bed, whilst no spouting was detected in the final mixture of 15 cm and 10 cm bed.

4.2 Mixing in V-Mixer

The photographs in Figure 7 was taken in order to investigate the mechanism of mixing, in which the mixer was stopped every certain time to examine the mixing quality. The figure shows the evolution of the surface composition for mixtures running at different time. It also shows that after 5 min, a minimal degree of mixing has occurred. It should be noted that common practice in industry to mix particles takes for only a few minutes.

In general, it was observed that the mixing quality of polymer particles increases with increasing mixing time. This is due to the fact that the exchange rate of particles between the two end of the arms and reaching join of arms is particularly sensitive to mixing time with revolution speeds, also the dispersion the particles inside the V-mixer.

The mechanisms of mixing formation at different rotation speeds, i.e. 20, 40, and 60 rpm are showed in Figure 8. From the photographs, it was observed that the mixture homogeneity at lower speed (i.e. 20 rpm) is less than the mixtures at higher rotation speeds (i.e. 40, and 60 rpm) at same conditions. Therefore, mixing index increases with an increasing rotation speeds. Results observed that a well mixed state was expected in each case, but it appeared that perfect mixing of polymer occurred at identical volume (i.e. 50 %) and optimum time for 40 rpm.

4.3 Power Consumption

Process optimization is important in order to produce the required product at a minimum energy or power consumption. From the study, it was proved that different operating parameters and different types of mixer gives the different optimal condition. Thus, to get homogenous mixtures at optimal conditions, the relation between the power consumption and the mixing index was established.

For mixing in V-mixer and Nauta-mixer, the ideal calculation indicated that the mixing index depends on the rotation speeds, as well as filled up levels, which indicate the amount of energy used.

The combination of these two parameters will indicate the optimum operation, namely to give the maximum value of mixing index, M at the lowest power consumed. Justification should be made to produce the largest amount of product but at the least amount of energy usage. In this case the energy consumed, E, is calculated by [1.047198*10-3.Rpm.t)/M] (J/kg).

The various mixing index can be compared on the basis of the specific energy consumption (J/kg). As seen in Figure 9 for mixing by V-mixer, the lowest overall energy losses (in J/kg) is at the mixing index value of 0.98 that is at the conditions of 40 % filled up level with 20 rpm and 40 % filled up level with 40 rpm. The minimum energy consumption is at 20 rpm rotation speed i.e. E = 8.5 and 9 J/kg at 20 and 40 rpm, respectively. However, the minimum energy consumption to achieve as low as 0.99 mixing index value, i.e. to produce the best homogenous mixture is given from runs at 40 filled up level with 40 rpm. 40 % filled up level with 40 rpm is slightly homogenous than 40 % filled up level with 20 rpm but consumed more energy, (in J/kg).

For mixing by fluidized bed, the optimal mixing index depends on the gas flow rate, where the power consumption

increases as gas flow rate increases. Figure 10 shows the results for specific energy consumption in mixing by fluidized bed. The results proved that fluidized bed consume very low energy that is in the range of 0.015 to 0.02 J/kg.

In order to calculate the realistic values of the specific energy consumption (in J/kg) it is necessary to make assumptions about the pressure drops across the distributor plate, as well as across the fluidized bed. Of course if the pressure drops are assumed to be the same for all the cases an alternative value can be calculated simply based on the gas flow rate and mixing time per mixing index and mass of solids quantity, K namely, $(Q.\rho g.t)/(M.m)$ against the Lacey mixing index. In this case the optimum operation would be given by the condition at which the K value is minimum for a specified M value. From Figure 11, it is observed that the optimum operation for fluidized bed is at 17 cm bed depth with $1.38 U_{mf}$ because it offers the minimum value of K, means minimum specific energy consumption, based on mixing index of 0.99.

4.4 Optimization

From Figures 9 and 10, the optimum conditions for the V-mixer and fluidized bed mixer, respectively were compared and presented in Table 4. The mixing index of 0.99 can be regarded as an ideal mixing condition.

5. Conclusion

Two type of mixer are introduced in this study namely, the V-mixer and fluidized bed mixer. In conclusion, it was proved that fluidized bed is the most efficient and economical compared to V-mixer. The advantages of fluidized bed are: easy to handle and the complete mixing is attained in few seconds and consumed the lowest power losses.

References

Chandnani, P. P. and Epstein, N. (1986). Fluidization V, ed. K. Ostergaad and A. Sorensen, Engineering Foundation, New York, p. 233

Fan, L. T., Chen, Y. M. and Lai, F. S. (1990). Recent development in solids mixing. *Powder Technology*, 61, 255-287

Geldart, D. (1973). Type of gas fluidization, *Powder Technology* , 7, 285-292

Lacey, P. M. C. (1943). The mixing of solid particles, *Transactions of the Institution of Chemical Engineers*, 21, 53-59

Lacey, P. M. C. (1954). Developments in the theory of particulate mixing. *Journal of Applied Chemistry*, 4, 257-268.

Rhodes, M. J. (1998). Introduction to Particle technology, John Wiley, Chichester

Stein, M., Ding, Y. L., Seville, J. P. K. and Parker, D. J. (2000). Solids motion in bubbling gas fluidized beds, *Chemical Engineering Science*, 55,5291-5300

Table 1. Physical Properties Of Polymers Used In This Study

Parameters	Polymer A (white)	Polymer B (black)
Mean particle size, d_p (μm).	3465	3502
Particle density, ρ_p (kg/m³)	923	1105
Bulk density, ρ_{ba} (kg/m³)	617	745
Geldart classification (1973)	D	D
Size range, d_p (μm).	4750-2360	4750-2360

Table 2. Experimental series for mixing in a fluidized bed

Parameters	Range of values
U_{mf} (m/sec)	1.35
Operating gas velocity	$U_{mf,}$ $1.15 U_{mf}$ and $1.38 U_{mf}$
Bed depth, H (cm)	10, 15 and 17
Bed weight, m (kg)	1.042, 1.563 and 1.772
H_{msc} (cm)	18.98
Duration, t (sec)	5,10,12,15,20 and 30

Table 3. Parameters used in the V-mixer.

Parameter	Range of values
Rotation speed (rpm)	20, 40 and 60
Filled up level %	40, 50 and 70
Duration, t (min)	5, 10 and 20

Table 4. Optimum mixing time at best parameters condition and power consumption for each mixer

Type of mixer	Mass (kg)	Velocity	Mixing index (-)	Optimum time (sec)	Power consumption (J/kg)
Fluidized bed	17 cm bed depth=1.772	Gas velocity = $1.38U_{mf}$	0.99	7	0.015
V-mixer	40% filled up 0.467	Rotation speed 40 rpm,	0.99	240	9
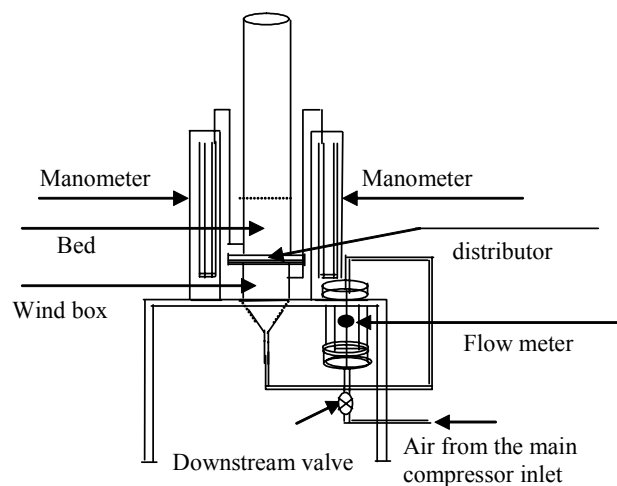
Figure 1. Experimental set-up of the mixing fluidized bed
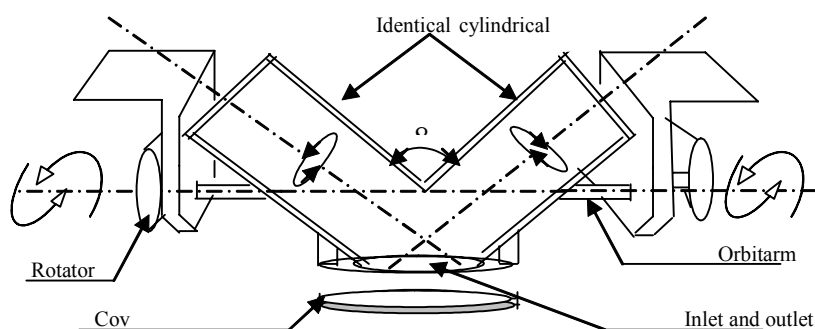
Figure 2. The schematic diagram of the V-mixer

t=0 s   *t=1 s*   *t=3 s*   *t=5*   *t=6 s*   *t=9s*   *t=12 s*
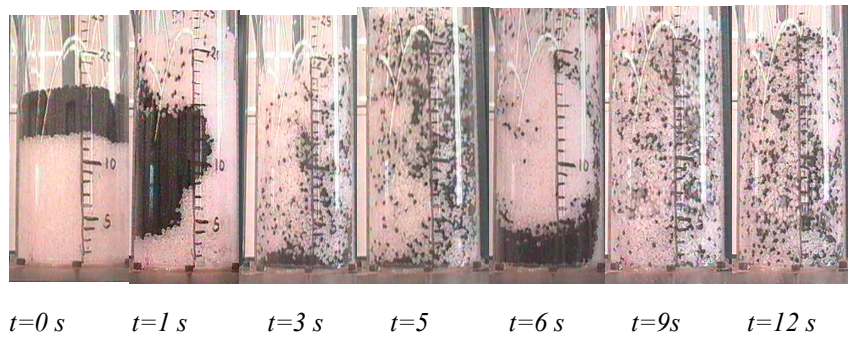
Figure 3. An illustration of the process of mixing (bed depth = 17 cm, superficial   gas velocity = 1.38 U_{mf})

(a)   (b)
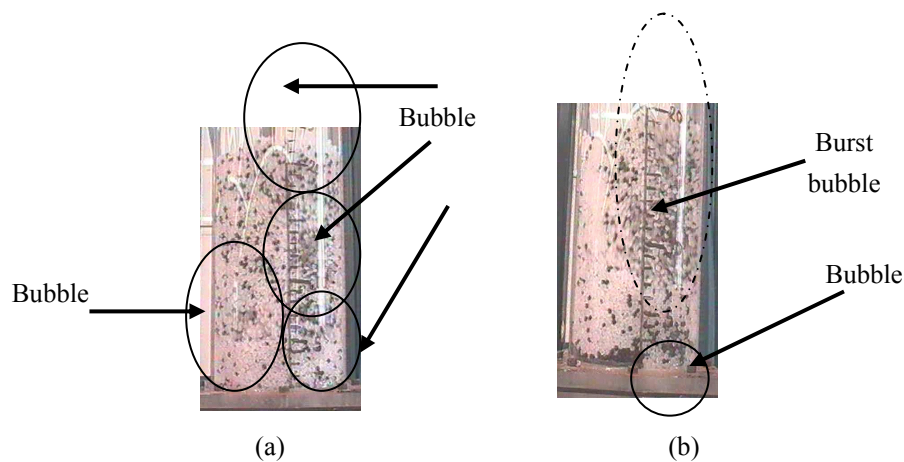
Figure 4. An illustration the bubbles behaviour of polymers mixing

(a)   (b)   (c)
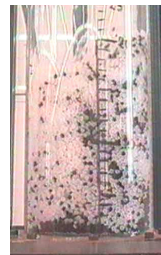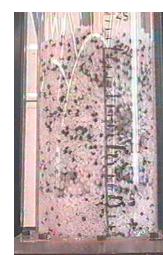
H = 15 cm, t = 5 s   H = 17 cm, t = 5 s   H = 17 cm, t = 9 s

Figure 5. Influence of bed depth on the degree of homogeneity of mixtures with time
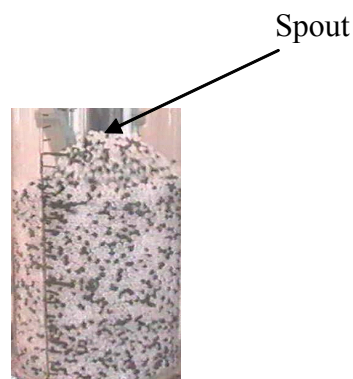
Spout

Figure 6. Photograph shows the spout of homogenous mixture at bed depth of 17 cm and gas velocity of 1.38U_{mf}

| t = 0 s | t = 1 s | t = 13s | t=28 s | t=1 min | t=1.5 |

| t = 2 min | t=3 min | t= 4 min | t=5 min | t= 7 min | t = 9 min |
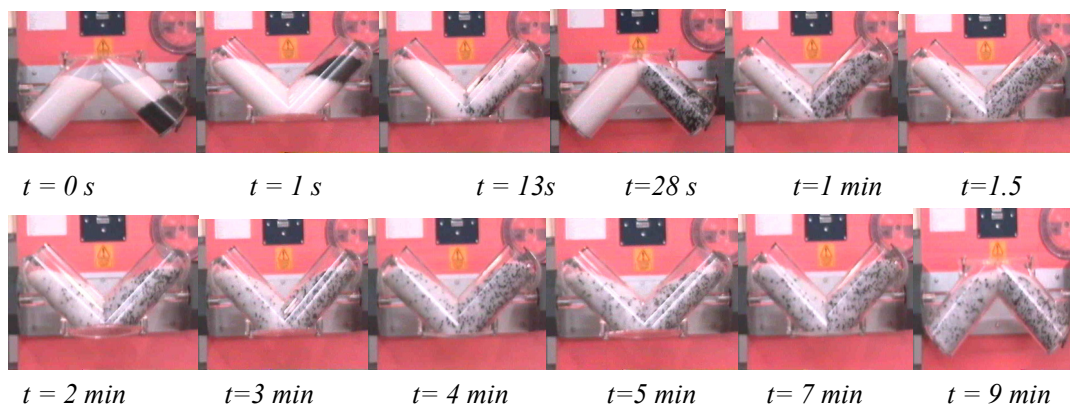
Figure 7. Photographs illustration the mechanism of mixing formation of polymers,

also it shows surface composition at different time, (70%, 60 rpm)

20 rpm   20 rpm

40 rpm   40 rpm

60 rpm   60 rpm
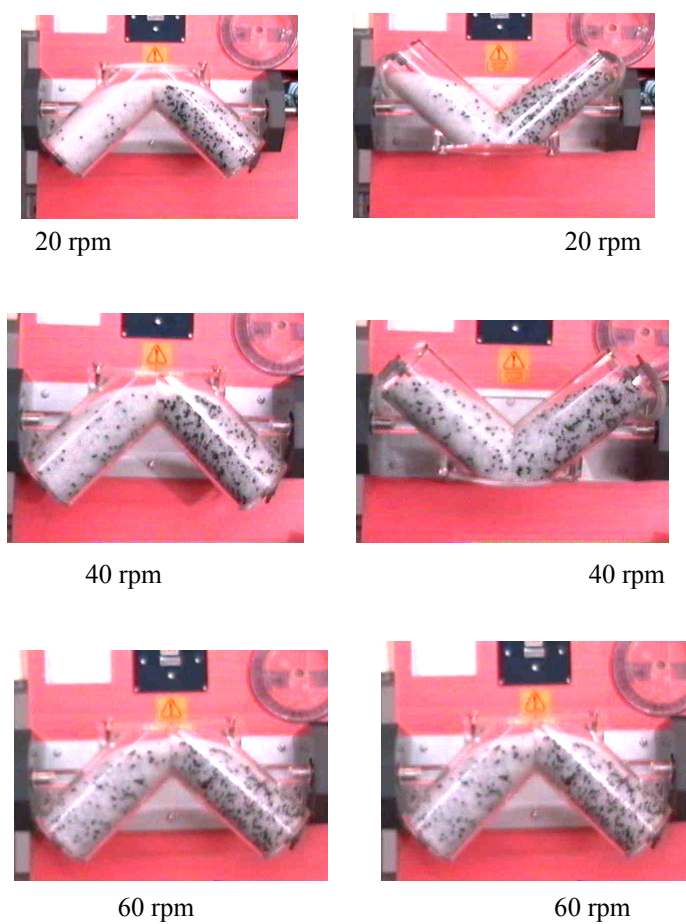
Figure 8. Effect of rotational speeds on mixing index at 70 % filled up and t=10 min
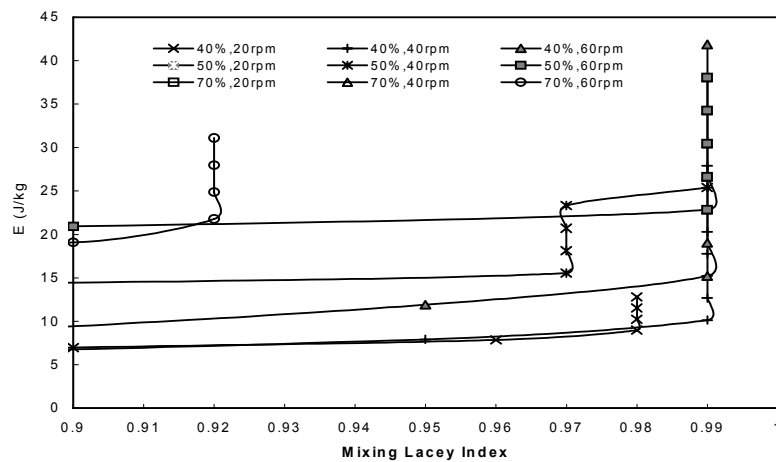
Figure 9. Specific energy consumption, *E* (J/kg) .vs. Lacey mixing index, *M* (-) for mixing in V-mixer
with mixing index, *M* from 0.9 to 1
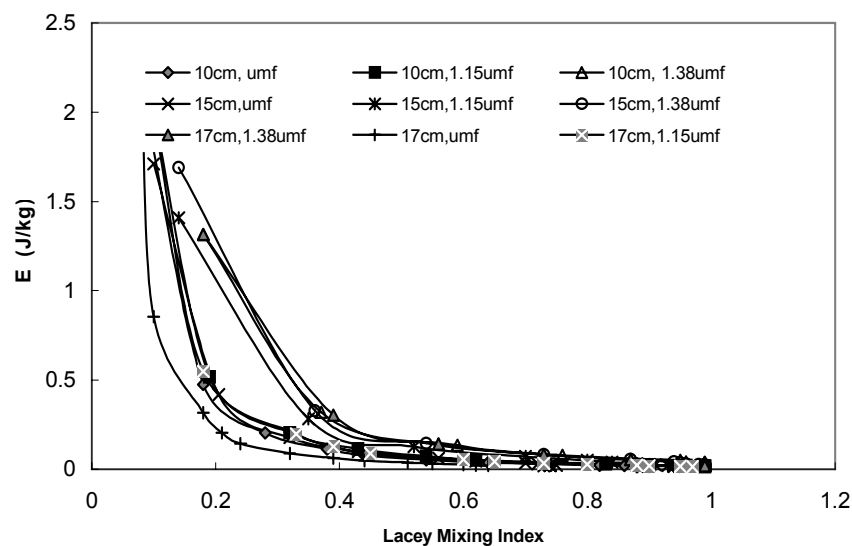
Figure 10. Specific energy consumption, E (J/kg) .vs. Lacey mixing index, M (-) for Fluidized bed;
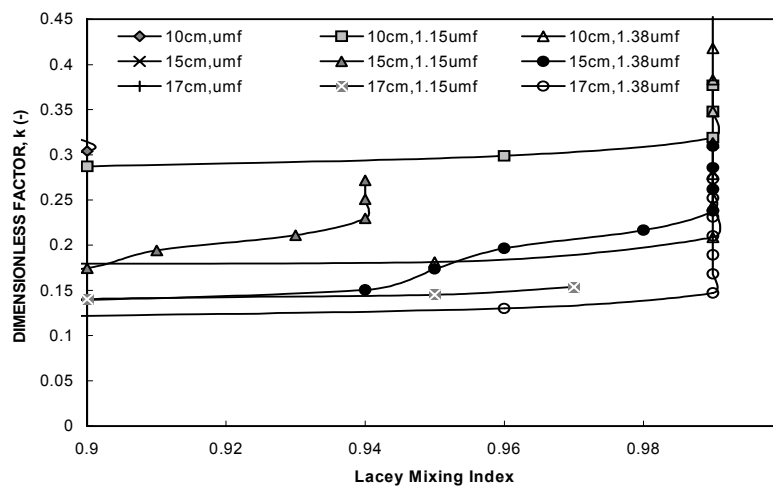For energy consumption from 0 to 2.5 J/kg

Figure 11. Dimensionless mixing factor, *K* .vs. Lacey mixing index, *M* (-) for Fluidized bed;
(a) For mixing index, *M* from 0 to 1, (b) For mixing index, *M* from 0.9 to 1

Study on the Product Symbol System for Brand R&D

Qin Wang

School of Mechanical and Electronic Engineering, Dongguan University of Technology

Dongguan 523808, China

Tel: 86-769-2307-8216   E-mail:wangqinjaney@126.com

Abstract

The development orientations of the product brand design in the market are toward conception and symbolization. Based on the design semantics and the product semantics, the design thoughts and levels of the product symbol system was studied in the article. The results of the article could help design personnel in enterprises to more deeply understand the importance of the strategic development of new products and the effective application of the product symbol system.

Keywords: Product symbol system, Interaction design, Cultural semantics, Symbolization

1. Introduction

The word of "semiotics" was first proposed by the Switzerland linguist Sauaure and American philosopher and pragmatics Pierce. Though the academe has not formed complete uniform definition of the symbol, but most scholars thought that the symbol could be regarded as the material carrier of social information, and it could load certain information and transfer thoughts, and it could be the signified things such as English letter, Arabic numerals and finger alphabet for special things, and it could be the symbolization of certain abstract concept. Three necessary characters of the symbol include that (1) symbols must be matters, (2) symbols must transfer the information which is different to the carrier in nature, i.e. symbols must represent other things, (3) symbols must transfer a sort of social information which are established by the public not by the individual. Above opinion organically combine the material character of the symbol with the thought character, and it could enlighten people to understand the deep semiotics and human connotation of the symbol.

There are methods to classify the symbols. American semeiotic scientist and esthetician Suzanne Lenglen classified symbols as "deduction symbols" and "simultaneous symbols". She thought that the former meant the language symbols specially, and the latter was a sort of presentational symbol (i.e. a sort of complex symbol system, or the direct combination of color, line and subject, or the vision image directly combined by parabolic and poetic languages, and it is presented by the total imago, and it is also called as "presentational symbol" or "symbol of art"). According to the interactive relationship among three factors (agent, objective and explanation) of symbols, American philosopher Pierce established the "symbols classified method of three in one", and the core types included icon, index and symbol. According to the characters of "signified and signifier" of symbols, some scholars put forward five types including omen symbol, signified symbol, induction symbol, language symbol and substitute symbol (Xu, 2008).

Though the extension of symbol is wide, but in practical application, the symbols in the product design are mainly used to connect the objective and consumers to realize the interactive communication by the forms such as information and culture. The design elements and the basic measures are regarded as the symbols to increase and diffuse the information cultures of products and establish the innovational brands through integrating these elements.

Human researches and practices indicated that symbolized thinking and behaviors were the most representative characters in human life, and all cultural forms were forms of symbol, and the symbol design held the balance in the whole human social evolvement. Just as Cassirer said, "symbol thinking overcomes human natural inertia, and endows human a new ability to continually update the world". In the days that the science and technology develop quickly, the products updating speed is so quick, and the consumption demand contents change fundamentally, the establishment of the utilization of the design semeiotics based on product semeiotics and the innovational design of the product symbol system will help enterprises to effectively develop the new products, establish special brands and enhance the market competitive forces of products.

Based on above contents, the application of the product symbol system in the innovational design of brand will be deeply analyzed from the concept and levels of the product symbol system in the article.

2. Concept analysis of the product symbol system design

Usually, product symbols are some design elements attached on the modeling of product, or the icons or visualized operation indications which represent special brand. How ever, the interactive integration of multiple subject knowledge

will widen the view of product design and enrich the methods of product design. Letter, language, Chinese traditional lines, various propagation forms in the nature, and many indicative expressions with designers' emotions and totems deduced from abstracted distortion all can be integrated into the product design process as the symbol elements.

But the design of modern industrial products can not only stay on the simple level of two-dimensional symbol element, and the single two-dimensional level design has not fulfill enterprises' requirements to research and develop strategic brand for a long time, and only the multi-dimensional product symbol system design can really fulfill the demands of the future market and establish special brand.

Generally speaking, the product symbol system includes three dimensions, i.e. the technical material dimension (including technology and materials), the semantics dimension of the technology object (configuration), and the syntactics dimension of technical function (composing). With the alterable freedom degrees of these three dimensions, the product can be turned into the design object, and only the product with these three dimensions, the product can acquire the symbol character. The organizer of the brand must completely grasp these three dimensions and exactly understand the referential function of the product symbol combining with the knowledge about the semeiotics and syntactics to establish applied product symbol system with bright features combining with consumers' psychological and sensible appeals.

3. Level analysis of the product symbol system design

The levels of the whole product symbol system directly influence the design of the innovational brand. From following aspects, the different levels of the product symbol system will be analyzed, and corresponding opinions will be proposed.

3.1 Interaction layer analysis of the symbol system

As the modern brand product design is required to not only fulfill consumers' demands from the appearance and function, but consider consumers sensible demands. Therefore, the design and R&D of the product symbol system should comprehensively consider the appearance, function, consumers' minds, ergonomic engineering, the design concept, emotion and cultures which are easily identified and trusted by consumers. As the agent of the bilateral communication between designers and consumers, the operation instruction symbols in the product should make consumers exactly know how to operate and use the product, and consider the cultural differences in different regions and the combination of the culture and technology, i.e. consider the three dimensions of the system. The interaction is represented in that the design should take the consumer as the design topic, and take certain information and culture as the core of the whole product symbol design system to realize the mutual communication between consumers and products. The good interaction of the symbol system requires that the interaction could be integrated into the hard and soft sensibility. The structure relation of the interactive symbol system proposed in the article is seen in Figure 1.

3.1.1 Image vision symbol interaction of the system

The vision information of innovational product includes three aspects such as configuration, color and materials (Mao, 2008). The image interaction of the system in the hard and soft design innovations could directly leave good effects to consumers. Taking the automatic smile shutter mode of Sony digital camera as the example, based on the face automatic focus technology of the camera, users can select this mode and press the shutter button of the camera when screening portrait, Cyber-shot will look for the smile in the screening process and make the photo when detecting the smile face. Smile shutter mode can also distinguish adult's smile and child's smile, and the degree of the smile can be enacted as low, middle and high. Thus, the camera could automatically catch the most wonderful instant in the life (seen in Figure 2). The "happy face retouch" function of Sony digital camera could turn the suffering face into the happy face by the digital processing (seen in Figure 3). The mode which could realize the function innovation of product could accord with human taste habits and fulfill human mental appeals. As the bright point of the brand product, the smile face which is a sort of symbol with apperception and emotion is liked deeply by consumers.

3.1.2 Sound hearing symbol interaction of the system

The most natural, fluent, convenient information communication mode is language, and the most abundant and exact signification in the semeiotics is the sound symbol. The researches of ergonomics indicated that the hearing information and the vision information could offer human intensive third dimension and proximity sensibility simultaneously, but the detection speed of the hearing information is quicker than the detection speed of the vision singles. Generally speaking, the sound contains language, music and sound effect. As the designer completely grasps the sound symbol system, he could process the sounds emitted by the product based on art and sensibility to make the product could transfer certain special information to consumers through the ergonomic interaction. For example, the single tone of short message warning tone and the incoming tone of Nokia phone have been the bright point of the Nokia brand culture because the "single tone" accords with human language habits and hearing habits. The special rings have been the special symbol of Nokia and the diffusion media of the brand of Nokia.

3.1.3 Behavior touching symbol interaction of the system

The handle is consumers' feeling when they directly contact the materials and configuration of the product. Good operation and control feeling could maximally exert the function of the product (Cheng, 2008 & Cupar, 2006). The design of the feeling sense symbol system closing the body has been the development direction of the design, so the establisher and developer of the brand should be good at combining the correlative principles of ergonomics to create the product symbol system according with consumers' physiological and psychological demands. For the Wii game console brand established by Japan Nintendo Corporation, as the optimal exterior fittings of the Wii game console, Wii Fit can not only offer various games, but do various fitting sports for consumers. The Wii game console adopts revolutionary handle operation and control mode to change the key-press control mode in the past, and innovates in the concept of the game console, and it can control the game tasks by the actions of the body by using the balance instrument in the remote control handle. In Figure 4, player can use Wii to play baseball, and the handle of Wii equals to the baseball bat, and users' occasion and speed of flinging the handle will influence batting effects. Here, the handle of Wii becomes into the touching symbol, and it has been turned into certain special concept, i.e. the new life mode of body-building and amusement. The design concept of "the revolution of TV game" of Wii brand has wined many consumers' favors.

In conclusion, the interactive product symbol system is multi-dimensional, and when it is applied in the design practice, above sensibility interactive modes should be comprehensively used to form the integrated technology which can really express the sensible cognition and whole taste experience for certain product, and make finite symbol express infinite recurrence of language environment and product image and establish the special image of the product.

3.2 Innovational semantic expression level analysis of the symbol system

In the product design process, designers endow their thoughts and ideas to the product, which will form the interior meanings with the attributes of the product, and utilize many methods such as association, memory and metaphor in the semeiotics to endow the configuration, image symbol and language full of originalities to the product, which will produce a sort of communication of meaning between designers and consumers to make consumers fully understand the connotation of the product, and simultaneously, the communication of spirit culture will be implemented between designers and consumers through the symbol system, and the resonance between the product and the consumer will be produced to some extent through the emotion creation of the product and originality of the emotion value.

Taking the MrP little shamed reading lamp design of Propaganda brand in Figure 5 as the example, the switch is the forbidden zone, and if consumers don't touch it, the lamp will not be turned on. As consumers adapt this switch slowly, face it and abuse it, which is a sort of innovational semantics of the product. The facetious symbol of the product can express unique semantics, and added joking paronomasia and hinted ardor symbolic language can stimulate consumers' interior freedom sense and make them indulge themselves to the top of their bents.

3.3 Symbolization expression level analysis of the symbol system

The symbol of the product symbolizes certain culture, and its cultural value can be called as the subjective value. The symbolized semantics contains designer's thoughts and intentions, and designer could express the time culture, enterprise spirit and culture through the product. However, the symbol is not established at will, and it must possess common character with object, and make consumers could associate and deeply understand the cultural connotation according to their own knowledge background from the one to the other. Therefore, good innovational product should seek the optimal vision expression of the originality from the relations among signified, signifier and signifying, and exactly grasp the symbolized meaning of the symbol.

Taking the torch design of 2008 Beijing Olympics as the example, the torch adopted the symbolized technique of the symbol (seen in Figure 6). The "clouds lines" symbol of the torch is the recurrence of the traditional design element in the Chinese Huaxia Civilization, and it symbolizes the Huaxia Civilization of "born in same origin and being in harmony", and it can diffuse the harmonious culture and oriental civilization through the oriental spirit of "the world should be natural and the people should be full of interior and open-minded tolerance" and the image of the lucky clouds. Based on above meanings, the Legend Group which assumed the design of the Olympics torch created the brand product with national cultural characteristics.

4. Some opinions about the product symbol system for enterprises to research and develop special brands

To design the innovational product favored by consumers, designer should grasp following aspects of the product symbol system.

(1) The product symbol system should possess the character of difference. The existing symbol language should be abstracted, or distorted, or decomposed to form innovational symbol language. The innovational symbol system (including the trademark on the product, packaging symbol, the modeling and function indication of the whole produce, and the whole image concept) should make consumers can distinguish and remember the product, and be interesting to

the brand, which will help the product to cultivate a passel of seed consumers and loyal consumers to extend the brand effect.

(2) The symbol semantics should possess the character of national culture. Designers should consider the national culture characters, and select the symbol language with the characters of national culture, and skillfully pick up and rebuild the symbol elements which could reflect the national characters to design the successful brand product which could map the connotation of the national culture. For example, the "lucky clouds torch" design in 2008 Beijing Olympics and the torch design in 2000 Sydney Olympics all possess bright national culture characteristics.

(3) The symbol should possess the affinity. The emotion communication is realized in the "friendly" communication process of the symbol, so the establishment of modern product brand should emphasize the "non-material design" and the emotional design.

(4) Designers should fully consider consumers' psychological acceptance. According to the "MAYA" threshold proposed by Raymond Loewy, i.e. the most advanced yet acceptable range, the design and utilization of symbol should consider the acceptable ability of the market and the public, and try to fulfill consumers' cultural background and psychological demands. In this way, consumers could distinguish and understand the symbolized meaning of the symbol, and the innovational brand could be favored and trusted by consumers, or else, the symbol language with more originality will run counter to consumers' psychologies.

(5) The thinking of symbol should possess the flexibility in the time space. The symbol should possess the character of variable thinking, and designer should flexibly utilize the symbol according with the characteristics of the times. As the symbol is continually developing with the variance of the time and space, designers should grasp the time and space applicability of the symbol, select or dig the symbol skillfully to exactly transmit the information and express the originality of the times.

5. Conclusions

Abundant product symbol system design with characteristics is the key for enterprises to strategically research and develop new product, and the key to start the innovational brand design. With the high-speed development of the information technology and the interactive integration of multiple subjects knowledge, and the design and development of the product symbol system is more and more emphasized by designers. How to enhance the symbol value of the product, and skillfully utilize the symbol system design to extend the brand effect has been the problem continually probed by designers. The research results are expected to be used for some references for the brand design.

References

Cao, Jujiang. (2007). Product Design Acceptance Based on Consumer. *Packaging Engineering.* No.2.

Cheng, Dinglv & Jiang, Xiao. (2008). The Signified of Semiotics in Interaction Design. *Art and Design.* No.8.

Cupar (US). (2006). *The Road of Interaction Design.* Beijing: Publishing House of Electronics Industry. March, 2006.

Li, Ni. (2006). Research of Fun Product Design on the Basis of Semiotics. *Packaging Engineering.* No.5.

Mao, Jingjing & Li, Shiguo. (2008). Interaction Design in the Sense Times. *Consume Guide.* No.1.

Wang, Hongjian & Yuan, Baolin. (1997). *The Concept of Art.* Beijing: Higher Education Press. April, 1997.

Xu, Shihu & Liu, Lijuan. (2008). The Enlightenment of Traditional Graphic Symbol to the Furniture Design. *Innovational Thinking and Practice.* No.3.

Yang, Wenfa. (2008). Cultural Design of Product. *Design and Culture.* No.3.

Zhang, Linghao. (2006). *The linguistic Meanings of Product.* Beijing: China Architecture & Building Press.
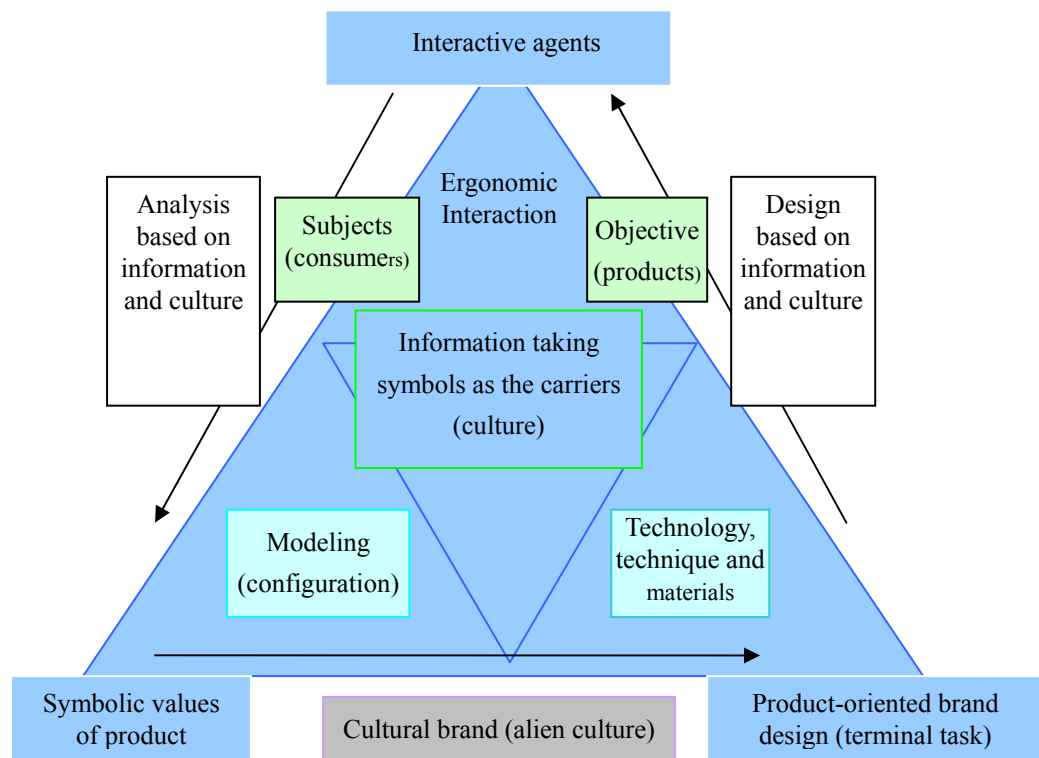
Figure 1. System Structure Relation of Interactive Product Symbols

Figure 2. The "cyber-shot" Smile shutter Mode of Sony

Figure 3. The Happen Face Retouching Function of Sony

Figure 4. Touching Symbol Function of Wii Game Console Lever

Figure 5. MrP Little Shamed Reading Lamp of Propaganda Brand

Figure 6. Design of Lucky Clouds Torch in 2008 Olympics

Microwave Sintering of Niobium Co-doped Yttria Stabilized Zirconia

S.Manisha Vidyavathy (Corresponding Author)

Department of Ceramic Technology, Anna University Chennai

Chennai – 600 025, India

Tel: 44 – 2220-3541   E-mail: mvidyavathy@yahoo.com

Dr.V.Kamaraj

Department of Ceramic Technology, Anna University Chennai

Chennai – 600 025, India

Tel: 44 – 2220-3514   E-mail: kamaraj@annauniv.edu

Abstract

Y_2O_3 and Nb_2O_5 doped tetragonal zirconia polycrystals were sintered at 1550ºC by conventional and microwave sintering. The effect of co-doping yttria stabilized tetragonal zirconia polycrystal with Nb_2O_5 was analyzed. The micro structural changes due to conventional and microwave sintering was studied using SEM and it was found that microwave sintering resulted in uniform microstructure with small grains. The phases were analyzed using X-ray diffraction analysis.

Keywords: Tetragonal zirconia polycrystals, Y_2O_3 and Nb_2O_5 co doped zirconia, Microwave sintering

1. Introduction

Partially stabilized tetragonal and fully stabilized cubic zirconia are important engineering ceramics with numerous applications. When ZrO_2 is utilized for technical applications the high temperature polymorphs cubic and tetragonal phases should be stabilized at room temperature by the formation of solid solutions which prevent deleterious tetragonal to monoclinic transformation(T.K.Gupta et al 1977). The alloying oxides which lead to the stabilization are alkaline earth, rare earth and actinide oxides.

Tetragonal zirconia polycrystals has been known as a structural ceramic due to its high strength and fracture toughness. Tetragonal zirconia polycrystals stabilized by doping with oxides such as Y_2O_3 and CeO_2 show a rising crack growth resistance with crack extension due to the formation of the transformation zone behind the crack tip as a result of the stress induced phase transformation (Ping Li et al 1994, 1993). Although yttria stabilized tetragonal zirconia polycrystals possess high strength and toughness at room temperature, they suffer low temperature strength degradation because of the spontaneous tetragonal (t) to monoclinic (m) phase transformation when annealed at temperatures from 100 to 500 ºC in air .

The addition of Ta_2O_5, Nb_2O_5 and HfO_2 to bulk Y_2O_3 stabilized ZrO_2 increases the transformability   (t to m transformation temperature) of the resulting zirconia ceramics. The enhanced transformability is related to the alloying effect on the tetragonality (c/a – cell parameters ratio) of stabilized tetragonal ZrO_2,so the addition of these oxides increases the tetragonal distortion of the cubic lattice. The increase in the tetragonality due to alloying is consistent with the increase in the fracture toughness and the increase in the t to m transformation temperature. Evidently from t-ZrO_2 become unstable as their tetragonality increases towards 1.020, which corresponds to the c/b ration of   m-ZrO_2 at room temperature. On the other hand, they become stable as the tetragonality decreases towards unity, which corresponds to c-ZrO_2. This relationship allows the classification of oxides into either a stabilizer (decreasing tetragonality) or destabilizer (increasing tetragonality) for the t-ZrO_2 phase (Ping Li et al 1994,Bartalome et al 2007).

Numerous investigations, so far, have explored the effectiveness of microwave sintering on the evolution of densification in ceramic systems. Rapid developments in the microstructure of basic ceramics have introduced many materials for many applications. The properties of these materials are determined by their microstructures; therefore, to control their micro structural development and to achieve fine microstructures, the sintering parameters must be optimized (Xin Guo et al 1998, Sharon A Nightingale et al 1997, Mehdi Mazaheri et al 2008) .

Employing microwave radiation for sintering of ceramic components has recently appeared as a newly focused scientific approach. Microwave sintering has numerical advantages such as rapid end volumetric heating, improved production rate, enhancement in densification and grain growth prohibition of ceramics. Heating under microwave is a

result of an interaction between electromagnetic waves and the molecules of the material. The intrinsic characteristics of the material are, therefore influence on the responds of the so – called element against the sintering heat.

The present work is aimed at exploring the general effect of microwave heating on the sintering procedure of tetragonal zirconia polycrystals co doped with yttria and niobium oxide and on revealing the major contribution of high heating rates on the micro structural improvement of microwave sintered samples.

2. Experimental Procedure

The starting powders were prepared by mixing ZrO_2 [obtained by sol – gel synthesis using zirconium oxy-chloride and oxalic acid as starting materials], Y_2O_3 [99.5% purity] and Nb_2O_5 [99.5% purity] using ball mill for 24 hours in an ethanol medium. Zirconia balls were used for the milling process. After milling the powders were dried at 110 ºC. The dried powders were pressed into pellets and then sintered by conventional sintering and microwave sintering. Conventional sintering was carried out at 1550 ºC using the heating rate of 5ºC/min without any holding time at the maximum temperature. Microwave sintering was conducted in a 1.1kW, 2.45 – GHz multimode microwave cavity using susceptor materials as auxiliary heating elements. The final densities of the compacts were measured by the Archimedes method and 99% theoretical density was acheieved. The microstructures of the conventional sintered and microwave sintered samples were analyzed using the scanning electron microscope. X-ray diffraction studies was done on the sintered specimens to identify the phases present.

3. Results and Discussion

3.1 Effect of co-doping with Nb_2O_5

When a trivalent oxide e.g Y_2O_3 is added to ZrO_2 as a stabilizer, a certain amount of lattice defects e.g oxygen vacancies and negatively charged solutes are produced in the ZrO_2 lattice. Pentavalent oxides are positively charged, opposite to the stabilizer, when dissolved in the ZrO_2 lattice, the addition of these oxides in the partially stabilized zirconia will definitely affect the original defect structure, thus also its properties. The effect of doping with pentavalent oxides such as niobia indicate that the ions reside as substitutional defects in the zirconium lattice annihilating oxygen vacancies generated by yttria doping (T.Ebadzadeh et al 2008) . The addition of pentavalent oxides such as Nb_2O_5 enhances the transformability and thus the instability of tetragonal zirconia as evidenced by the increase in the t to m and m to t phase transformation temperature. The instability probably originated from an increased internal strain in the tetragonal lattice that was caused by the annihilation of oxygen vacancies in the tetragonal zirconia which results in a strained cation network and oxygen overcrowding in t-ZrO_2. The oxygen vacancies in tetragonal zirconia are formed to maintain electrical neutrality ; Y^{3+} ions substitute for Zr^{4+} ions following the reaction

$$Y_2O_3 \rightarrow 2Y'_{Zr} + V_O^{\cdot\cdot} + 3O_O^x,$$
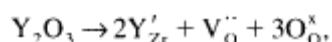
Where Y'zr represents the negatively charged yttrium ion that substitutes for the zirconium ion and Vo represents the positively charged oxygen vacancy. Doping of Nb_2O_5 into yttria stabilized zirconia is likely to diminish the number of oxygen vacancies in the above reaction because of the substitution of Nb^{5+} ions for Zr^{4+} ions according to the reaction

$$2Nb_2O_5 \xrightarrow{ZrO_2} 4Nb_{Zr}^{\cdot} + V_{Zr}^{''''} + 10O_O$$

$Y_2O_3 + Nb_2O_5 \rightarrow$[2Yzr' + 2 Nbzr'] + 8 Oo
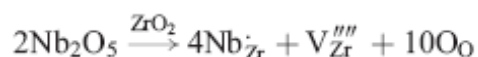
The probable reduction in the vacancy concentration can be revealed in the change in the properties of niobium codoped yttria stabilized zirconia (Deuk Yong Lee et al 2002, 1998, Dae- Joon Kim et al 1990, 1998,.Xin Guo et al 1997, Sharon A Nightingale et al 1997)

3.2 Microstructural Studies

"Figure 1a & b" shows the SEM micrographs of the specimens sintered under conventional sintering and microwave sintering. From the figure, one can observe a uniform microstructure with small grains it was also observed that in microwave sintering the grains were spherical and uniform in shape when compared with conventional sintering where the grains were large and irregular in shape. It was also confirmed that in microwave sintering better densification and microstructure can be achieved in comparison with conventional sintering.

3.3 X-ray Diffraction Studies

The powders was subjected to X-ray diffraction analysis using a Reich – Seifert Diffractometer with Cu Kα(λ = 1.5418Å) radiation as shown in the "Figure 2 a & b" The sample was scanned over the range 10 to 60 degree at a scan rate of 2 degree/minute. The experimental values were found to agree well with the calculated 'd' values. It

was found that monoclinic phase was formed and it was found that the crystalline quality of yttria, niobium stabilized zirconia by microwave sintering is good when compared to conventional sintering shown in "Figure 2a & b".

4. Conclusion

The combination of transformation toughening and ductile particle reinforcements improves substantially the crack growth resistance and flaw tolerance. The presence of Nb_2O_5 is beneficial to tetragonal to monoclinic transformation. Dense, uniform and fine microstructure was obtained using microwave sintering. Decrease in grain size is attributed to fast heating and cooling rate in the case of microwave sintering.

References

BartolomeJ.H, Gutierrez-Gonzalec.C.F, Pecharroman.C, & Moya,J,S (2007). Synergetic Toughening Mechanism in 3Y-TZP/Nb Composites. *Acta Materialia*, 55, 5924 – 5933.

Dae – Joon Kim. (1990). Effect of Ta_2O_5, Nb_2O_5 and HfO_2 alloying on the transformability of Y_2O_3 stabilized Tetragonal ZrO_2, *Journal of American Ceramic Society*, 73[1], 115-120.

Dae-Joon Kim, Hyung – Jin Jung, Joo-Wung Jang, Hong – Lim Lee (1998). Fracture Toughness, Ionic Conductivity, and Low Temperature Phase Stability of tetragonal Zirconia codoped with Yttria and Niobium Oxide, *Journal of American Ceramic Society*, 81[9]2309 – 2314

Deuk Yong lee, Dae-Joon Kim, Bae – Yeon Kim. (2002). Influence of alumina particle size on fracture toughness of (Y,Nb) – TZP/Al_2O_3 composites, *Journal of European Ceramic Society*, 2173 – 2179.

Deuk YongLee, Dae –Joon Kim, Duk-Ho Cho, (1998). Low Temperature Phase Stability and Mechanical Properties of Y_2O_3 and Nb_2O_5 co-doped Tetragonal Zirconia Polycrystal Ceramics .*Journal of Material Science Letters* 17, 185-187

Ebadzadeh.T & Valefi.M(2008). Microwave Assisted Sintering of Zircon, *Journal of Alloys & Compounds*, 448, 246 – 249.

GuptaT.K, .Bechtold.J.H, Kuznicki.R.C, Cadoff .L.H & Rossing. R.D (1977). Stabilization of Tetragonal Phase in Polycrystalline Zirconia. *Journal of Material Science*, 12, 2421 – 2426.

Mehdi Mazaheri, Zahedi.A.M, & Hejazi.M.M. (2008). Processing of Nanocrystalline 8mol% YSZ by Conventional, Microwave Assisted and Two Step Sintering. *Material Science & Engineering A*, 261 – 267.

Ping Li & Wei Chen. (1994). Effect of Dopants on Zirconia Stabilization – An X-ray Absorption Study : 1 Trivalent Dopants. *Journal of American Ceramic Society*, 77[1], 118 – 128.

Ping Li, I-Wei Chen & James E Penner Hahn. (1993). X-ray absorption studies of ZrO_2 polymorphs II Effect of Y_2O_3 dopant on ZrO_2 Microstructure, *Physical Review B*, 48[14], 10074 – 10081.

Ping Li, I-Wei Chen, James E Penner Hahn. (1994). Effect of Dopants on Zirconia Stabilization – An X-ray Absorption Study : III Charge Compensating Dopants. *Journal of American Ceramic Society*, 77[5], 1289 – 1295.

Sharon A Nightingale, Worner H.K, Dunne .D.P (1997). Microstructural Development during the Microwave Sintering of Yttria – Zirconia Ceramics, *Journal of American Ceramic Society*, 80[2], 394 – 400.

Sharon A Nightingale, Worner.H.K & Dunne.D.P. (1997). Microstructural Development during the Microwave Sintering of Yttria – Zirconia Ceramics, *Journal of American Ceramic Society*, 394 – 400.

Xin Guo. (1997). Effect of Nb_2O_5 on the space charge conduction of Y_2O_3 stabilized ZrO_2, *Solid State Ionics*, 99, 137 – 142.

Xin Guo, & Zhu Wang. (1998). Effect of Niobia on the Defect Structure of Yttria Stabilized Zirconia, *Journal of European Ceramic Society*,18, 237 – 240.
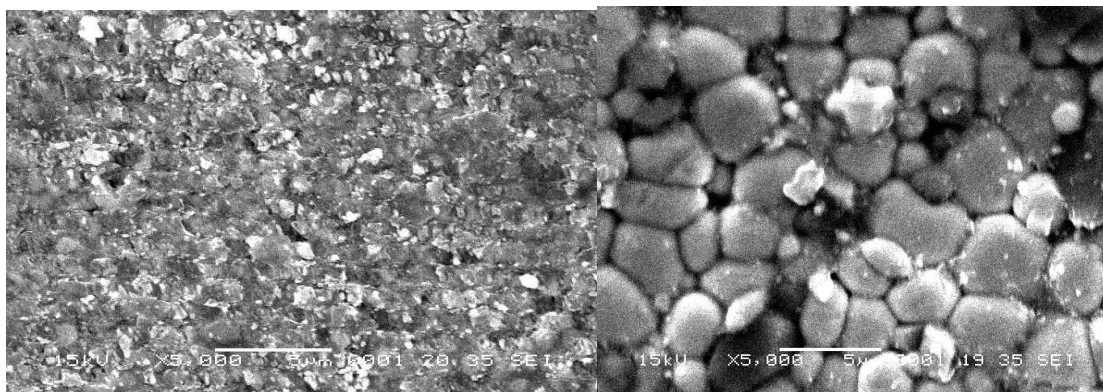
<center>(a) (b)</center>

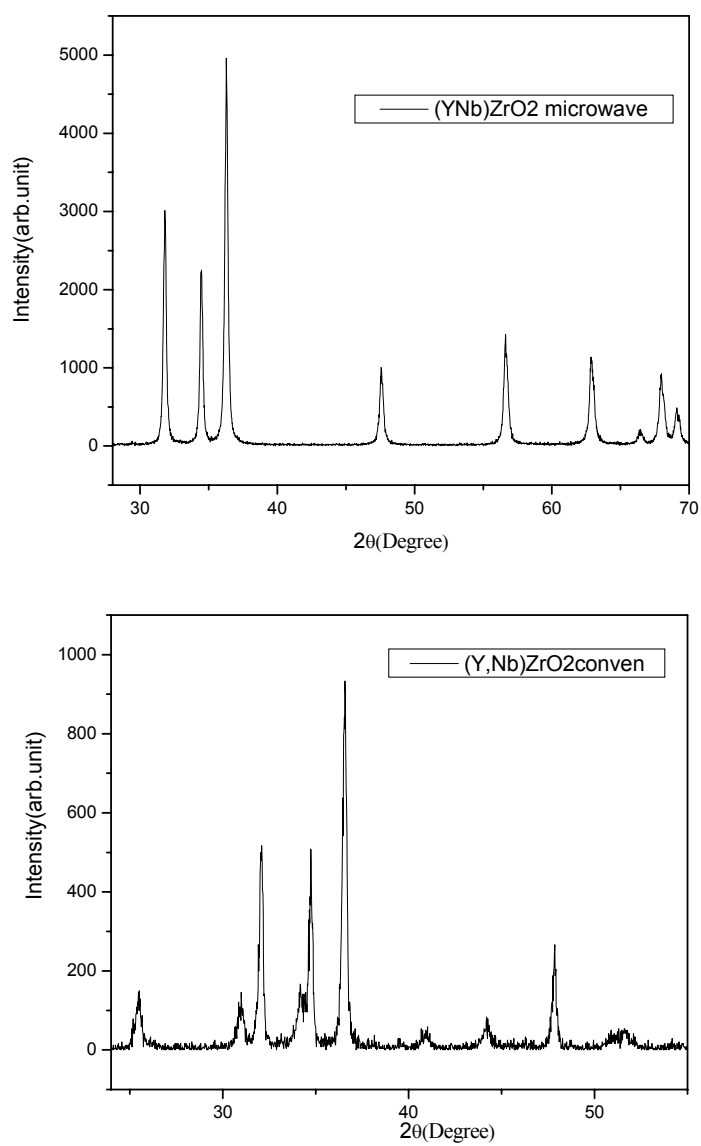Figure 1. SEM Micrographs of samples sintered by (a) Microwave Sintering (b) Conventional Sintering

Figure 2. X-ray Diffraction of Samples Sintered at 1550ºC (a) Microwave (b) Conventional

Research on Flocculation Property of Bioflocculant PG·a21 Ca

Yongzhang Pan, Bo Shi & Yu Zhang

Environmental Engineering Department

Jinan University, Guangzhou, Guangdong 510632, China

Tel: 86-20-8522-6615   E-mail: jnu_083002@163.com

Abstract

This paper investigates the flocculation performance of polyglutamic acid-based bioflocculant PG·a21 Ca by processing kaolin suspension, studies the effects on the flocculation efficiency from the amount of flocculant, pH, temperature, hydraulic condition and etc. The results show that the flocculation rate of PG·a21 Ca to 1 g/L kaolin suspension is 95.8% under the condition that the amount of PG·a21 Ca is 300 mg/L, pH is 7, temperature is 25 ºC, stirring speed of mixing is 350 r/min, stirring time of mixing is 50 s, stirring speed of reaction is 80 r/min, and stirring time of reaction is 4 min. Effects from wastewater processing show that bioflocculant PG·a21 Ca has better effects in treating domestic wastewater and higher removal rate of total phosphorus and ammonia nitrogen than the common chemical flocculants such as PAC and PFS. Meanwhile, PG·a21 Ca can effectively remove chlorophyll A in algae-contained lake water and make water clear, and partially remove COD and TP in wastewater from beer brewing.

Keywords: Bioflocculant PG·a21 Ca, Flocculation performance, Wastewater disposal, Polyglutamic acid

Flocculation technology has been widely applied in water processing field, especially in preprocess of various wastewater treatment. It has the benefits of low infrastructure investment and short processing time. There are two common flocculants at present: inorganic macromolecular compounds as represented by aluminum-iron series coagulant and synthesized organic macromolecular flocculants as represented by acrylamide polymer. However, it has been found that these flocculants have relatively serious safety issue and potential secondary pollution in practical applications. For example, aluminum ion may cause senile dementia; iron salt causes corrosion to equipment and may have relatively higher coloring; acrylamide polymer, an organic macromolecular flocculant, although non-toxic, is difficult to degrade and can cause secondary pollution; meanwhile, the original monomer acrylamide has strong neurotoxicity and can cause cancer. All above issues limit their applications. Therefore, it is necessary and important to develop a safe and non-toxic flocculant with high flocculating activity and without any secondary pollution.

Study on application of bioflocculant has reached wide areas including various wastewater disposal, such as suspension removal (Gong, Xiaoyan, 2003, p. 196-199; Li, Heping, 2000, p. 113-117; Huang, Xiaowu, 2004, p. 25-27), color removal (Zhuang, Yuanyi, 1997, p. 349-353; I. L. Shih, 2001, p. 267-272; Xin, Baoping, 2000, p. 97-102; J. Zhang, 2002, p. 517-522; Man, Yuezhi, 2003, p. 187-190). In recent years, the bioflocculant has attracted more and more attentions with its high efficiency, non-toxicity, easy decomposition, non secondary pollution, wide application areas, unique color removal effect and other benefits. Wang, Li (2008, p. 31-32) processed dyeing wastewater with Pullulans bioflocculant, its COD_{Cr} removal rate and turbidity removal rate are respectively 88.22% and 63.67%. Ma et al (2009, p. 196-200; 2008, p. 39-41) processed high algae-laden water by polymeric aluminum ferric chloride-compounded composite bioflocculant, wherein the composite bioflocculant was prepared with rice straw as substrate. The results indicated that the turbidity removal rates of chlorine dioxide-preoxided high algae-laden water by the same amount of composite bioflocculant and polymeric aluminum ferric chloride are 89.1% and 60.5% respectively. Gong et al (2008, p. 4668-4674) separated a bacteria from soil. The bioflocculant produced from this bacterium has better flocculation effects at processing effluents from river, beer factory, meatpacking, soy sauce plant and pulp-paper mill. Fujita et al (2001, p. 237-243) purified wastewater from manufacturing plants of deinking chemicals, carbon ink, paint and bean products by a flocculant obtained from Q3-2 bacteria strain separated from recycled sludge of wastewater processing plant. Its flocculation effects are excellent, especially for processing effluents from deinking chemicals plant, wherein its flocculation efficiency is 91.4% and SS removal rate is 99.2%. However, it is less effective in processing wastewater from bean products. H. M. Oh et al (2001, p. 1229-1234) screened and secondarily screened a bacteria of high flocculation activity from sludge, and processed petrochemical wastewater by a flocculant produced from this bacteria. The flocculation effect was good, and its turbidity removal rate was up to 90.1%.

This paper studies the flocculation effects of commercialized polyglutamic acid-based bioflocculant PG·a21 Ca, applies it and other common flocculants in processing wastewater, compares and investigates the actual application value of bioflocculant PG·a21 Ca.

1. Materials, equipments and methods

1.1 Materials

(1) Reagent

Bioflocculant PG·a21 Ca, grey powder, formulated with polyglutamic acid, Ca and other minerals, manufactured by PLOY-GLU Company of Japan; Polymeric aluminum chloride (PAC), light yellow solid; Polymeric ferric sulfate (PFS), reddish-brown liquid; Kaolin, CR. All are purchased.

(2) Kaolin suspension

Add 1 g kaolin powder into 1,000 mL distilled water, stir uniformly to get kaolin suspension with concentration of 1 g/L.

1.2 Equipments

2R4-6 mixer for coagulation test, PHS-3C precise acidometer and STZ-A24 turbidimeter.

1.3 Methods

Add flocculant into 500 mL kaolin suspension, adjust pH; Stir at 350 r/min for 50 s, then stir at 60 r/min for 4 min by 2R4-6 mixer for coagulation test; Keep stationary for 15 min, then determine the turbidity of supernatant fluid by STZ-A24 turbidimeter. The flocculation activity is expressed by flocculation efficiency calculated with the following formula:

$$\text{Flocculation efficiency} = (\text{Initial turbidity} - \text{Turbidity after flocculation})/\text{Initial turbidity}$$

The optimal application conditions are determined by comparing flocculation efficiency.

1.4 Analysis methods of water quality

Test COD, ammonia-nitrogen, TP and chlorophyll A respectively by potassium dichromate method, Nessler reagent photometric method, molybdenum-antimony anti-spectrophotometric method and acetone extraction-spectrophotometric method.

2. Results and Analysis

2.1 Process conditions affecting flocculation effects

2.1.1 Influence of the amount of PG·a21 Ca to flocculation

The amount of flocculant has a major effect on flocculation. In most of relevant literatures, the amounts of bioflocculants used for processing kaolin suspension are in the range of 1.0-20.0 mL/L, and most of cases need to add certain amount of calcium chloride or aluminum sulphate as coagulant aid. Their flocculation efficiencies can reach 90%. However, PG·a21 Ca is a bioflocculant from polyglutamic acid and Ca, its applied dosage is different from that of common bioflocculant. Figure 1 exhibits the influence of the amount of PG·a21 Ca to the turbidity removal effect of kaolin suspension. Figure 1 indicates that flocculation efficiency reaches 90% or more when the amount of PG·a21 Ca is above 250 mg/L; and small viscous floces are formed in solution, many suspended substances on the solution surface, and the turbidity of solution is high when the amount is at 50 mg/L. With the increased amount, floces in solution become bigger, suspended substances on the solution surface get less, and the solution is clearer. From the point of view benefit and cost, the optimal amount of PG·a21 Ca is about 300 mg/L.

2.1.2 Influence of pH to flocculation

Figure 2 exhibits the influence of pH to flocculation when initial turbidity is 123 NTU and the amount of PG·a21 Ca is 300 mg/L. From figure 2, we can see that flocculation efficiency is above 90% and keeps constant when pH is lower than 7, reaches the maximum when pH is exactly at 7, but decreases with the increase of pH when pH is higher than 7. It demonstrates that PG·a21 Ca is suitable to applying in acid circumstances and need to adjust pH if in alkaline environment. This is because biopolymer shows different electric states at different pH, in turn affects the surface electric property of kaolin powder. Flocculant is much easier to be absorbed onto the surface of kaolin particles when electrostatic repulsion is lower than electrostatic attraction between flocculant particles and kaolin particles.

2.1.3 Influence of stirring speed and stirring time to flocculation

It is required that flocculant is rapidly and uniformly mixed with wastewater during mixing stage, so rapid stirring in a short time is necessary. However, it is required not only to form floces of flocculant and impurities, but also to prevent floces from being deflocculated during the reaction stage, so slow stirring for a longer time is necessary.

With residual turbidity of supernatant after 15 min static settling as test index, a 4-factor-3-level orthogonal table is used to schedule 9 operation conditions of orthogonal experiment, with the four factors being stirring speed of mixing, stirring time of mixing, stirring speed of reaction and stirring time of reaction. The orthogonal experiment and the range analysis on it are shown in table 1.

From table 1, we can conclude that the influence from large to small is stirring speed of mixing, stirring time of reaction, stirring time of mixing and stirring speed of reaction. The optimal hydraulic conditions are respectively 350 r/min stirring speed of mixing, 3 min stirring time of reaction, 40 min stirring time of mixing and 80 r/min stirring speed of reaction.

2.1.4 Influence of temperature to flocculation

Figure 3 exhibits the influence of temperature to flocculation effect of PG·a21 Ca at the optimal hydraulic conditions when initial turbidity is 126 NTU and the amount of PG·a21 Ca is 300 mg/L. Figure 3 demonstrates that flocculation efficiency of PG·a21 Ca rises with the increase of temperature in the range of 5-60 ℃, but decreases with the increase of temperature when the temperature is above 60 ℃. It indicates that too high or too low a temperature of solution is unfavorable to the flocculation. This can be explained by chemical kinetics: suspended particle moves faster and collision frequency is greater at higher temperatures, this contributes to the increase in rate of reaction. However, when temperature is too high, although reaction speeds up, the formed floces are too small and have stronger hydrating trend, as a result, it is difficult to be separated by precipitation. When temperature is too low, reaction slows down, the increase of shear intensity of water to flocculant makes floces too small to be separated by precipitation.

2.2 Flocculation test of PG·a21 Ca on actual wastewater

Above test results indicate that bioflocculant PG·a21 Ca has good flocculation effects on kaolin suspension at proper conditions. For further study on the flocculation effects of PG·a21 Ca, flocculation tests of PG·a21 Ca on actual domestic wastewater, algae-contained lake water and wastewater from beer brewing were carried out, and its processing effects were compared with those of PAC and PFS.

2.2.1 Effects on actual domestic wastewater

Samples came from schoolyard domestic wastewater of Jinan University. Based on the preliminary tests, it is determined that the optimal amounts of PAC, PFS and PG·a21 Ca are 15 mg/L, 18 mg/L and 300 mg/L respectively. The processing results are shown in table 2. From table 2, we can see that the removal rate of COD, ammonia-nitrogen and total phosphorus by PG·a21 Ca is 50.6% (approximating that by PAC or PFS), 33.2% (much higher than that by PAC or PFS) and 85.1% (slightly higher than that by PAC or PFS). The concentration of COD, ammonia-nitrogen and total phosphorus in PG·a21 Ca-processed actual domestic wastewater meets the Grade 1 Level in the Integrated Wastewater Discharge Standard (8978-1996).

2.2.2 Effects on algae-contained lake water

Samples came from South Lake of Jinan University. Based on the preliminary tests, it is determined that the optimal amounts of PAC, PFS and PG·a21 Ca are 20 mg/L, 15 mg/L and 300 mg/L respectively. The results are shown in table 3. From table 3, we can see that the removal rate of total phosphorus by PG·a21 Ca is up to 97.8%, higher than that by PAC or PFS; removal rate of turbidity is above 90%, similar to PAC or PFS; removal rate of COD is slightly higher than that by PAC or PFS; removal rate of chlorophyll A and ammonia-nitrogen is much higher than that by PAC or PFS.

2.2.3 Effects on wastewater from beer brewing

Samples came from Zhujiang Bear. Based on the preliminary tests, it is determined that the optimal amounts of PAC, PFS and PG·a21 Ca are 400 mg/L, 350 mg/L and 400 mg/L respectively. The results are shown in table 4. From table 4, we can see that the removal rate of turbidity by PG·a21 Ca is up to 95.6%, higher than that by PAC or PFS; removal rate of total phosphorus and ammonia-nitrogen is much higher than that by PAC or PFS; removal rate of COD is slightly higher than that by PAC or PFS.

In short, the results of actual wastewater disposal demonstrate that floces from PG·a21 Ca is much bigger than that from PAC or PFS, and much easier to be separated by precipitation.

3. Conclusion

(1) The results of flocculation test indicate that PG·a21 Ca is a bioflocculant with high flocculation efficiency and stable flocculation property. It has much better effects on removal of ammonia-nitrogen than PAC, PFS and similar products, excellent effects on removal of phosphorus, and similar effects on removal of COD as PAC and PFS.

(2) The concentration of COD, ammonia-nitrogen and total phosphorus in PG·a21 Ca-processed actual domestic wastewater meets the Grade 1 Level in the Integrated Wastewater Discharge Standard (8978-1996). PG·a21 Ca can efficiently remove chlorophyll A and turbidity in algae-contained lake water, and partially remove COD and TP in wastewater from beer brewing.

(3) The dosage needed and the cost of PG·a21 Ca are relatively high, which cause high operation cost and limit the wide range applications of PG·a21 Ca.

References

Gong, Wenxin, Wang, Shuguang, Sun, Xuefei & et al. (2008). Bioflocculant production by culture of Serratia ficaria and its application in wastewater treatment. *Bioresource Technology*, 99, 4668-4674.

Gong, Xiaoyan, Wang, Shuguang, Luan, Zhaokun & Jia, Zhiping. (2003). Screening and optimization of a bioflocculant-producing bacterium and its application in water treatment. *Chinese Journal of Applied and Environmental Biology*, 9(2), 196-199.

H. M. Oh, S. J. Lee, M. H. Park & et al. (2001). Harvesting of Chlorella vulgaris using a bioflocculant from Paenibacillus sp. AM49. *Biotechnol. Lett.*, 23, 1229-1234.

Huang, Xiaowu, Cheng, Wen, Hu, Yongyou & Huang, Zhihua. (2004). A study of microbiological flocculants for treatment of wastewater. *Industrial Water & Wastewater*, 6, 25-27.

I. L. Shih, Y. T. Van, L. C. Yeh & et al. (2001). Production of a biopolymer flocculant from Bacillus licheniformis and its flocculation properties. *Bioresour. Technol.*, 78, 267-272.

J. Zhang, Z. Liu, S. Wang & et al. (2002). Characterization of a bioflocculant produced by the marine myxobacterium Nannocystis sp.NU-2. *Appl. Microbiol. Biotechnol.*, 59, 517-522.

Li, Heping, Zheng, Zegen, Zhu Zhu & Zheng Huaili. (2000). Microbial flocculant. *Journal of Chongqing Jianzhu University*, 22(3), 113-117.

M. Fujita, M. Ike & T. Hirao. (2001). Bioflocculant production from lower-molecular fatty acids as a novel strategy for utilization of sludge digestion liquor. *Water Sci. Technol.*, 44, 237-243.

Ma, Fang, Li, Dapeng, Zheng, Lina, Lv, Xiaolei & Qiu Shan. (2008). Combination of compound bio-flocculant and PAFC for treatment of algae-laden water. *China Water & Wastewater*, 24(3), 39-41.

Ma, Fang, Zhang, Huiwen, Li, Dapeng, Wei, Li & Hou, Ning. (2009). Compound bioflocculant produced by using rice straw as substrate. *China Environmental Science*, 29(2), 196-200.

Man, Yuezhi, Zhuang, Yuanyi, Xin, Baoping, Qiu, Jinquan, Wang, Wen & Yang Min. (2003). Study on affecting factors of biological adsorption of dyes and desorption conditions. *Environmental Protection of Chemical Industry*, 23(4), 187-190.

Wang, Li. (2008). Comparison of flocculation effect of bio-flocculant Pullulan and PAC and PAM on the dyeing wastewater. *Industrial Safety and Environmental Protection*, 34(5), 31-32.

Xin, Baoping, Zou, Qimeng, Zhuang, Yuanyi, Jin, Zhaohui, Hu, Guochen & Song Wenhua. (2000). Biosorption and decolorization of reactive brilliant blue KN-R by a specific strain GX2. *Acta Scientiae Circumstantiae*, 20(9), 97-102.

Zhuang, Yuanyi, Dai, Shugui, Li, Tong, Song, Wenhua, Zhuang, Lian, Gu, Wenxin,Li, Guichun, Yan, Hui, Sun, Qijun & Li Hui. (1997). Study of the flocculation of dyes in water by bioflocculants. *Technology of Water Treatment*, 23(6), 349-353.

Table 1. L$_9$(3^4) orthogonal experiment and the range analysis

Serial number	Stirring speed of mixing (r/min)	Stirring time of mixing (min)	Stirring speed of reaction (r/min)	Stirring time of reaction (min)	Residual turbidity (NTU)
1	350	50	100	4	6.9
2	300	50	80	2	7.3
3	250	50	60	2	9.7
4	350	40	80	3	5.1
5	300	40	60	4	9.3
6	250	40	100	3	9.5
7	350	30	60	3	7.8
8	300	30	100	2	10
9	250	30	80	4	10.4
K$_1$	9.87	9.40	8.93	9.00	
K$_2$	8.87	7.97	7.60	7.47	
K$_3$	6.60	7.97	8.80	8.87	
Extreme difference	3.27	1.43	1.33	1.53	

Table 2. Effects of flocculant on actual domestic wastewater

Item		COD	Ammonia-nitrogen	Total phosphorus
Before process (mg/L)		143	21.7	1.75
PAC	After process (mg/L)	75.0	17.1	0.35
	Removal rate (%)	47.5	18.6	80.2
PFS	After process (mg/L)	69.8	17.6	0.27
	Removal rate (%)	51.1	18.9	84.7
PG.a21 Ca	After process (mg/L)	73.3	14.5	0.09
	Removal rate (%)	50.6	33.2	85.1

Table 3. Effects of flocculant on high algae-laden lake water

Item		Turbidity (NTU)	Chlorophyll A (μg/L)	COD (mg/L)	Ammonia-nitrogen (mg/L)	Total phosphorus (mg/L)
Before process		18.2	48.3	132	2.2	0.48
PAC	After process	1.3	15.8	42	1.8	0.03
	Removal rate (%)	92.8	67.3	68.2	18.2	93.7
PFS	After process	1.1	12.6	39	1.7	0.02
	Removal rate (%)	93.9	73.9	70.4	22.7	95.8
PG.a21 Ca	After process	1.2	8.7	37	1.3	0.01
	Removal rate (%)	93.4	82.0	72.0	40.9	97.9

Table 4. Effects of flocculant on wastewater from beer brewing

Item		Turbidity (NTU)	COD (mg/L)	Ammonia-nitrogen (mg/L)	Total phosphorus (mg/L)
Before process		133	1925	21.4	10.54
PAC	After process	12.5	1182	17.1	5.41
	Removal rate (%)	90.6	38.6	20.1	48.7
PFS	After process	11.0	1161	16.3	5.25
	Removal rate (%)	91.7	39.7	23.9	50.4
PG.a21 Ca	After process	5.8	1122	14.1	4.39
	Removal rate (%)	95.6	41.7	34.1	58.3
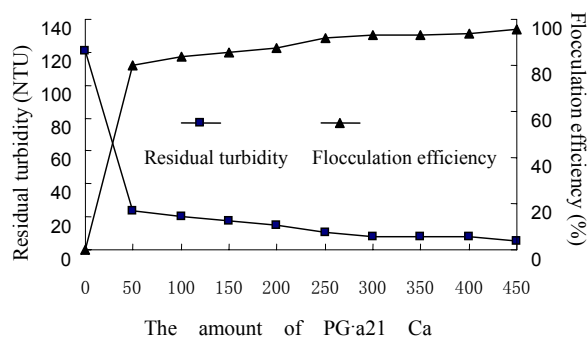
Figure 1. Influence of the amount of PG·a21 Ca to flocculation
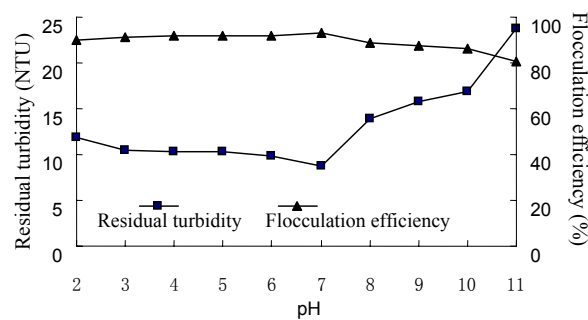
Figure 2. Influence of pH to flocculation
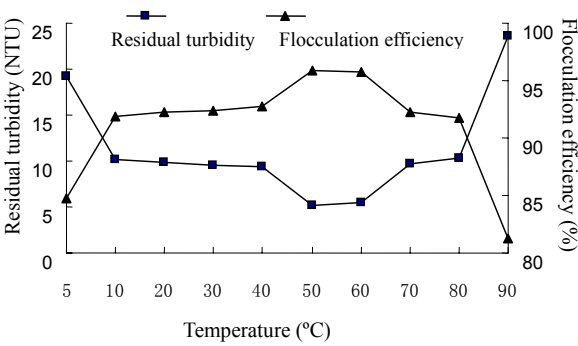
Figure 3. Influence of temperature to flocculation

The Application and Modeling

for Conditional Heteroscedasticity Time Series

Wenfang Su (Corresponding author)

Department of Science, Yanshan University

438 West of He Bei Avenue, Qinhuangdao 066004, China

E-mail:suwenfang0228@126.com

Rui Shan & Jun Zhang

Department of Science, Yanshan University

438 West of He Bei Avenue, Qinhuangdao 066004, China

Yan Gao

Jangheliu Senior High School

Hebei 053500, China

Abstract

This article mainly presents the fundamental theory, model and application of conditional heteroscedasticity residual sequence. And it also gives detailed, scientific and exact analysis and research on a financial security example. Then summarizing a conclusion: Financial Securities follows specific rules and tracks through above study. The research indicates that ARCH model only applies to a short-term, auto-correlative heteroscedastic function, whereas the amended GARCH model has the opposite result, that is, GARCH fits a long-term, auto-correlative heteroscedastic function. Meanwhile, SAS program presents more intuitive, exact tables and figures. All analysis and results show that AR (m)-GARCH fits well.

Keywords: Time series, Heteroscedastic function, ARCH, GARCH, SAS

1. Introduction

In recent years, with computing technology and signal processing technology, the theory and methods of time series analysis has been refined greatly, especially in the parameter estimation algorithm, model structure identification and intellectual computing technology integration and so on. Furthermore it gains fruitful achievement in these fields and covers an increasingly wide range of applications, and the results are at a high-level of level. For example, in the field of control engineering, motion control system for time series analysis modeling and forecast; in Internet technologies, network traffic analysis of time series model; theoretical studies in the database, data mining of time series methods; in electronic information field, random signals in time series modeling and analysis; in the field of biological engineering, DNA sequence analysis and calculation; in the field of biomedical engineering, biomechanical and electrical signals in time series analysis; in mechanical fault diagnosis study, non-destructive testing signals in time series analysis; fine chemical control in the use of time series spectral analysis techniques and so on.

Although the time series offers a variety of different models to fit the actual problem, and make short-term prediction, such as commonly used model has ARMA, ARIMA, etc…We are familiar with ARMA, ARIMA model and think its residual sequence is white noise sequence which meets $E(\varepsilon_t) = 0$; and also meets $D\varepsilon_t = \gamma(0) = \delta^2$, where, δ^2 is a constant. However, when Engle did research on the UK inflation rate in 1982, he surprisingly found that the classic ARIMA model has failed to achieve the desired effect of the fitting. After careful study on sequence of residuals, he discovered a problem in some time series of residuals with heteroscdasticity. In recent year scholars found many financial time series has emerged of the nature of heteroscdasticity in practice, and usually there is a positive relationship between the standard deviation and the level. That is, with low levels of sequence, the sequence of fluctuations small, with high levels of sequence, the sequence of fluctuations in large. Although we have made appropriate assumptions to heteroscedastic function, a lot of practice has proved that this assumption is too simplistic. Thus, in order to estimate heteroscedastic function more accurately, Engle made conditional heteroscedasticity ARCH and GARCH models.

2. ARCH model

The full name of ARCH model is autoregressive conditional heteroscedasticity model (autoregressive conditional heteroscedastic), it is made by Robert F. Engle, who is an American statistician, economist measurement. Set $\{x_t, t = 1,2,...\}$ is a time series, called the model with the following structure for the q-order Autoregressive Conditional Heterocedasticity Model, easily recorded as ARCH(q), its complete structure as follows:

$$x_t = f(t, x_{t-1}, x_{t-2},...) + \varepsilon_t$$
$$\varepsilon_t = \sqrt{h_t}\, e_t$$
$$h_t = \omega + \sum_{j=1}^{q} \lambda_j \varepsilon_{t-j}^2$$

Where, $f(t, x_{t-1}, x_{t-2},...)$ is the regression function of Auto-Regressive Model of $\{x_t\}$; $h_t = \omega + \sum_{j=1}^{q} \lambda_j \varepsilon_{t-j}^2$ is heteroscedasticity function; $e_t \overset{i.i.d}{\sim} N(0,1)$; $\{\varepsilon_t\}$ is white noise heteroscedasticity residual sequence which has $E(\varepsilon_t) = 0$.

3. GARCH model

After ARCH model was amended by Bollerslev, he proposed the GARCH model (generalized autoregressive conditional heteroscedastic), easily recorded as GARCH (p, q), its structure as follows:

$$x_t = f(t, x_{t-1}, x_{t-2},...) + \varepsilon_t$$
$$\varepsilon_t = \sqrt{h_t}\, e_t$$
$$h_t = \omega + \sum_{i=1}^{p} \eta_i h_{t-i} + \sum_{j=1}^{q} \lambda_j \varepsilon_{t-j}^2$$

Where, $f(t, x_{t-1}, x_{t-2},...)$ is the regression function of $\{x_t\}$; $e_t \overset{i.i.d}{\sim} N(0,1)$; $h_t = \omega + \sum_{i=1}^{p} \eta_i h_{t-i} + \sum_{j=1}^{q} \lambda_j \varepsilon_{t-j}^2$ is the GARCH model heteroscedasticity function, $\{\varepsilon_t\}$ is white noise heteroscedasticity residual sequence which has $E(\varepsilon_t) = 0$.

3.1 GARCH model constraints

GARCH model in the use of modeling practical problems should pay attention: its effective use must meet the following two constraints.

Condition 1: parameters of non-negative

$$\omega > 0, \eta_i \geq 0, \lambda_j \geq 0 ;$$

Condition 2: parameters have limit

$$\sum_{i=1}^{p} \eta_i + \sum_{j=1}^{q} \lambda_j < 1$$

3.2 GARCH (p, q) modeling thought

GARCH model fitted to follow the six steps:

Step1. According to observations of the nature of sequences, fitting regression model;

Step2. Test the residual sequence autocorrelation through statistic DW;

Step3. The use of statistic PQ and LM for heteroscedasticity autocorrelation test;

Step4. Through the DW test results, residual autocorrelation sequence diagram as well as PQ and LM test statistic for the fitted-order model fitting;

Step5. The use of maximum likelihood estimation method to estimate the unknown parameters;

Step6. Finally the use of Bear-Jarque normality test statistic for testing the validity of the model.

4. AR (m)-GARCH

When the GARCH model of regression function $f(t, x_{t-1}, x_{t-2},...)$ can not extract the sequence $\{\varepsilon_t\}$ of the relevant information fully, the residual sequence may have a nature of auto-correlation, rather than pure randomness. At this point the need for $\{\varepsilon_t\}$ first fitting autoregressive model, and then inspecting autoregressive residual sequence $\{v_t\}$ whether meets $D\varepsilon_t = \gamma(0) = \delta^2$ or not. If $\{v_t\}$ is heteroscedasticity, GARCH model is fitted. This model called AR (m)-GARCH (p, q) model, its structure as follows:

$$x_t = f(t, x_{t-1}, x_{t-2},...) + \varepsilon_t$$
$$\varepsilon_t = \sum_{k=1}^{m} \beta_k \varepsilon_{t-k} + v_t$$
$$v_t = \sqrt{h_t}\, e_t$$

$$h_t = \omega + \sum_{i=1}^{p} \eta_i h_{t-i} + \sum_{j=1}^{q} \lambda_j v_{t-j}^2$$

Where, $f(t, x_{t-1}, x_{t-2}, ...)$ is the regression function of $\{x_t\}$; $e_t \overset{i.i.d}{\sim} N(0,1)$

5. SAS Program Results and Discussion

Table 1 shows security data about Reserve Bank of Australia from 1969, 1 to 1994, 9. Then we will analyze these data and fit an appropriate model to dignify them. Table 2 gives the DW test results. The results show residual sequence has obvious positive auto-correlativity. Parameter estimation demonstrates the regressive model parameters are all remarkable. From table 3, we know residual sequence autocorrelation has a long-term auto-correlativity, and the coefficient decreases slowly. Table 4 demonstrates PQ and LM test results. The results show remarkable heteroscedastic nature and long-term relation. From table 5, we can make sure that the value of different parameters in the AR (2)-GARCH (1, 1). Last we can acquire the formula of AR (2)-GARCH (1, 1) model, as follows:

$$x_t = 0.0358t + u_t$$
$$u_t = 1.0754u_{t-1} - 0.081u_{t-2} + \varepsilon_t$$
$$\varepsilon_t = \sqrt{h_t}\, a_t, a_t \overset{i.i.d}{\sim} N(0, 0.35041)$$
$$h_1 = 0.34 + (2.554E - 23)\varepsilon_{t-1}^2 + 0.0298h_{t-1}$$

Figure 1 shows the curve track of $\{x_t\}$. From figure 1, we can see the curve presents remarkable linear increasing tendency, and the range of fluctuation increases with time extends. So we fit the linear regressive model. Figure 2 shows the curve of AR (2)-GARCH (1, 1). Comparing with figure 1, we see the two curves are quite similar.

6. Conclusions

From the above example of analysis and study, we acquire such conclusion: the AR (m)-GARCH model usually applies to Financial Sequence which has a long-term ,auto-correlative heteroscedasticity function, the AR(2)-GARCH(1, 1) fits well from the two figures. So under the heteroscedasticity conditions, we find a better model to fit this kind of practical problems.

References

Gao, Huixuan. (1998). *SAS System, SAS/ETS Software User Manual*. Beijing: China Statistics Press. pp. 116-153.

James D. Hamilton. (1999). *Time Series Analysis*. Beijing: China Social Science Press. pp. 799-819.

Pan, Hongyu. (2006). *Time Series Analysis*. Beijing: Foreign Economic and Trade University Press.

Wang, Yan. (2005). *Application of Time Series Analysis* [M]. Beijing: China People University Press. pp.167-207.

Wang, Zhenlong. (2007). *Time Series Analysis*. Beijing: Science Press.

Zhang, Xiaolong. (2007). Inventory Control under Temporal Demand Heterosedasticity. *European Journal of Operational Research*.2007 182 (pp127-144).

Table 1. Reserve Bank of Australia data diagram

4.99 5.00 5.03 5.03 5.25 5.26 5.30 5.45 5.49 5.52 5.70 5.68 5.65 5.80 6.50 6.45 6.48 6.45 6.35 6.40 6.43 6.43 6.44 6.45 6.48 6.40 6.35 6.40 6.30 6.32 6.35 6.13 5.70 5.58 5.18 5.18 5.17 5.15 5.21 5.23 5.05 4.65 4.65 4.60 4.67 4.69 4.68 4.62 4.63 4.90 5.44 5.56 6.04 6.06 6.06 8.07 8.07 8.10 8.05 8.06 8.07 8.06 8.118.60 10.80 11.00 11.00 11.00 9.48 9.18 8.62 8.3 8.47 8.44 8.44 8.46 8.49 8.54 8.54 8.50 8.44 8.49 8.40 8.46 8.50 8.50 8.47 8.47 8.47 8.48 8.48 8.54 8.56 8.39 8.89 9.91 9.89 9.91 9.91 9.90 9.88 9.86 9.86 9.74 9.42 9.27 9.26 8.99 8.83 8.83 8.83 8.82 8.83 8.83 8.79 8.79 8.69 8.66 8.67 8.72 8.77 9.00 9.61 9.70 9.94 9.94 9.94 9.95 9.94 9.96 9.97 10.83 10.75 11.20 11.40 11.54 11.50 11.34 11.50 11.50 11.58 12.42 12.8513.10 13.12 13.10 13.15 13.10 13.20 14.20 14.75 14.60 14.60 14.45   14.50 14.80 15.85 16.20 16.50 16.40 16.40 16.35 16.10 13.70 13.50 14.00 12.30 12.00 14.35 14.60 12.50 12.75 13.70 13.45 13.55 12.60 12.00 11.00 11.60 12.05 12.35 12.70 12.45 12.55 12.20 12.10 11.15 11.85 12.10 12.50 12.90 12.50 13.20 13.65 13.65 13.50 13.45 13.35 14.45 14.30 15.05 15.55 15.65 14.65 14.15 13.30 12.65 12.70 12.80 14.50 15.10 15.15 14.30 14.25 14.05 14.70 15.05 14.05 13.80 13.25 13.00 12.85 12.60 11.80 13.00 12.35 11.45 11.35 11.55 10.85 10.90 12.30 11.70 12.05 12.30 12.90 13.05 13.30 13.85 14.65 15.05 15.15 14.85 15.70 15.40 15.10 14.80 15.80 15.80 15.00 14.40 13.80 14.30 14.15 14.45 14.10 14.05 13.75 13.30 13.00 12.55 12.25 11.85 11.50 11.10 11.15 10.70 10.25 10.55 10.25 10.30 9.60 8.40 8.20 7.25 8.35 8.25 8.30 7.40 7.15 6.35 5.65 7.40 7.20 7.05 7.10 6.85 6.50 6.25 5.95 5.65 5.85 5.45 5.30 5.20 5.55 5.15 5.40 5.35 5.10 5.80 6.35 6.50 6.95 8.05 7.85 7.75 8.60

Table 2. DW Test Results

Ordinary Least Squares Estimates				
SSE	2774.27594	DFE		306
MSE	9.06626	Root MSE		3.01102
SBC	1562.52428	AIC		1555.06408
Regress R-Square	0.1933	Total R-Square		0.1933
Durbin-Watson	0.0303	Pr < DW		<.0001
Pr > DW	1.0000			
		Standard		Approx
Variable	DF	Estimate	Error	t Value	Pr > |t|
Intercept	1	7.5194	0.3440	21.86	<.0001
t	1	0.0165	0.001930	8.56	<.0001

Table 3. Estimation of Autocorrelation

Estimates of Autocorrelations			
Lag	Covariance	Correlation	-1 9 8 7 6 5 4 3 2 1 0 1 2 3 4 5 6 7 8 9 1
0	9.0074	1.000000	| |********************|
1	8.8341	0.980764	| |******************|
2	8.6228	0.957299	| |****************** |
3	8.4323	0.936155	| |****************** |
4	8.2226	0.912870	| |***************** |
5	7.9961	0.887726	| |***************** |
6	7.7979	0.865717	| |**************** |
7	7.5974	0.843466	| |**************** |

Table 4. PQ and LM Test Results

Q and LM Tests for ARCH Disturbances				
Order	Q	Pr > Q	LM	Pr > LM
1	286.1017	<.0001	283.4412	<.0001
2	545.0776	<.0001	283.6751	<.0001
3	782.4323	<.0001	283.8243	<.0001
4	995.5900	<.0001	284.2103	<.0001
5	1183.6297	<.0001	284.2391	<.0001
6	1353.8193	<.0001	284.6598	<.0001
7	1507.0917	<.0001	284.7027	<.0001
8	1638.3835	<.0001	285.3592	<.0001
9	1750.6976	<.0001	285.3872	<.0001
10	1842.9918	<.0001	286.2225	<.0001
11	1919.1500	<.0001	286.5690	<.0001
12	1981.4862	<.0001	286.6223	<.0001

Table 5. The fitted-model Results

The AUTOREG Procedure					
GARCH Estimates					
SSE		107.927726	Observations		308
MSE		0.35041	Uncond Var		0.35041436
Log Likelihood		-275.54282	Total R-Square		0.9969
SBC		579.736136	AIC		561.085637
Normality Test		4322.0655	Pr > ChiSq		<.0001
			Standard		Approx
Variable	DF	Estimate	Error	t Value	Pr > |t|
t	1	0.0358	0.0285	1.26	0.2086
AR1	1	-1.0754	0.0760	-14.15	<.0001
AR2	1	0.0810	0.0777	1.04	0.2971
ARCH0	1	0.3400	0.008580	39.63	<.0001
ARCH1	1	2.554E-23	2.352E-15	0.00	1.0000
GARCH1	1	0.0298	0.003006	9.90	<.0001

Modern Applied Science
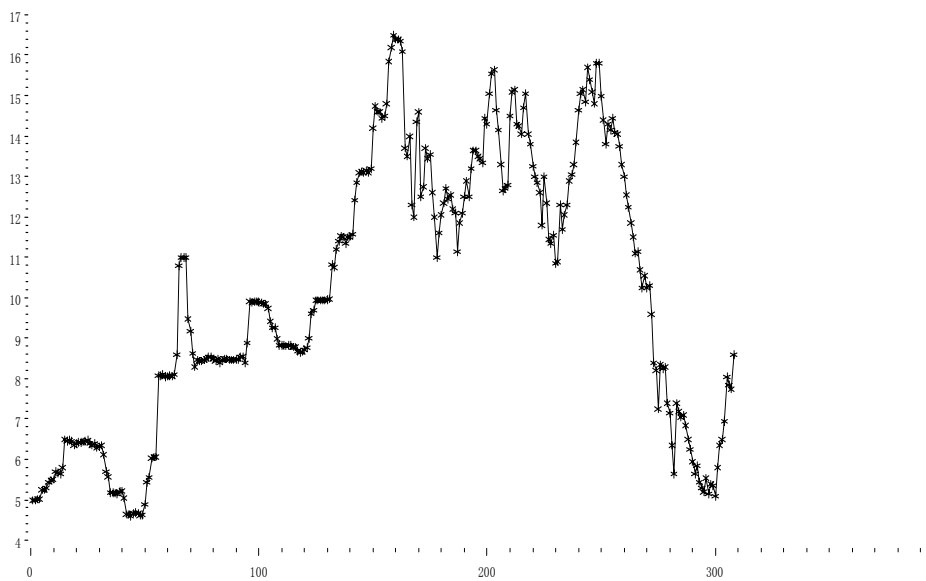
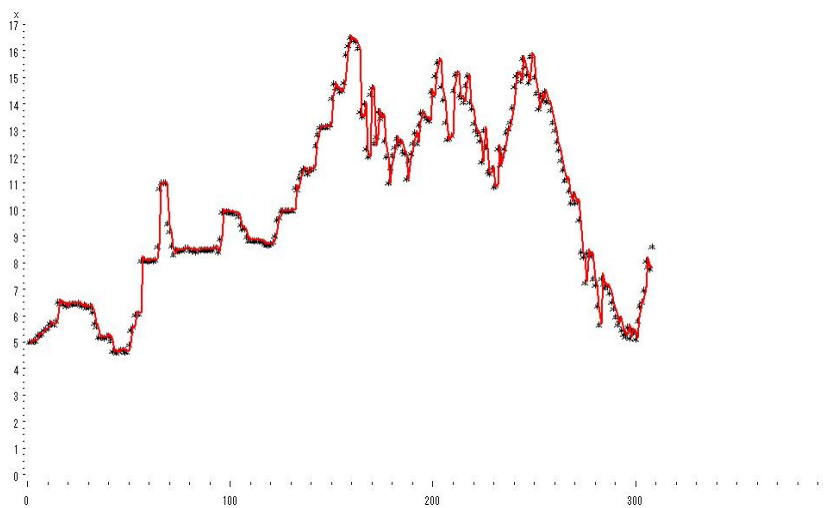Figure 1. The figure of time series { x_t }

Figure 2. The figure of fitted-model

Research for Characteristics of Rotating

Dipole Acoustic Source in Spatial Acoustic Field

Zhihong Liu

Center of Energy and Environment, The QingDao Technology University

11 FuShun Road, QingDao 266033, China

E-mail: lzhqingdao@163.com

Chuijie Yi

Center of Energy and Environment, The QingDao Technology University

11 FuShun Road, QingDao 266033, China

E-mail: Chuijieyi@vip.163.com

Qian Zhang

Center of Energy and Environment, The QingDao Technology University

E-mail: Qianzhang@163.com

Abstract

Formula for calculating the acoustic pressure of spin dipole acoustic source at any point in space was deduced on the base of frequency-domain solution of turning point acoustic source and acousticfield in free space .Which discussed the acoustic field characteristics during the harmonic dipole source rotating and studied the impact on the acoustic field and acoustic pressure at different source frequency, rotating frequency. Study shows that: dipole acoustic field is of an intense space directivity, the characteristics of acoustic field and acoustic source are closely related.

Keywords: Dipole Acoustic Source, Characteristics of acoustic field, Rotating acoustic source

1. Frequency-domain Solution of Spin Dipole AcousticSource:

The acoustic pressure radiated by pulsating sphere acoustic source is discribed as:

$$P(r,t) = \frac{Q(a)}{4\pi r} \frac{-i\omega\rho}{1-ika} e^{ik(r-a)} e^{-i\omega t} \tag{1}$$

Where: ρ is for air-space density, ω is for circular frequency, k is for wave number.

Q(a) is for the intensity of spherical acoustic source, defined as the surface of the spherical acoustic source multiplied by the speed of the surface.Supposed if the radiusof a point acoustic source tends to zero and $\lim\limits_{a\to 0} Q(a) = Q_0$, Q_0 is

for the intensity of the point acoustic source,then formula(1) is :

$$P(r,t) = -i\omega\rho Q_0 \frac{e^{ikr}}{4\pi r} e^{-i\omega t} \tag{2}$$

According to the literature [1,3,4,5], the radiation of acoustic pressure of a rotating Point Source in free space is expressed as:

$$P(X,t) = \frac{1}{4\pi} \int_{-\infty}^{\infty} \frac{Q(\tau)}{r_s} \delta(t-\tau-r_s/c_0) d\tau \tag{3}$$

(X,t) are for the location and time coordinates of observing. (ξ,τ) are for the location and time coordinates of point acoustic source. Q(a) is for the intensity of acoustic source. $r_s = |X - \xi(\tau)|$ is for the distance between point acoustic source and observation point. $(t-\tau-r_s/c_0)$ is for time delay. c_0 is for the velocity of sound in medium. Taking the Fourier transform on both sides of the formula (3) can get frequency-domain solution of arbitrary movement of a

acoustic source and field:

$$P(X,\omega) = \frac{1}{2\pi} \int_{-\infty}^{\infty} Q(\tau) \frac{e^{ik_0 r_s}}{4\pi r_s} e^{i\omega\tau} d\tau \tag{4}$$

According to the literature [2], taking $\dfrac{e^{ik_0 r_s}}{4\pi r_s}$ expanded by Legendre and addition principle, supposed initial of point source is $(r_0, \theta_b, \varphi_b)$, the location of rotating is $(r_0, \theta_0, \varphi_0)$, observation location is (r, θ, φ), $\varphi_0 = \varphi_b + m\Omega$, we can get the frequency domain solution of a rotating point source in free space and the acoustic field g_ω caused by unit intensity and harmonic point source.

$$g_\omega(r/r_0) = \sum_{n=0}^{\infty} ik_0 [(2n+1)/4\pi] j_n(k_0 r_<) h_n(k_0 r_>) \sum_{m=0}^{n} \varepsilon_m \frac{(n-m)!}{(n+m)!} P_n^m(0) P_n^m(\theta)$$
$$* \left(e^{im(\varphi_b-\varphi)} \delta(\omega + m\Omega - \omega_t) + e^{-im(\varphi_b-\varphi)} \delta(\omega - m\Omega - \omega_t) \right) \tag{5}$$

through the differential coordinates of the acoustic source, multi-pole field can be generated from the monopole field, so the dipole acoustic field is generated by unit intensity point source at the direction of $Z(\theta = 0)$:

$$g_z = -\partial g_\omega / \partial z = -(\partial g_\omega / \partial r) \cos\theta \tag{6}$$

Taking g_ω into formula (6):

$$g_z(r/r_0) = \sum_{n=0}^{\infty} (-ik_0^2)[(2n+1)/4\pi] \cos\theta H_n' \sum_{m=0}^{n} \varepsilon_m \frac{(n-m)!}{(n+m)!} P_n^m(0) P_n^m(\cos\theta)$$
$$* \left(e^{im(\varphi_b-\varphi)} \delta(\omega + m\Omega - \omega_t) + e^{-im(\varphi_b-\varphi)} \delta(\omega - m\Omega - \omega_t) \right) \tag{7}$$

Among the forluma:

$$H_n' = \begin{cases} j_n(kr_0) h_n'(kr) & r > r_0 \\ j_n'(kr) h_n(kr_0) & r < r_0 \end{cases} \qquad \varepsilon_m = \begin{cases} 1/2 & m = 0 \\ 1 & m = 1 \cdots n \end{cases}$$

$k_0 = \omega / c_0$ is acoustic wave number, ω is for acoustic circular frequency, Ω is for rotating circular frequency, ω_t is for source vibration frequency, Similarly, the dipole acoustic field is generated by unit point source at the direction of φ_0 dipole :

$$g_\varphi = -\frac{1}{r_0} \frac{\partial g_\omega}{\partial \varphi}$$

Taking g_ω into the formula above:

$$g_\varphi(r/r_0) = \sum_{n=0}^{\infty} (-ik_0/r_0)[(2n+1)/4\pi] j_n(k_0 r_<) h_n(k_0 r_>) *$$
$$\left\{ P_n(0) P_n(\theta) \delta(\omega - \omega_t) - \sum_{m=1}^{n} \frac{(n-m)!}{(n+m)!} P_n^m(0) P_n^m(\theta) \right.$$
$$\left. * im \left[e^{im(\varphi_b-\varphi)} \delta(\omega + m\Omega - \omega_t) - e^{-im(\varphi_b-\varphi)} \delta(\omega - m\Omega - \omega_t) \right] \right\} \tag{8}$$

formula (7) and (8) set up the acoustic field frequency-domain solution of a rotating dipole source respectively. In order to discuss the directivity, the above directive function of the acoustic field $D(\theta, \varphi)$ was set up according to the definition of far-field directivity of the acoustic field:

$$D_z(\theta, \varphi) = r e^{-ikr} g_z(r, \theta, \varphi), \quad D_\varphi(\theta, \varphi) = r e^{-ikr} g_\varphi(r, \theta, \varphi) \tag{9}$$

2. The Acoustic Field Characteristics of Rotating Dipole Sound Source

In order to compare with the characteristics of the monopole rotating sound source , relevant parameters were selected according to the literature [2], namely

$\varphi_b = 0$, $\varphi = -pi/4$, $\omega_t = 6800 rad/s, 2300 rad/s$, $\Omega = 560 rad/s, 112 rad/s$, $\omega = \omega_t + k\Omega$.

Here k is for arbitrary integer, set $k = -5, \cdots, 5$. ω_0 for rotating circular frequency substitute for Ω, Y substitutes for θ, valued $0, pi/18, pi/6, pi/3, pi/2$.

2.1 The Characteristics of Far-Field Acoustic Pressure

For far field $r = 2$, $r_0 = 0.3$, we can calculate the value changes of acoustic pressure with the frequency and directivity. harmonic distribution of acoustic pressure as Fig1and Fig. 3. Acoustic pressure amplitude distribution along the observation angle as Fig2and Fig. 4 . We can conclude from figures: ①Fig1(a)~Fig1(d), far-field acoustic pressure amplitude increases with the auto-oscillation frequency increasing in direction of Z and decreases with the observed angle increasing, the scope of harmonic expands. ② There is only fundamental frequency in the direction of $\theta = 0$,namely the direction of rotation axis and acoustic pressure reaches the maximum amplitude; There is not harmonic distribution in the direction of $\theta = \pi / 2$ namely plane of rotation. ③Fig1(e), with the increasing of rotation frequency , it shows Doppler shift apparently ,and the changes of rotation frequency have a greater impact on the harmonic distribution at a larger observation angle. ④Fig3 (a)~(d), far-field acoustic pressure amplitude is impacted greately by the auto-oscillation frequency,the scope of whose harmonic expands with the observed angle increasing in direction of Y. ⑤There is only fundamental frequency in the direction of $\theta = 0$,namely the direction of rotation axis; Harmonic distribution is the most abundant in the direction of $Y = \pi / 2$ namely plane of rotation. ⑥The frequency change greatly impacts on the harmonic distribution, consistent with it in the direction of Z. ⑦Directivity aspect ,there is an intensive space directivity in the direction of Z and Y.With the decreasing of auto-oscillation frequency and rotation frequency ,there is more harmonic deviated from the fundamental frequency distributed near the plane of the observed angle $\theta = \pi / 2$,range from 300 to 900 in the direction of Z. With the increasing value of k,it points to $\theta = 0$ gradually,and when k=o,it points to $\theta = 0$ intensively. The changes of auto-oscillation frequency and rotation frequency impacts on directivity mildly in the direction of Y,and there is more harmonic deviated from the fundamental frequency distributed near the plane of the observed angle $\theta = \pi / 2$, With the increasing value of k,it points to $\theta = 0$ gradually,and when k=o,it points to $\theta = 0$ intensively.

2.2 The Characteristics of Near-Field Acoustic Pressure:

For near-field $r = 0.4$, $r_0 = 0.3$,the other parameters are the same as far-field,and discusses its acoustic characteristics in accordance with the above points similarly.It can be seen from Fig1.a to Fig1.d that near-field affects the harmonic distribution acoustic pressure amplitude mildly in the case of small θ, but it impacts intensively in the case of θ close to $\pi / 2$ in the direction of Z. With the increasing value of θ,the acoustic pressure amplitude decreases gradually,but the scope of harmonic distribution expands. Reducing the rotation frequency affects the acoustic pressure amplitude and the scope of harmonic distribution mildly.Reduction of the auto-oscillation frequency descreases the acoustic pressure amplitude and the scope of harmonic distribution remarkable. It can be seen from Fig1e for near-field: ①When the rotation frequency is below 100Hz, the changes of it does not affect the distribution of harmonics, but there will be frequency shift when the value of θ is big . ②When the rotation frequency is above 1000Hz, the changes of it affects the distribution of harmonics intensively, and there will be Doppler frequency shift remarkable. ③There is an intensive directivity in the direction of $\theta = 0$ and harmonic distribution is abundant near the plane of $\theta = \pi / 2$.

It can be seen from Fig3.a to Fig3.d that near-field affects the harmonic distribution acoustic pressure amplitude mildly in the case of big θ, but it affects intensively in the case of θ close to $\pi / 2$ in the direction of Y. With the increasing value of θ,the acoustic pressure amplitude increases gradually,but it affects the scope of harmonic distribution mildly. Reducing the rotation frequency affects the acoustic pressure amplitude and the scope of harmonic distribution mildly. Reduction of the auto-oscillation frequency descreases the acoustic pressure amplitude and the scope of harmonic distribution remarkable. It can be seen from Fig1e for near-field : ①When the rotation frequency is below 100Hz, the changes of it does not affect the distribution of harmonics. ②When the rotation frequency is higher, the changes of it affects the distribution of harmonics intensively, and there will be Doppler frequency shift remarkable. ③ There is an directivity in the direction of $\theta = \pi / 2$ and harmonic distribution is abundant in the plane of $\theta = \pi / 2$ .when k=0,it points to $\theta = 0$.

3. Conclusion

From the rerults of the study we can get the key point of the ratoting source acoustic traits.

1) The spatial dipole acoustic field is of an intense space directivity, specally in the direction of

   $\theta = 0$ and $\theta = \pi / 2$.

2) The characteristics of acoustic field is closely depended on the traits of acoustic source.

3) The auto-oscillation frequency and rotation frequency of source impacts the directivity mildly in the direction of $\theta = 0$ and $\theta = \pi / 2$.

References

A. Zinoviev, D.A. Bies. (2004). On acoustic radiation by a rigid object in a fluid flow. *Journal of Sound and Vibration*. PP. 535–548.

C. Testa, S. Ianniello, G. Bernardini, M. Gennaretti. (2007). Sound scattered by a helicopter fuselage in descent flight

condition, AIAA Paper13th AIAA/CEAS Aeroacoustics Conference.

Ju Hongbin. (1995). The Analysis of the Near-Field Acoustic Characteristics about the rotating sound source. *Journal of Aerospace Power*. PP. 131-134.

M. Gennaretti, C. Testa. (2008). A boundary integral formulation for sound scattered by elastic moving bodies. *Journal of Sound and Vibration* 314. PP. 712–737.

WuJiuhui, Chen Hualing, HuangXieqlng. (2000). Acoustic Solution of RotatingPoint Source in Frequency Domain. *JOURNAL OF XI AN JIAO'TONG UNIVERSITY*.PP.71-75.

(a) $w_t = 6800rpm, w_0 = 560rpm$

(b) $w_t = 6800rpm, w_0 = 112rpm$

(c) $w_t = 2300rpm, w_0 = 560rpm$

(d) $w_t = 2300rpm, w_0 = 112rpm$

(e) $w_t = 2300rpm, Y = pi / 3$
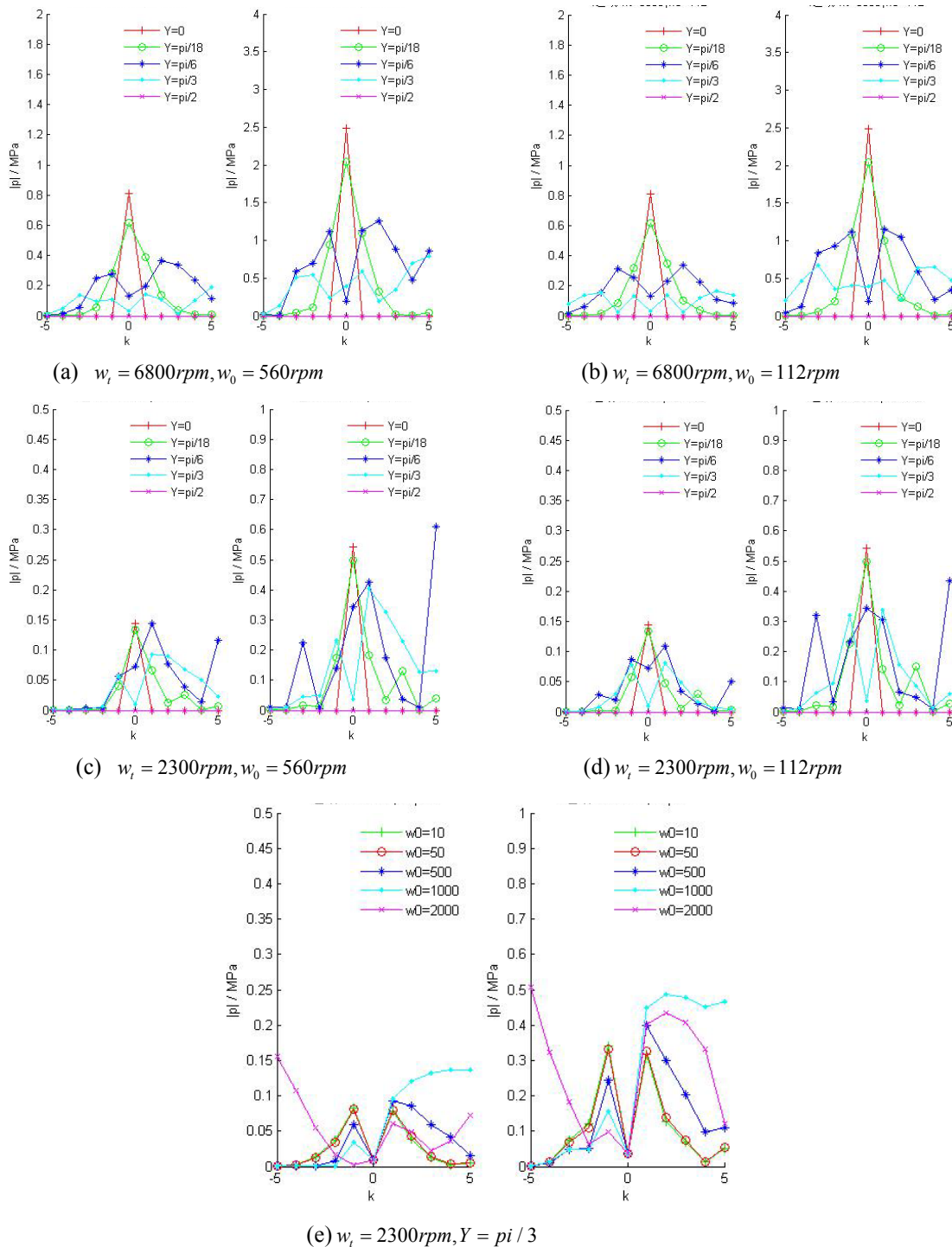
Figure 1. Acoustic pressure harmonic distribution of of the far-field
on the left and the near-field on the right in the direction of Z
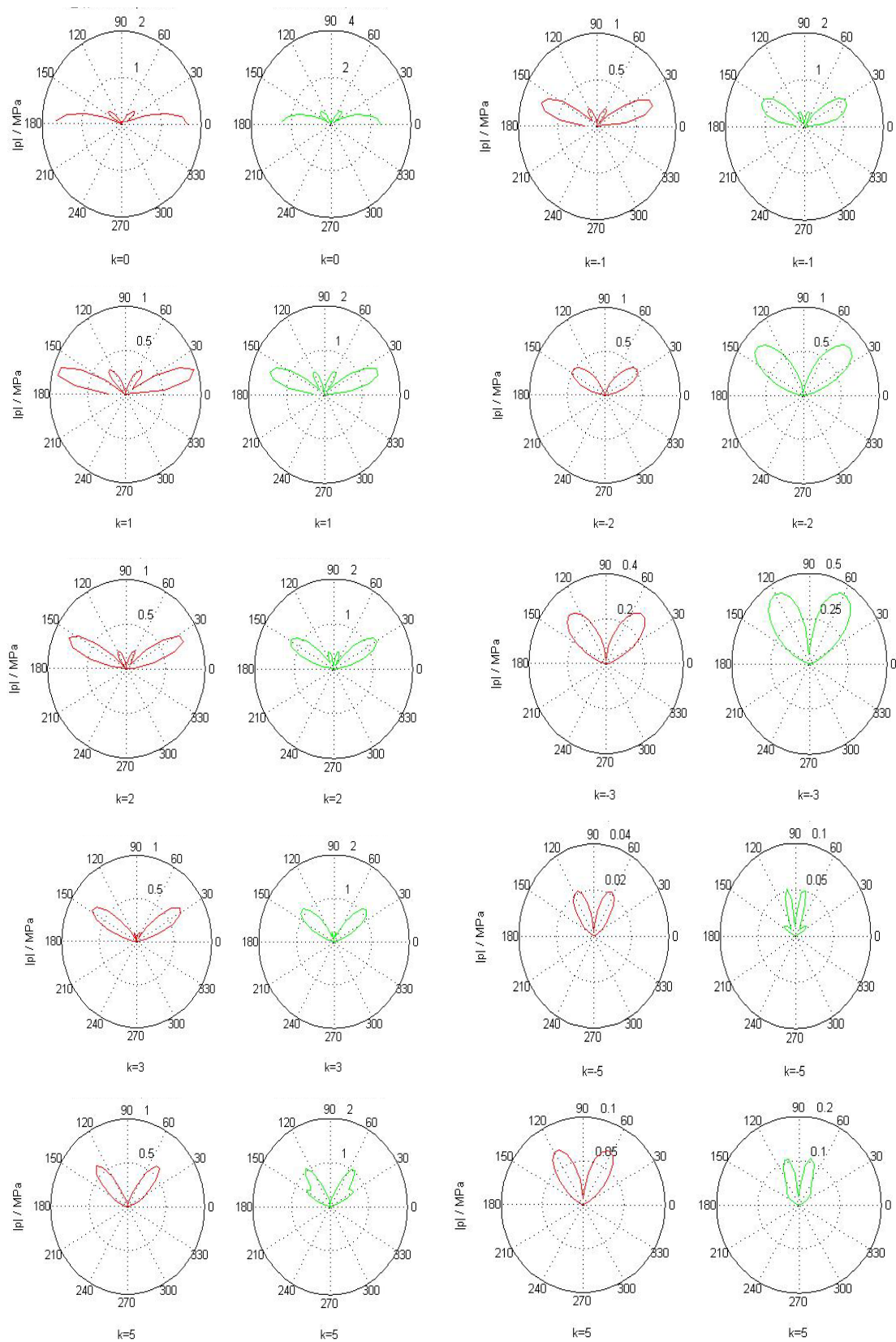
Figure 2. Acoustic pressure amplitude distribution along the observed angle of the far-field
on the left and the near-field on the right in the direction of Z at the rotate speed $w_t = 6800rpm, w_0 = 560rpm$

(a)　$w_t = 6800rpm, w_0 = 560rpm$

(b)　$w_t = 6800rpm, w_0 = 112rpm$

(c)　$w_t = 2300rpm, w_0 = 560rpm$

(d)　$w_t = 2300rpm, w_0 = 112rpm$

(e)　$w_t = 2300rpm, Y = pi/3$
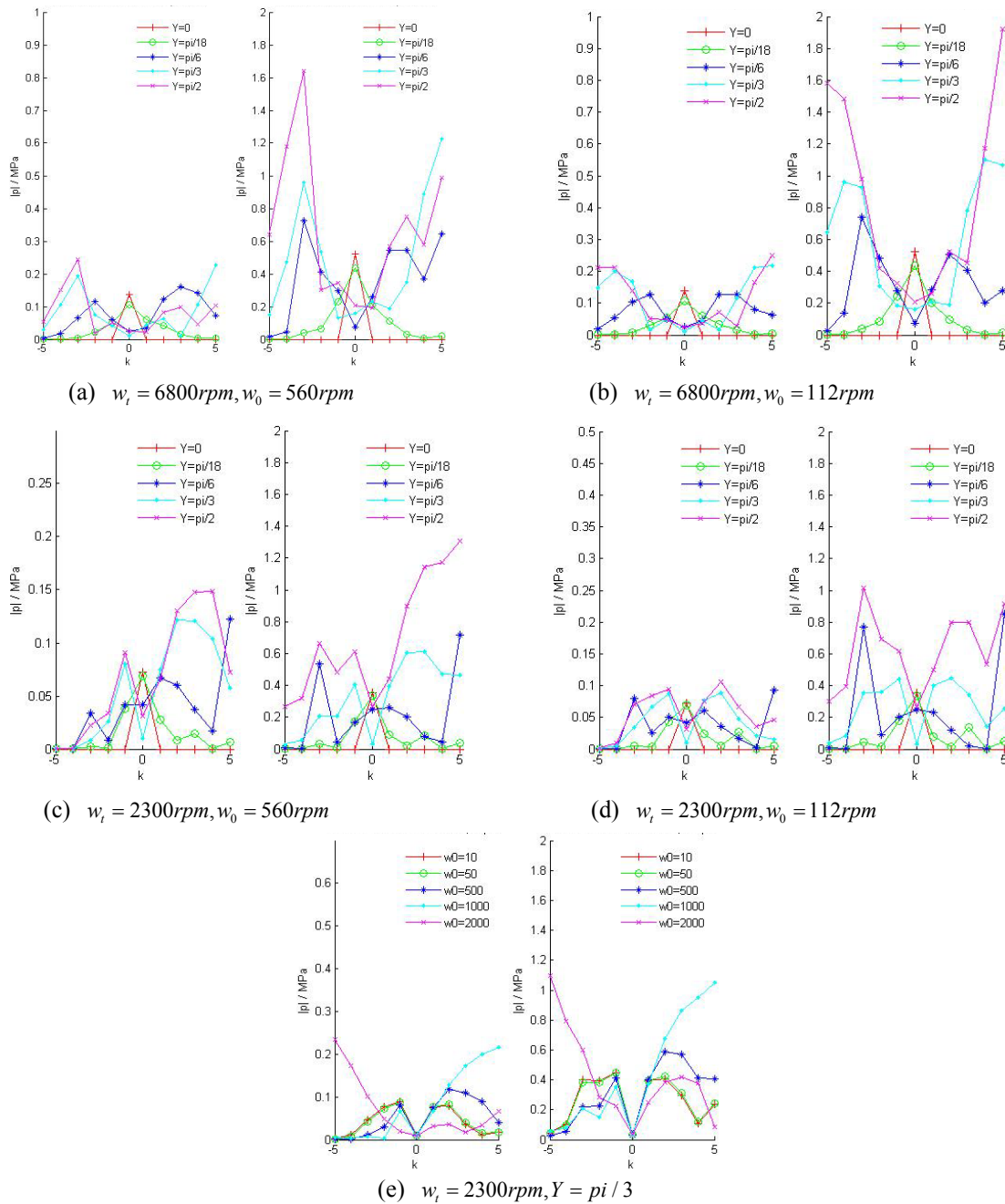
Figure 3. Acoustic pressure harmonic distribution of of the far-field
on the left and the near-field on the right in the direction of Y
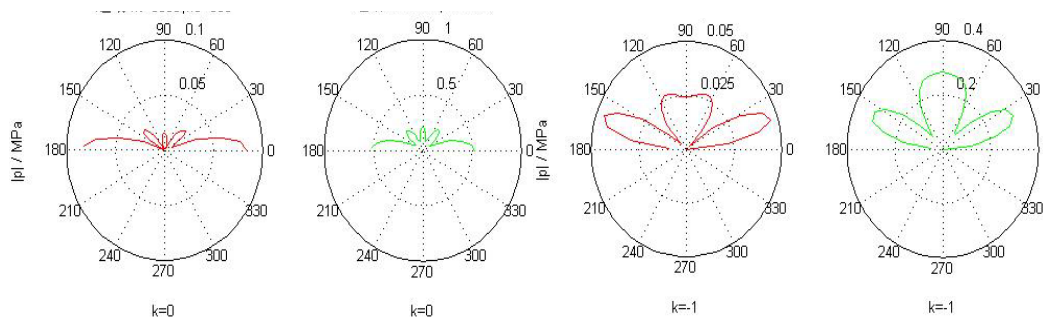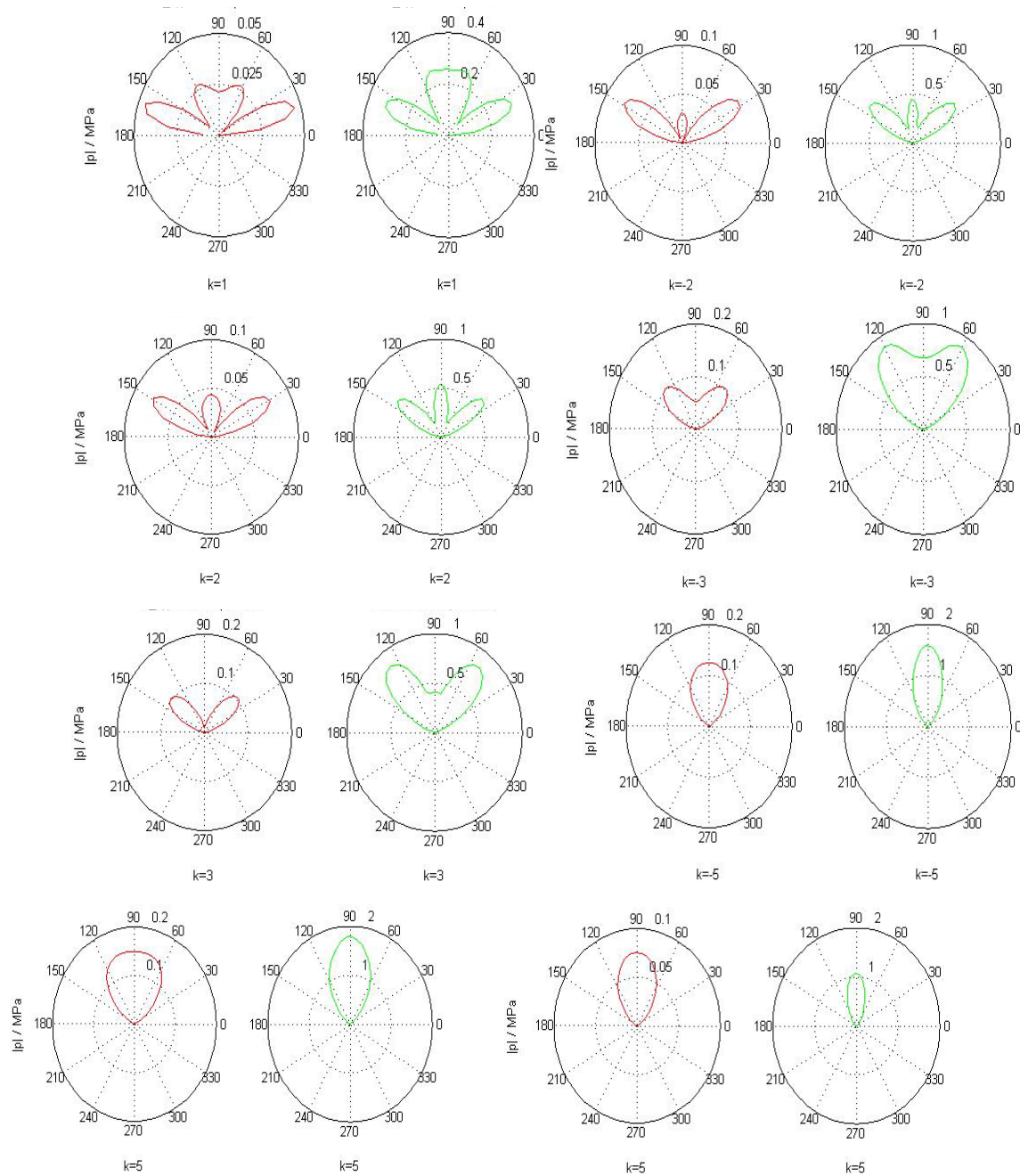
Figure 4. Acoustic pressure amplitude distribution along the observed angles of far-field
on the left and the near-field on the right in the direction of Y at the rotate speed $w_t = 6800rpm, w_0 = 560rpm$

One Type of Optimal Portfolio Selection in Birandom Environments

Limei Yan

Mathematics Department, Dezhou University

Shandong 253023, China

E-mail: yanlimei9898@163.com

Abstract

In order to solve the portfolio problem when security returns are birandom variables, firstly we propose a new definition of risk, then one type of portfolio selection based on expected value and risk is provided according to birandom theory. Furthermore, A hybrid intelligent algorithm by integrating birandom simulation and genetic algorithm is designed. Finally, one numerical experiment is provided to illustrate the effectiveness of the hybrid intelligent algorithm.

Keywords: Birandom variable, Portfolio selection, Expected value operator, Confidence curve, Hybrid intelligent algorithm

1. Introduction

The theory of portfolio selection was initially provided by Markowitz (1952, p.77) and has been greatly developed since then. It is concerned with selecting a combination of securities among portfolios containing large number of securities to reach the goal of obtaining satisfactory investment return. In his path-break work, Markowitz proposed a principle that when making investment decision, an investor should always strike a balance between maximizing the return and minimizing the risk, i.e., the investor maximize return for a given level of risk, or one should minimize risk for a predetermined return level. More importantly, Morkowitz initially quantified investment return as the expected value of returns of securities, and risk as variance from the expected value. After Maokowitz's work, scholars have been showing great enthusiasm in portfolio management, trying different mathematical approaches to develop the theory of portfolio selection. Traditionally, returns of individual securities were assumed to be stochastic variables, and many researchers were focused on extending Markowitz's mean-variance models and on developing new mathematical approaches to solve the problems of computation. Peng (2007,p.433) proposed concept of birandom variable and the framework of birandom programming. However, investors may come across birandom returns in portfolio selection situations. For example, security returns are usually regarded to be normally distributed random variables, but the expected value may be still random variable, thus investors have to face random returns with random parameters, to deal with this type of uncertainty, we propose the security returns could be regarded as birandom variables. As a general mathematical description for this kind of stochastic phenomenon with incomplete statistical information, birandom variable is defined as a mapping with some kind of measurability from a probability space to a collection of random variables.

In general, there are three types of risk definitions in portfolio selection problems. Variance is the earliest and most commonly accepted definition of risk for portfolio selection initially proposed by Markowitz (1952, p.77). A variety of extensions to Markowitz's mean-variance models has been proposed. Semivariance is the second type of risk definitions, and was also proposed by Markowitz (1959). Semivariance is an improvement of variance because semivariance only measures portfolio return below the expected value. Many models have been built to minimize semivariance in different cases. The third popular definition of risk is a probability of a bad outcome initially by Roy (1952, p.431). Much research has been undertaken to find ways of minimizing the probability of the bad outcome. Recently, Huang (2007, p.5404) proposed another new definition of risk for portfolio selection in fuzzy and random fuzzy environments. The detailed exposition on the definition of risk had been recorded in the literature, the interested readers may consult it. We can regard it as the fourth type of risk. Her work has enriched the risk theory for portfolio selection. We try to do something for portfolio selection in birandom environments, and give a new risk definition and a model for portfolio selection according to the proposed risk.

The rest of this paper is arranged as follows. After reviewing some necessary knowledge about birandom variable in section 2, in section 3, one type of risk for portfolio selection model under birandom environment is proposed. In section 4, we give a model for portfolio selection from the point of the new definition of risk. To provide a general method for solving the new models, in section 5, a hybrid intelligent algorithm integrating genetic algorithm and birandom simulation is designed. To better illustrate the modeling idea and demonstrate the effectiveness of the proposed algorithm, one numerical example is provided in section 6.

2. Preliminaries

Birandom variable theory was introduced by Peng (2007, p.433). To better understand the proposed model for portfolio selection, let us briefly review some necessary knowledge about birandom variable.

Definition 1 A birandom variable ξ is a mapping from a probability space (Ω, A, Pr) to a collection of random variables such that for any Borel subset B of the real line R, the induced function $\text{Pr}\{\xi(\omega) \in B\}$ is a measurable function with respect to ω.

Example 1 Let $\Omega = \{\omega_1, \omega_2\}$, and $\text{Pr}\{\omega_1\} = \text{Pr}\{\omega_2\} = 1/2$. Assume that ξ is a function on (Ω, A, Pr) as follows.

$$\xi(\omega) = \begin{cases} \xi_1, & \omega = \omega_1 \\ \xi_2, & \omega = \omega_2 \end{cases}$$

where ξ_1 is a uniformly distributed random variable on $[0,1]$ and ξ_2 is a normally distributed random variable with mean 0 and variance 1, i.e., $\xi_1 \sim U[0,1]$ and $\xi_2 \sim N(0,1)$. Then ξ is a birandom variable according to the definition.

The following are the definitions of the expected value operator and variance of birandom variance and the primitive chance of birandom event.

Definition 2 (Peng (2007, p.4330)). Let ξ be a birandom variable defined on the probability space (Ω, A, Pr). Then the expected value of birandom variable ξ is defined as

$$E[\xi] = \int_0^\infty \text{Pr}\{\omega \in \Omega \mid E[\xi(\omega)] \ge t\} \, dt - \int_{-\infty}^0 \text{Pr}\{\omega \in \Omega \mid E[\xi(\omega)] \le t\} \, dt$$

provided that at least one of the above two integrals is finite.

Definition 3 (Peng (2007, p.4330)). Let $\xi = (\xi_1, \xi_2, \cdots, \xi_n)$ be a birandom vector on (Ω, A, Pr), and $f: R^n \to R^m$ be a vector-valued Borel measurable function. Then the primitive chance of birandom event characterized by $f(\xi) \le 0$ is a function from $(0,1]$ to $[0,1]$, defined as

$$\text{Ch}\{f(\xi) \le 0\}(\alpha) = \sup\{\beta \mid \text{Pr}\{\omega \in \Omega \mid \text{Pr}\{f(\xi(\omega)) \le 0\} \ge \beta\} \ge \alpha\}.$$

Theorem 1 (Peng (2007, p.4330)). Let $\xi = (\xi_1, \xi_2, \cdots, \xi_n)$ be a birandom vector on (Ω, A, Pr), and $f: R^n \to R^m$ be a Boral measurable function. Then the chance

$$\text{Ch}\{f(\xi) \le 0\}(\alpha)$$

is a decreasing and left-continuous function of α.

Theorem 2 (Peng (2007, p.4330)). Let ξ be a birandom variable and α a given number in $(0,1]$, then the chance distribution

$\text{Ch}\{\xi \ge x\}(\alpha)$ is a decreasing and left-continuous function of x.

3. New definition of risk

In reality, some investors are only sensitive to one preset bad case. They regard as safe those securities whose chance of this bad case occurring is lower than the investors' tolerance level. Other investors consider all the possible unfavorable cases, and only those securities whose chance of every unfavorable case occurring is lower than the investors' tolerance level are regarded as safe. We will define the risk from this perspective.

Definition 4 Let ξ be a birandom variable on the probability space (Ω, A, Pr), and δ the preset confidence level and b the target return. Then the curve $f(\delta, r) = \text{Ch}\{b - \xi \ge r\}(\delta), \ \forall r \in R$ is called the risk curve of an

investment in the portfolio, and r the loss severity indicator.

The greater the indicator r, the more severe the loss $b - \xi$. The risk curve $f(\delta, r)$ gives the chance of the occurrence of all events when the birandom return ξ is r less than the target return b.

From theorem 1 and theorem 2 we can derive that the risk curve $f(\delta, r)$ is a decreasing function with respect to δ and r, that is, the greater the δ, the smaller the $f(\delta, r)$ value, the greater the r, the smaller the $f(\delta, r)$.

To determine whether a portfolio selection is risky, an investor must first decide what is his or her maximum tolerance level of each bad event occurring. Usually, the worse the event, the lower the tolerance level. Then for every loss severity indicator $r_0 \in R$, the investor always can give a confidence level corresponding $\alpha(r_0)$, thus the confidence level $\alpha(r)$ is a function of the loss severity indicator r, the function $\alpha(r)$ is called the confidence curve.

Let ξ be a birandom return of a portfolio A, and $\alpha(r)$ the confidence curve. We can say that A is safe if $f(\delta, r) = \mathrm{Ch}\{b - \xi \geq r\}(\delta) \leq \alpha(r)$ for every $r \in R$, where b is the target return and δ the preset credibility level. The number r denotes all possible loss severity indicator. If the investor is only concern with one special loss severity indicator r_0, then the risk becomes the chance $\mathrm{Ch}\{b - \xi \geq r_0\}(\delta)$, Which is exactly the ordinary chance measure of birandom variable.

4. Birandom portfolio selection

Let us select a portfolio according to the definition of risk in the preceding content. Let x_i denotes the investment proportions in security i, ξ_i the birandom return for the ith security, $i = 1, 2, \cdots, n$, respectively. Let r denote the loss severity indicator, and $\alpha(r)$ the confidence curve preset by the investor. To obtain the maximum investment return and avoid risk, the investor should select an optimal combination of securities from the portfolio safe point. We use the expected value of the securities to express the investment return. Thus we should set a goal of maximizing the expected return of a portfolio, and require that the risk curve $f(\delta, r)$ is not larger than the confidence curve $\alpha(r)$. Let b be the target return and δ the preset credibility level. Then the model is formulated as follows:

$$\max_x E\left[\sum_{i=1}^n x_i \xi_i\right]$$
$$\text{subject to}$$
$$\mathrm{Ch}\left\{b - \sum_{i=1}^n x_i \xi_i \geq r\right\}(\delta) \leq \alpha(r), \ \forall r \geq 0 \tag{1}$$
$$\sum_{i=1}^n x_i = 1$$
$$x_i \geq 0, \ i = 1, 2, \cdots, n$$

When the birandom returns degenerate to random, the chance constraint becomes

$$\Pr\left\{b - \sum_{i=1}^n \xi_i x_i \geq r\right\} \leq \alpha(r), \ \forall r \geq 0,$$

thus the model is the following

$$\max_x E\left[\sum_{i=1}^n x_i \xi_i\right]$$
$$\text{subject to}$$
$$\Pr\left\{b - \sum_{i=1}^n x_i \xi_i \geq r\right\} \leq \alpha(r), \ \forall r \geq 0 \tag{2}$$
$$\sum_{i=1}^n x_i = 1$$
$$x_i \geq 0, \ i = 1, 2, \cdots, n$$

Furthermore, if the investor only concerns one preset loss severity level r_0, then the model (2) can be converted into the formulation:

$$\max_{x} E[\sum_{i=1}^{n} x_i \xi_i]$$

subject to

$$\Pr\{b - \sum_{i=1}^{n} x_i \xi_i \geq r_0\} \leq \alpha(r_0) \qquad (3)$$

$$\sum_{i=1}^{n} x_i = 1$$

$$x_i \geq 0, \quad i = 1,2,\cdots,n$$

5. Hybrid intelligent algorithm

Since the two-fold uncertainty of birandom variable, it is difficult to analytically solve the models (1), (2) and (3). To provide a general solution to the models, we design a hybrid intelligent algorithm integrating genetic algorithm (GA) and birandom simulation. Roughly speaking, in the proposed hybrid intelligent algorithm, the technique of birandom simulation is applied to compute the expected value and the chance measure, then birandom simulation and GA are integrated for solving the birandom models.

5.1 Birandom simulation

In this section, we first discuss the calculation of the expected value and the chance measure of birandom variables. Let ξ_i be birandom variables and x_i decision variables, $i = 1,2,\cdots,n$, respectively. Write $f(x,\xi) = \sum_{i=1}^{n} x_i \xi_i$, where $x = (x_1, x_2, \cdots, x_n), \xi = (\xi_1, \xi_2, \cdots, \xi_n)$. Let b be the target return and δ the preset credibility level. The number r denotes all possible loss severity indicator. In order to solve the proposed models, we must handle the following two types of uncertain function.

$$U_1 : x \rightarrow E\{f(x,\xi)\}$$
$$U_2 : x \rightarrow Ch\{b - f(x,\xi) \geq r\}(\delta) \geq \alpha(r), \forall r \geq 0.$$

$U_1(x)$ may be estimated by the following procedure.

Algorithm 1 (birandom simulation for $U_1(x)$)

Step 1. Set $E[f(x,\xi)] = 0$.

Step 2. Generate ω from Ω according to the probability measure Pr.

Step 3. $E[f(x,\xi)] \leftarrow E[f(x,\xi)] + E[f(x,\xi(\omega))]$ may be calculated by stochastic simulation.

Step 4. Repeat the second to the third steps N times.

Step 5. $E[f(x,\xi)] \leftarrow E[f(x,\xi)]/N$.

Algorithm 2 (birandom simulation for $U_2(x)$)

Step 1. Set $l = 1$.

Step 2. randomly generate a real number r according to the confidence curve given by the investor.

Step3. Generate $\omega_1, \omega_2, \cdots, \omega_N$ from Ω according to the probability measure Pr.

Step 4. Compute the probability $\beta_n = \Pr\{b - f(x,\xi(\omega_n)) \geq r\}$ for $n = 1,2,\cdots,N$, respectively, by stochastic simulation.

Step 5. Set N' as the integer part of δN.

Step 6. Return the N'th largest element $\overline{\beta}$ in $\{\beta_1, \beta_2, \cdots, \beta_N\}$.

Step 7. If $\overline{\beta}$ is no larger than $\alpha(r)$, then $l = l*1$, else $l = l*0$.

Step 8. repeat the second to the fifth steps for a given number times.

Step 9. If $l = 1$, then return **YES**, else return **NO**.

Remark: here YES means that the investment proportion x is feasible; NO means that x is infeasible.

5.2 Genetic algorithm

Representation structure: A solution $x = (x_1, x_2, \cdots, x_n)$ is represented by the chromosome $V = (v_1, v_2, \cdots, v_n)$, where the genes $v_1, v_2, \cdots, v_n$ are randomly generated in the interval $[0,1]$, and the relation between x and V are

formulated as follows:

$$x_i = v_i /(v_1 + v_2 + \cdots + v_n), i = 1,2,\cdots, n,$$

which ensures that

$x_1 + x_2 + \cdots + x_n = 1, \ x_i \geq 0, \ i = 1,2,\cdots, n$ always holds.

Initialization process: pop_size number of chromosomes are initialized randomly by generating points $(v_1, v_2, \cdots, v_n)$ from the hypercube $[0,1]^n$ pop-size times. Since the constraint required that $x = (x_1, x_2, \cdots, x_n)$ satisfy $x_1 + x_2 + \cdots + x_n = 1$, based on the relation between x and V, the feasibility of the randomly generated chromosomes is obvious.

Evaluation function: Evaluation function, denoted by $Eva(V)$, is to assign a probability of reproduction to each chromosome V so that its likelihood of being selected is proportional to its fitness relative to the other chromosomes in the population. That is, the chromosomes with higher fitness will have more chance to produce offspring by using roulette wheel selection. One well-known evaluation function is based on allocation of reproductive trial according to rank rather than actual objective values. We can rearrange the pop-size chromosomes according to their objective values to make better chromosome take smaller ordinal number. That is, after rearrange, among pop-size chromosomes $V_1, V_2, \cdots, V_{pop\_size}$, V_1 is the best chromosome, and V_{pop_size} the worst one, then a parameter $a \in (0,1)$ in the genetic system is given. We can define the rank-based evaluation function as follows:

$Eva(V_i) = a(1-a)^i, \ i = 1,2,\cdots, pop\_size$.

Note that $i = 1$ means the best individual, $i = pop\_size$ the worst one.

Selection process: Firstly, calculate the cumulative probability q_i for each chromosome V_i,

$$q_0 = 0, \ q_i = \sum_{j=i}^{i} Eva(V_j), i = 1,2,\cdots, pop\_size$$

Secondly, generate a random number r in $(0, q_{pop\_size}]$, and select the chromosome V_i if r satisfies $q_{i-1} < r \leq q_i$.

Repeat the second and third steps pop_size times and obtain pop_size copies of chromosome.

Crossover operation: A parameter p_c of a genetic system as the probability of crossover is defined first. The parents for crossover operation are selected by doing the following process repeatedly from $i = 1$ to pop_size: Generating a random number r from the interval $[0,1]$, the chromosome V_i is selected as a parent if $r < p_c$, the selected parents are denoted by $V_1', V_2', V_3', \cdots$ and divided into the pairs: $(V_1', V_2'), (V_3', V_4'), (V_5', V_6'), \cdots$. The crossover operation on each pair is illustrated by (V_1', V_2'). At first, we generate a random number c from the open interval $(0,1)$, then the operator on V_1' and V_2' will product two children X and Y as follows:

$X = cV_1' + (1-c)V_2', \quad Y = (1-c)V_1' + cV_2'$.

If both children are feasible, then we replace the parents with them. If not, we keep the feasible one if it exists, and then redo the crossover operator by regenerating a random number c until two feasible children are obtained or a given number of cycles is finished. In this case, we only replace the parents with the feasible children .

Mutation operation: A parameter p_m of a genetic system as the probability of mutation is defined first. This probability gives us the expected number of $p_m \cdot pop\_size$ of chromosomes undergoing the mutation operations. We repeat the following steps from $i = 1$ to pop_size: Generating a random number r from the interval $[0,1]$, the chromosome V_i is selected as a parent if $r < p_m$. For each selected parents V_i, we mutate it in the following way.

Let M be an appropriate large positive number. We choose a mutation direction d in R^n randomly. If $V + M \cdot d$ is not feasible, then we set M as a random number between 0 and M until it is feasible. If the above process cannot find a feasible solution in a predetermined number of iterations, then we set $M = 0$. Anyway, we replace the parent V_i with its feasible child $V + M \cdot d$.

The following is the hybrid intelligent algorithm integrating birandom simulation and genetic algorithm.

Algorithm 3 (hybrid intelligent algorithm)

Step 1 Initialize pop_size chromosomes.

Step 2 Calculate the objective values for all chromosomes by birandom simulation.

Step 3 Given the rank order of the chromosomes according to the objective values, and the values of the rank-based evaluation function of the chromosomes.

Step 4 Compute the fitness of each chromosome according to the rank-based evaluation function.

Step 5 Select the chromosomes by spinning the roulette wheel.

Step 6 Update the chromosomes by crossover and mutation operations.

Step 7 Repeat the second step to the sixth step for a given number of cycles.

Step 8 Take the best chromosome as the solution of portfolio selection.

6. Numerical example

To illustrate the modeling idea and to test the effectiveness of the designed hybrid intelligent algorithm, let us consider one numerical example. The example is performed on a personal computer by using C++ programming language. The parameters in the HIA are set as follows: the probability of crossover $p_c = 0.3$, the probability of mutation $p_m = 0.2$, the parameter $\alpha = 0.05$ in the rank-based evaluation function.

Example 2 Assume that there are 5 securities, the returns of securities are all birandom variables.

$$\max_{x} E[\sum_{i=1}^{5} x_i \xi_i]$$

subject to

$$\mathrm{Ch}\{b - \sum_{i=1}^{5} x_i \xi_i \geq r\}(\delta) \leq \alpha(r), \ r \geq 0$$

$$\sum_{i=1}^{5} x_i = 1$$

$$x_i \geq 0, \ i = 1, 2, \cdots, 5$$

Where

$\xi_1 \sim N(\mu_1, 1)$ with $\mu_1 \sim U(0, 1)$,

$\xi_2 \sim N(\mu_2, 1)$ with $\mu_2 \sim U(1, 2)$,

$\xi_3 \sim N(\mu_3, 1)$ with $\mu_3 \sim U(2, 3)$,

$\xi_4 \sim N(\mu_4, 2)$ with $\mu_4 \sim U(3, 4)$,

$\xi_5 \sim N(\mu_5, 1)$ with $\mu_5 \sim U(4, 5)$.

Suppose that the investor has given the confidence curve and other parameters :

$$\alpha(r) = \frac{1}{(r+1.1)^4}, \ r \geq 0 . b = 0.9, \delta = 0.9 .$$

Here, $N(\mu, \sigma^2)$ represents the normally distributed random variable with mean μ and standard variance σ and $U(a, b)$ denotes the uniform distribution on the interval (a, b). A run of the hybrid intelligent algorithm with 3000 generations shows that among 5 securities, in order to gain maximum expected value of the total securities return the investor should assign his money according to the optimal solution:

$$x_1^* = 0, \ x_2^* = 0.1325, \ x_3^* = 0.2236, \ x_4^* = 0.2782, \ x_5^* = 0.3657 .$$

References

A. Charnes & W. W. Cooper. (1965). Chance-constrained programming. *Management Science*, 6, 73-79.

A. D. Roy. (1952). Safety first and the holding of assets. *Econometrics*, 20 ,431-449.

B. Liu. Uncertainty theory, 3rd edition. http://orsc.edu.cn/lliu/ut.pdf.

H.Markowit z. (1952). Portfolio selection. *Journal of Finance* , 7, 77-91.

H.Markowitz. (1959). Portfolio selection: Efficient diversification of investment, Wiley, New York.

Jin peng. (2007). Birandom variables and birandom programming. *Computer & Industrial Engineering*, 53, 433-453.

Xiaoxia Huang. (2006). Fuzzy chance-constrained portfolio selection. *Applied mathematics and computation*, 177, 500-507.

Xiaoxia Huang. (2007). A new perspective for optimal portfolio selection with random fuzzy returns. *Information science* ,177, 5404-5414.

A Small Power SMP Based TOPSwitch

Tingjian Zhong, Hongxing Luo & Wenjin Dai

Jiang Xi Vocational & Technical College of Electricity, Nanchang 330032, China

School of information Engineering, Nanchang University, Nanchang 330029, China

E-mail: jxdlztj@163.com

Abstract

In designing small power switching mode power supply (SMPS),its functions, tech-parameter and cost should be considered at the same time. TOPSwitch has stronger functions than the discrete components. It is easy and flexible to design SMPS based TOPSwitch and the products always get less cost. SMPS based on UC3842 or UC3843 is compared to the one based TOPSwitch in the paper. Then an actual project used flyback convertor is put forward.

Keywords: TOPSwitch, Switching mode power supply, Flyback Digests

1. Forewords

Today, TOPSwitch has been usually applied on SMP. But for some matter, people are inclined to use UC3842 or UC3843 as controlling IC when making mention of SMP. In fact, in a small power SMP, especially the SMP as an auxiliary power of system, TOPSwitch should be the best choice and the SMPs based TopSwicth have more vantages compared to the else of based UC3842 or UC3843.

A low power SMP based TOPSwitch which power is less than 200W would be used less parts and make circuit simple, volume and weight minishing, cost low.

2. System designing

2.1 Introduction of component

First, we introduce the three-terminal off-line PWM Switch-TOPSwitch. It is a combination element that integrates a MOSFET power switch with PWM controller. It makes efficiency and stability of SMP higher and at the same time makes the system cost, volume and weight lower. TOPSwitch incorporates all functions necessary for a switched mode control system into a three terminal monolithic IC: power MOSFET, PWM controller, high voltage start up circuit, loop compensation and fault protection circuitry. Power Integrations, Inc. provides several packages for TOPSwitchⅡ.

The SMPs based TOPSwith compared to the else adopted discrete parts have some good points:

(1)Low cost With 15 fewer components, it cuts cost, increases reliability and allows for a smaller and lighter

solution. Source connected tab for low EMI and the gate driver is designed to turn the output MOSFET on at a controlled rate to minimize common-mode EMI. As result, the cost for EMI could be greatly reduced.

(2) High efficiency Compared to discrete MOSFET and controller, TOPSwitch is built-in start-up and its current limit reduce DC losses, cuts switching losses and adopts CMOS controller/gate driver to power consume lower.

(3) Simplifies Design TOPSwitch Integrates PWM Controller with high power MOSFET. It is not demanded R for start-up. Only one external capacitor is needed for compensation, bypass and start-up/auto-restart functions.

(4) Perfect fault-protection function TOPSwitch has auto-restart and cycle by cycle current limiting functions, which can handle both primary and secondary faults. It has on-chip latching thermal shutdown,which can protects the entire system against overload at the same time.

(5) Highly Versatile TOPSwitch can be implemented buck, boost and flyback or forward topology.And it interfaces easily with both opto and primary feedback.

2.2 Comparison of Project

Some people always choose forward project, because flyback topology is difficult to design, especially in the case that the transformer has both store energy function and isolated and voltage conversion functions. However we think the flyback topology is better choice when designing off-line term SMP.

The causes are as follows:

(1) The flyback converter is more flexible to afford multiple voltage outputs, because we can get any expectant voltages by regulating duty ratio(D).Flyback converter outputs voltages can not be restricted by input voltage. There are the proofs as follows:

As shown in Fig.1, when Q is conducted, the current flows throw primary coils and store energy. The rectifier diode suffers negative voltage and the energy is not be transmitted to load R. We can get:

$I_p = V_s t / L_p$

where, i_p is primary current, V_s is primary voltage , L_p is the primary inductance.

When Q is shut off, the magnetic field sharply reduces, the secondary voltage reverses and the diode conducts to charge capacitor C and transfers current to load, at the same time we can get:

$$I_s = I_{sm} - V_o t / L_s ,$$

Where, I_s is the secondary current, I_{sm} is the secondary current maximum, V_o is the output voltage, L_s is the secondary inductance.

According to energy conversation law:

$$\int_0^{Ton} V_s^2 \, t/L_p \, dt = \int_{Ton}^{Ton+Toff} V_o (I_{sm} - V_o t/L_s \, dt)$$

it is easy to get:

$$\int_0^{Ton} V_s^2 \, t/L_p \, dt = \int_0^{Toff} V_o^2 \, t/L_s \, dt$$

Where, T_{on} is conduction time, T_{off} is shut-off time.

So:$V_o = \dfrac{N_s}{N_p} V_s D/(1-D)$ \hfill (1)

where $D = T_{on}/(T_{on} + T_{off})$

(2) The flyback transformer in the flyback converter also can be called induct store energy transformer. It has the functions of voltage isolation, storing energy and voltage transform in simultaneity. Energy is transferred by magnetism and disturbance of line can not come into load directly. So the system has better anti-jamming faculty. The rectifier inductors are not necessary, because the transformer is inductor itself. So compared to the othe isolated power convection circuit, the parts of the flyback circuit, especially magnetism parts, can be reduced and the cost is saved too.

2.3 Design technique

2.3.1 Design of high-frequency transformer

High frequency transformer is important part in energy storing and transferring. Its performances are always the key of a SMP's quality. It affects not only the power supply's efficiency but also EMC of power supply. We must design it elaborately. There are several methods being used as follows

(1) Depressing leakage inductance

(2) Choosing soft ferrite that is sufficed to 100KHz switch frequency,which has higher resistivity, lower eddy current loss and lower price.

(3) Choosing sharp of EI or EE, whose air gas should be on the mid columniation,which makes convenient to reel coils and flux minimal.

(4) Reeling all kinds of windings one by one, in which primary winding is inner, feedback winding second and secondary winding at last.

(5) Confirming appropriate primary inductance Flyback transformer's primary inductance is essential for its inductor energy transfer-method. It must be proper neither too big nor too small.

Here, a simply method is present to calculate the primary inductance

from $\qquad\qquad V_s = L_p I_{pm}/T_{on}$

and $\qquad\qquad 0.5 \; \eta \, I_{pm} D T U_s = P_o$

So the primary inductance : $L_p = \dfrac{U_s^2 D^2 T \eta}{2 P_o}$ \hfill (2)

Where, D is duty ratio, T is switch period, P_o is output power and then η is efficiency.

In calculation, I_{pm} should be magnified 20%.

For switch supply power of this paper, its lowest input voltage is 88Vdc, so order:

V_s =88V, D = 0.66, T = 10us, η =0.7, P_o =11.3W, and I'_{pm} =1.2 I_{pm}, then L_p=870uH is easy to be gotten.

Design transformer is a course of repeating calculation. The primary inductance needs calculate time and again. For cutting down the works of design, Power Integrations, Inc. offers a set of Excel table to design the transformer.

2.3.2 Design feedback circuit

TOPSwitch is a self biased and protected linear control current-to- duty cycle converter with an open drain output. The internal output MOSFET duty cycle linearly decreases with increasing CONTROL pin current as shown in Figure 2. As to control mode, we adopt opto+TL431. TL431 serves as exterior amplifier. The sampling voltage is gotten from R103 and R104 partitioning the output voltage 5V. The sampling voltage compares with the fiducial voltage. when the output voltage exceeds to 5V, I_c will increases by optocoupler. Then D decreases and the output(5V) voltage reduces. So the output voltage is steady.

The optocoupler has insulation functions when it works in linear mode. From Fig.2, it is easy to find that Ic must work in 2-6mA. Therefore the optocoupler CTR should be proper too. If CTR is too little, D doesn't increase with the feedback current reducing. If CTR is too big, it is easy to work in nonlinear scope, Consequently, TOPSwitch works abnormally. Commonly, 100%-300% is recommended.

In addition, the apex voltage from leakage inductance could destroy TOP223P.TVS D104 and SRD D103 are used to clamping voltage for protection. Of course,DRC could be adopt too, but at the cost of more power loss.

3. System assembly & test result

The system assembly is shown in Fig.3. We design a sample and make some correlative tests. The test outcomes show the SMP can work steadily in 110V or 220V(dc & ac).Under the rated input voltage- 220VAC, the system efficiency is 70%.Underthe rated load, when input voltage is 85V AC~265V AC, the output voltage regulation

ratio is Sv=ΔV/Vo=0.5%.Under the rated input voltage, when load is 10%~100% rated load, the load regulation ratio is Si=ΔV/Vo=1%(ΔV is the variation of output voltage). It is easy to see that the system has very good work characteristics.

References

Chuanwen, Ji, and Keyue. M. Smedley. Cross Regulation in Flyback Converters: ANALYTIC MODEL. PESC99.

Gao, Yan, Zhu, Zhongni,Pan, Yulong. (2004). the Analysis and Design of Forward Mode Power Supply Adopted TOPSwitch [J].*Power supply technique application*, 2004, 4.

Power Integrations, Inc.. TOPSwitch Flyback Transformer Construction Guide[Z]. AN-18. (1996).

Power Integrations, Inc..TOP221-227 TOPSwitch-II Family Three-terminal Off-line PWM Switch[Z].(2001).

Zhang, Zhansong. (1992). *High frenqucy switch steady-vlotage supply power[M]*.Guo Dong science&technology publishing company.1992, 4.
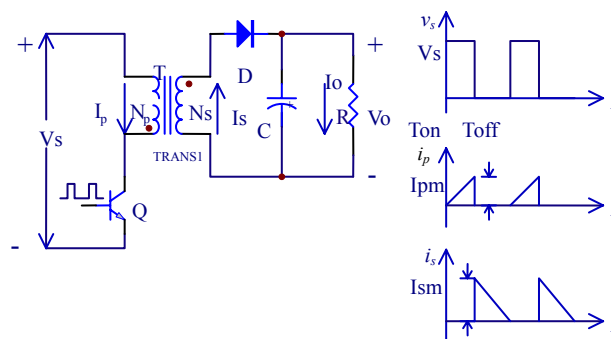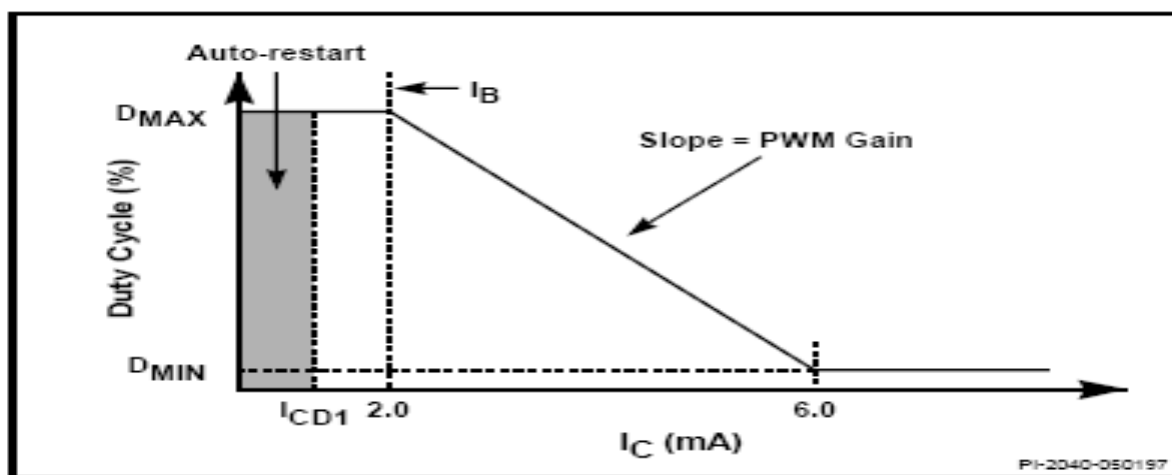
Figure 1. flyback converting-circuit

E

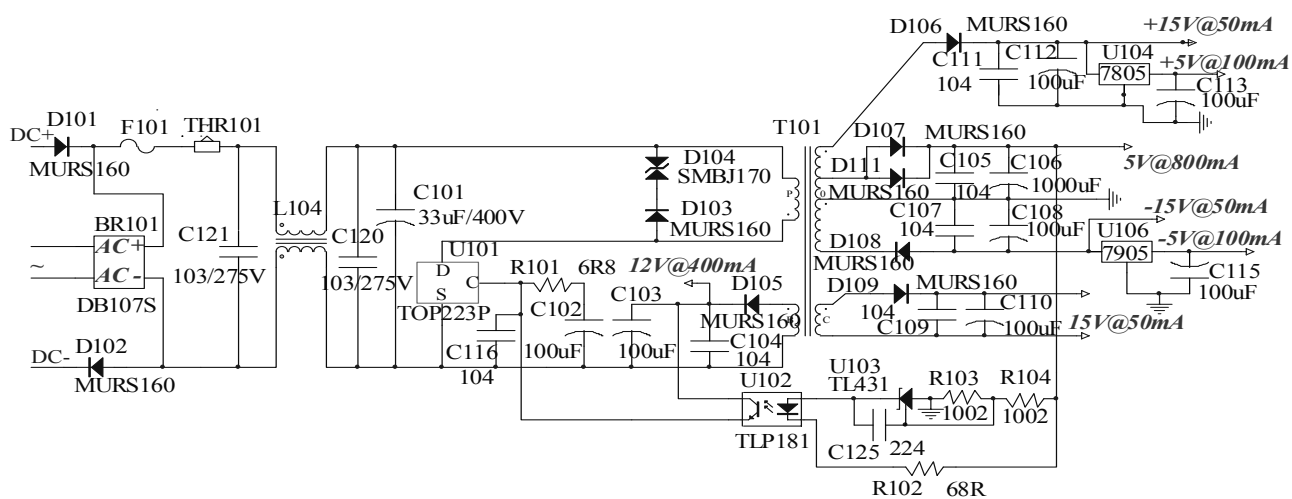Figure 2. Relationship of Duty Cycle to CONTROL Pin Current

Figure 3. Circuit digram of system

Influence on Lubricant Properties of Anti-wear

Agent Containing Nitrogen, Boron and Molybdenum

Xuguo Huai & Shihai Zhao

School of Mechanical and Electronic Engineering, Tianjin Polytechnic University

Tianjin 300160, China

E-mail: xuguo.huai@163.com

Abstract

The lubricant property of composite lubrication oils was studied through the friction and wear experiment of the A3 steel-GCr15 steel pairs on the ring-block wear testing machine. The composite lubrication oils were prepared from base oil added various content (0, 2%, 3%, and 4%) of organic anti-wear agent, which contains Nitrogen, Boron and Molybdenum. In order to research the influence of the base oil, the non-brand base oil was selected to compare with the brand one. The results show that adding the anti-wear agent can enhance lubricant property and improve the frictional and wear resistance of materials. When the anti-wear agent content reached 3% in the composite lubrication, the A3 steel-GCr15 steel pairs possess the lowest friction coefficient and wear rate. The lubricant property of the non-brand base oil can be enhanced by adding anti-wear agent, even better than that of the brand with the same concentration (3%).

Keywords: Anti-wear agent, Lubricant property, Friction and wear

1. Introduction

Friction-wear failure of mechanical components is among the most common problems that limit productivity. Frequently repairing or replacing worn parts costs businesses both time and money. Therefore, the reduction of surface wear is a common goal in many industries. Generally there are two ways to solve this problem. The first is surface improvement of material. So, protective coatings have been used against friction and wear, such as plasma nitriding (Xia Yanqiu, 2006, pp.145), Al2O3-TiO2 coating (Narulkar VV, 2008, pp.582) and Al/Al2O3 Composite Coatings (Yin ZJ, 2007, pp.1430-1437). Adding anti-wear agent has become the other popular way and the most successful techniques for reducing the wear of materials and equipments. There are two kinds of anti-wear agents, that is, organic anti-wear agent and inorganic anti-wear agent. The organic anti-wear agents contain metal 8-hydroxyquinolinates (M.W Sulek, 2003, pp.301-307) and Nitrogen-containing compound (Qiao Yulin, 1998, pp.165-169). And the inorganic anti-wear agents contain nanocopper (Yu Helong, 2006, pp.433-438), nanometer Titanium (Hu Zeshan, 2000, pp.292-295), and so on. In this experiment, the new organic anti-wear agent contains Nitrogen, Boron and Molybdenum, simultaneously.

In the present work, the composite lubrications were prepared from vary base oil with various concentrations (0~4%) of the anti-wear agent, which contains Nitrogen, Boron and Molybdenum. And the friction and wear properties of the A3 steel- GCr15 steel pairs were studied under oil lubrication on M-2000 wear testing machine. The friction coefficient and wear rate were researched to demonstrate the influence of the anti-wear agent and the base oil.

2. Experimental

2.1 Preparation

The specimen preparation of A3 steel process is as follows: Firstly, the samples of A3 steel were prepared though polishing to bright specular surface with emery paper and fabric. Then, those samples were ultrasonic cleaning with anhydrous alcohol for 0.5h. Lastly, the specimens were dried at 85℃ for an hour.

2.2 Experimental measurement and characterization

The friction and wear properties were studied on M-2000 ring-block wear testing machine under oil lubrication. The A3 steel is bonding on the metal fixture as the upper sample and the counterpart ring is GCr15 steel, which inner bore is 16mm and external diameter 40mm. The counterpart is sliding friction at a load of 200N and 0.42 m/s for 40 minutes.

The lubrications were prepared from brand base oil (named B lubrication) added the anti-wear agent of 0%, 2%, 3%, 4%, respectively, which were signed by the symbol 0-B, 2-B, 3-B and 4-B. In order to demonstrate the influence of the base oil, the non-brand base oil with the anti-wear agent (named N lubrication) was selected to compare with the brand oil.

The friction coefficient was calculated by the formula (1):

$$\mu = \frac{T}{RP} \times \frac{\alpha + Sin\alpha Cos\alpha}{2Sin\alpha} \tag{1}$$

Where T is the friction torque (N/m), which was recorded every five minutes, P is the load of pressing the surfaces (N), R is radius of lower sample (m), 2α is the contact angle of the upper sample with the counterpart and μ is the friction coefficient of A3 steel/ GCr15 pairs as a function.

The wear rate of A3 steel sample, which is the rate of weight loss, was calculated by comparing its mass with an electronic balance (sensitivity 0.1mg) before and after friction. Prior to weighing, the samples were ultrasonic cleaned with anhydrous alcohol and dried half an hour, respectively. Thus the wear rate can be calculated.

The worn surface morphology was observed by OLYMPUS BX51 System Microscope.

3. Results and discussion

3.1 The influence of the content of the anti-wear agent

The friction coefficient curves of A3 steel/ GCr15 pairs, as a function of sliding time, are shown in Fig.1. It can be seen that the friction coefficient decreases more rapidly early and is relatively steady after about 30min of sliding time. Under the lubrication of 3-B, the friction coefficient A3 steel/ GCr15 steel pairs was the lowest.

Fig.2 shows the wear rate of A3 steel samples under the lubrication of 0-B, 2-B, 3-B and 4-B, respectively. It clearly indicates that the wear rate of sample under 0-B was the highest, and the wear rates of A3 steel under B lubrication with anti-wear agent were lower than that under B lubrication, so the anti-wear agent can enhance the lubrication performance of the base oil. When the anti-wear agent content is 3% in the composite lubrication, the A3 steel-GCr15 steel pairs possess the lowest friction coefficient and the least wear rate.

Corresponding worn surfaces of A3 steel are shown in Fig.3, which the magnification used for indentation measurement is 1500. For under base oil (as shown in Fig.3a) alone, the friction surface fracture shedding and ploughing were evident. Local delamination was observed and the damage region was more extensive. All the other three had less fracture shedding and ploughing than under base oil. And under the lubrication of 3-B, the friction surface had the least scratched lines and ploughings.

So, as is said above, the anti-wear agent can reduce the depth of subsurface plastic deformation and prevent the development of long subsurface ploughing, which led to surface spalling. And under the lubrication oil, the A3 Steel sample possesses of lower friction coefficient and wear rate. It can conjecture that the surface of A3 steel maybe form the ceramic film in the process of sliding friction.

3.2 The influence of the base oil

As discussed above, the lubricant property of base oil with 3% anti-wear agent is the best. So we choose the 3-N lubrication (N lubrication added 3% anti-wear agent), for comparison with the 3-B lubrication.

Fig.4 shows the friction coefficient of A3 steel/ GCr15 pairs as a function of sliding time. In evidence, the friction coefficient under 3-N was lower than 3-B. At the same, the friction coefficient of two samples decreased and was relatively steady after about 30min of sliding time.

Fig.5 shows the wear rate of two samples under B and N lubrication with the same content anti-wear agent. Under the 3-N lubrication, the wear rate was much lower than 3-B lubrication.

Fig.6 shows the worn surfaces of A3 steel under the lubrication of 3-B and 3-N. For Fig.6a, the friction surface fracture shedding and ploughing were evident. The surface of A3 steel under the 3-N lubrication was generally smooth, although some scratched lines were seen.

Through the above analysis, under the non-brand base oil added this anti-wear agent, the A3 Steel expresses lower friction coefficient and wear rate. And the lubricant property of the composite lubrication based the non-brand oil is even better than the brand one added the same concentration. The reason may be that the anti-wear agent can have a

synergic potentiation with one additive of the non-brand base oil. And the Synergetic enhancement mechanism will try to be analyzed in another project.

4. Conclusions

The following conclusions can be drawn from the present study:

(1) Adding the anti-wear agent can enhance lubricant property and improve the frictional and wear resistance of A3 steel.

(2) When the anti-wear agent content reached 3wt% in the composite lubrication, the A3 steel-GCr15 steel pairs possess the lowest friction coefficient and wear rate.

(3) The non-brand base oil, added the same content (3%) anti-wear agent, can show the better lubricant property than that of the brand one.

References

Hu, Zeshan., Wang, Liguang., and Huang, Ling. (2000). Preparation and Tribological Properties of Nanometer Copper Borate as Lubricating Oil Additive. Tribology, 20, 292-295

KsenijaTopolovec, Miklozic., Jocelyn, Graham., and Hugh, Spikes. (2001). Chemical and Physical Analysis of Reaction Films Formed by Molybdenum Dialkyl-Dithiocarbamate Friction Modifier Additive Using Raman and Atomic Force Microscopy. Tribology Letters, 11, 71-81

M.W, Sulek., and A, Bocho-Janiszewska. (2003). the Effect of Metal 8-Hydroxyquinolinates as Lubrication Additives on the Friction Process. Tribology Letters, 15, 301-307

Narulkar, VV., Prakash, S., and Chandra, K. (2008). Effects of Temperature on Tribological Properties of Al2O3-TiO2 Coating. Defence Science Journal, 58, 582-587

Qiao, Yulin., Liu, Weimin., and Qi, Shangkui. (1998). The Tribochemical Mechanism of the Borate Modified by N-Containing Compound as Oil Additive. Wear, 215, 165-169

Xia, Yanqiu., Zhou, Feng., and Lin Yimin. (2006). Study on Friction and Wear Properties of Plasma Nitriding 45# Steel under Different Lubrication. Tribology, 26, 145-149

Yin, ZJ., Tao, SY., and Zhou, XM. (2007). Tribological Properties of Plasma Sprayed Al/Al2O3 Composite Coatings, Wear, 263.1430-1437

Yu, Helong., Xu, Binshi., and Xu, Yi. (2006). Friction and Sliding-wear Behavior of Steel-Aluminum Tribopair Improved by Nanocopper Additive. Tribology, 26, 433-438
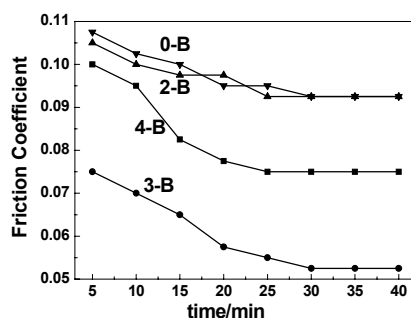
Figure 1. The friction coefficient of A3 steel/ GCr15 steel pairs as a function of sliding time

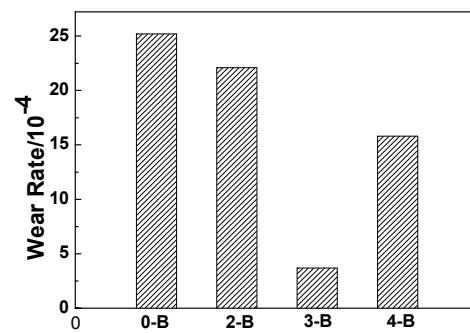under B lubrication with different content anti-wear agent

Figure 2.The wear rate of A3 steel samples under B lubrication with different content anti-wear agent

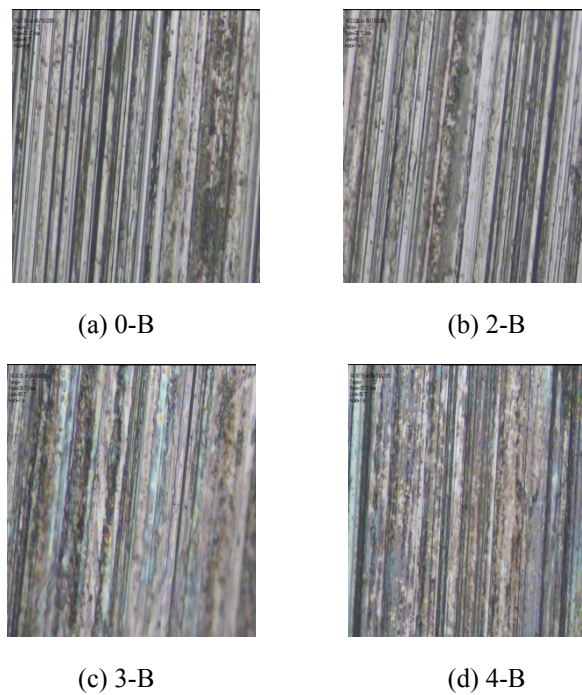(a) 0-B (b) 2-B

(c) 3-B (d) 4-B

Figure 3. Micrographs of A3 steel worn surface under B lubrication with different content anti-wear agent
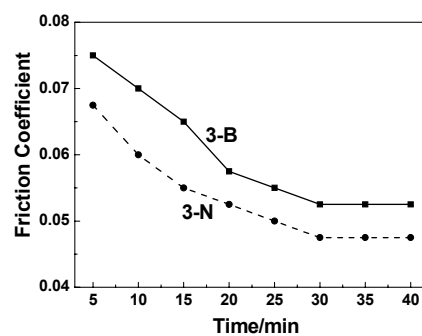

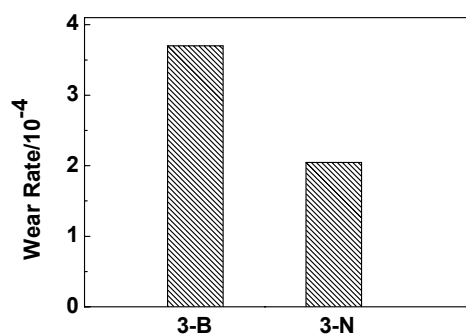Figure 4. The friction coefficient of A3 steel/ GCr15 steel pairs as a function of sliding time

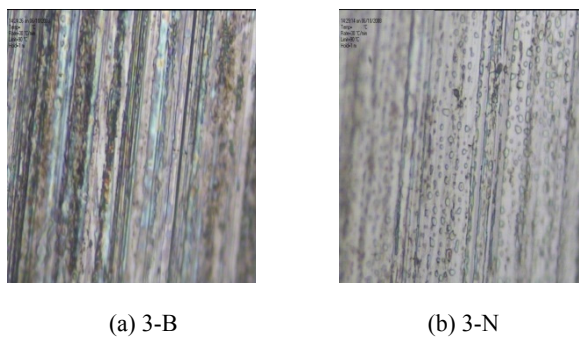Figure 5. The wear rate of A3 steel samples under B and N lubrication with the same content anti-wear agent

(a) 3-B   (b) 3-N

Figure 6. Micrographs of A3 steel worn surface under B and N lubrication with the same content anti-wear agent

Research on Vectorization of Embroidery Images Consisting

of Straight Lines & Circular Arcs

Jinglan Li

College of Engineering

Linyi Normal University

Linyi 276005, China

E-mail: lijinglan1229@163.com

Huaiqiang Liu

Department of Physics

Linyi Normal University

Linyi 276005, China

E-mail: huaiqiang1019@163.com

Abstract

A novel method for inputting embroidery images is presented. The method can convert BMP image format to DXF graphics format automatically. Firstly, the embroidery image is captured by a scanner; secondly, the image will be converted to a graphics by means of image processing and multinomial fitting algorithm; finally, a special graphics file will be created to be the DXF graphics format. Test results using this method showed that the algorithm achieved a good quality and improved the efficiency of inputs greatly.

Keywords: Embroidery image, Vectorization, Image processing, Multinomial fitting

1. Introduction

With the development of CAD technique currently, the vectorization becomes a focus of researches in many fields such as CAD and so on, which makes graphics inputs from human computer interaction technique to computer input automatically. In this way, vectorization can not only save memory but also improve the intelligent level and the efficiency of graphics inputs. Thus the vectorization becomes one novel method to solve the prevalence and application of the CAD technique and has an important theoretical and practical significance.

Now the computer embroidery CAD system(Diao Hongquan, 2003) is prevalent in the world. Its strongpoint is the precision of the input .But the cost is very high and the efficiency is low. The paper presents a novel method which is to take images captured by scanner as inputs .A graphics can be acquired by a digital image which is preprocessed. The cost is low and the efficiency is relatively high. This paper introduces briefly BMP format and DXF format at first, then the course of vectorization which has four steps. Firstly, a BMP image is captured by a scanner. Secondly, the image is preprocessed for removing noise. Thirdly, lines and circular arcs are followed automatically. Finally, the paper presents fittings of lines and circular arcs and pick-ups of characteristic points and realizations of vectorization.

2. Raster image and vector graphics

This paper introduces the raster format and vector format briefly. A raster image is considered a matrix which has some elements. Each element corresponds with a pixel. The structure of BMP images has four-part: BIT-MAPFILEHEADER, BITMAP INFOHEADER, RGBQUAD and an array to store a matrix. This array stores datum from the bottom to the top of an image. The number of byte in one row must be the multiple of 4.The total number of byte in one drawing lies on the number of color and the width of pixel. A vector graphic is constituted by some lines and circular arcs and so on. Each element saves only some characteristic points. For example, start points and end points of straight lines and the centre of a circle, radius, start and end angles of circular arcs. Saving all points in vectors is unnecessary.

3. Preprocessing images

Before vectoring images, we should preprocess images: image segmentation, image simplification and image removing noise. Image segmentation is to divide images into some special parts. We divide images according to the hue, which reduces the complexity of image processing and increases conversion speed, so the next method can be taken:

Conversion RGB multicolor space to HIS multicolor space:

$$I = (R + G + B)/3$$
$$S = 1 - [\min(R, G, B)/I]$$
$$H = 1/360[90 - \arctan(F/\sqrt{3}) + \{0, G > B; 180, G < B\}]$$
$$F = (2R - G - B)/(G - B)$$

H0 is the value of hue that should be taken as the threshold of picking up datum. Although it isn't strict with the colors information of vector graphics, it is necessary to save its color features. The array—PrcBmp[256][] saves datum of each color, which brings much convenience. An improved Hilditch arithmetic(Song Xiaoyu, 2000) is adopted in the image simplification. The methods of shrinking, expanding and flowing are good for image to remove noise. The expanding is combined with the shrinking repeatedly to remove noise in the bi-level image.

4. Automatic follow

Following vector is required before a vector is recognized. The aim of follow is to pick up the outline of brink. A main task is that the image preprocessed is saved into chains of datum which is the most original datum. Recognition and pick-up later are based on the datum. The pixel information of images can be seen clearly from the result of images preprocessed. The scheme is under the condition of Visual C++ 6.0. The object-oriented technique is used for saving chains of datum. The method of chain-in-chain in Visual C++ 6.0 is adopted:

Step1: The class CColor can classify the drawing according to the color of points. The function JudgeIfPointBelong(int hue) is to judge whether the hue of the current point is saved or not. If it isnotsaved, we can add the hue of the point to the hue-line through the function AddHue(int hue) and set layerlist[i] to be true. Otherwise, goes to Step2.

Step2: The class CLineListClass processes the current point. One struct(tagLineElem) which is structured by the class CListClass is a double-direction list. The function JudgeIfPointBelong (PointElem* Point) judges whether the point belongs to the current list-line or not. If not, the function AddList(PointElem point) add the point to the list-line. Otherwise, goes to Step3.

Step3: The class CListClass processes the current point. The function JudgeIfPointBelong(PointElem* Point) judges whether the point belongs to the current list-point or not. If yes, the function AddList(PointElem point) adds the point to the list-point.

When all points in the image are processed completely in this way, the automatic follow is finished. The image is divided into many layers according to the different colors. The lists of same color are saved in one layer.

5. Fitting and picking up

The fitting of straight lines & circular arcs is necessary to judge whether a list above is a straight line or a circular arc(Hori O, 1993). METHOD of LEAST SQUARE(Zou Shuyi, 1999) is presented to fit the straight lines & circular arcs in the paper. Some characteristic points represent the shape of vectors. The pick-ups of characteristic points are the key to fitting vectors.

5.1 Fitting straight lines & picking up characteristic points

METHOD of LEAST SQUARE is adopted to compute the extremum. The equation for straight line is: Ax +y+ C=0. At first we judge whether a list-point can make up of a line or not. When the slope of the line is $\|- A\| < 1$, the vertical coordinate y_i of the point (x_i, y_i) is subtracted from the corresponding vertical coordinate on the equation. The result's square is a standard to measure the line equation. METHOD of LEAST SQUARE of curve is shown as follows:

$$\|\delta\|^2 = \sum_{i=0}^{m} \|\delta_i^2\| = \sum_{i=0}^{m} - Ax_i - C - y_i)^2$$

According to it, the partial derivatives to A, C are equal to zero and the minimum of δ and the value of A, C can derive from these equations. The experimental data of the error ε is predicted to 0.02. If $\delta \geq \varepsilon$, the list-point cannot make up a line. If $\delta \leq \varepsilon$, it can do. The starting and ending points of automatic follow are the characteristic points of the line. If $\|A\| > 1$, x & y are interchanged in the equation above.

5.2 Fitting circular arcs & picking up characteristic points

METHOD of LEAST SQUARE added to the least radial error fits circular arcs. The method can revise datum during the course of automatic follow. The result is global optimum. We have a hypothesis that the distances between the

points on circular arcs and on the list-point are the least .The equation of circular arc is $(x-x_0)^2+(y-y_0)^2=R^2$, (x_0,y_0) is the centre of a circle, R is the radius). Suppose $f(x_0,y_0,R)=\sum((x_i-x_0)^2+(y_i-y_0)^2-R^2)^2$, two restricted conditions are added: $f(x_u,y_u)=f(x_v,y_v)=0$, where (x_u,y_u) and (x_v,y_v) are the coordinates of starting and ending points and partial derivatives to $x_0,y_0 \& R$ are supposed to be zero. When the $f(x_0,y_0,R)$ is the minimum, the fitting of circle is optimum. Under this condition, x_0,y_0,R starting angle and ending angle are the characteristic points of the circular arcs.

6. Output of vector

The ultimate aim for vectorization is that the current drawing can be used by some software for computers to process vector graphics. That is to say, the output format must be the format that some software can recognize. DXF format is one of them. A whole DXF file is made up from six SECTION and one end tag which is HEADER, TABLES, BLOCKS, ENTITIES and END OF FILE. One vector graphics can be saved if these characteristic points are found. A line saves only starting and ending points while the fitting of circular arcs uses the method of perpendicular bisector. A line segment L0 is connected with another line L1. The two line segments are on the same list-point and are considered the seeds of a circular arc. The point P1 is the intersection of the two perpendicular bisectors. The point is considered the approximate centre of the circle. The average of distances between the centre and all the apexes of the list-point is considered the approximate radius. When the next line segment L2 is connected with L1, we repeat the task above. If the new radius and the center of a circle are near to the last ones, the line L2 belongs to the circle arc. This task continues until the circle arc breaks. The values of distance between every centre of a circle and all sides are computed. If a variance between one average value and the values correspondingly is the least, the centre and radius are characteristic points of the circle arc. The layer of color in table section is added in the DXF file and the final graphics consists of many color layers automatically. The result is realized as follows (Fig.2).

7. Conclusion

A scanner is an equipment of input for two-dimensional graphics. The paper presents an automatic vectorization algorithm for embroidery images. The algorithm realized an automatic conversion from raster image to vector graphics which is efficient and adaptive. To some extent, the method has an applicable value. Currently the system is on the developing state and doesn't have a mature product, but it must have a bright market future.

References

Diao, Hongquan, & Yan, Gangfeng. (2003). Integral design scheme of computerised embroidery machine's control system. *Journal of Engineering Design*, 10(4), 188-190.

Hori O, & Tanigawa S. (1993). Raster-to-vector conversion by line fitting based on contours and skeletons. *Proceedings of the 2nd International Conference on Document Analysis and Recognition*,623-626.

Liu, wenyin, Dov Dori. (1999). From Raster to Vectors: Extracting Visual Information from Line Drawings. *Pattern Analysis & Applications*, 10~21.

Saber Eli, Tekalp A Murat, Eschbach Reiner & Knox Keith. (1996). Automatic Image Annotation Using Adaptive Color Classification. *Graphical Models and Image Processing*, 58(2), 115- 126.

Song, Xiaoyu, Wang, Yonghui. (2000). Research on Automatic Vectorization Algorithm of Engineering Drawing. *Computer Engineering and Applications*, 36(3), 41-43.

Y. Wei. (2001). A fast finding and fitting algorithm to detect circles. *Proceedings of IEEE International Symposium on Geoscience & Remote Sensing*, 2 (6), 1187~1189.

Zou, Shu-yi, Guan, Chengxiang & Wu, Mingxian. (1999). Improving of intervening computation's precision by METHOD of LEAST SQUARE. *Journal of Physics*, 20 (1), 100 -102.
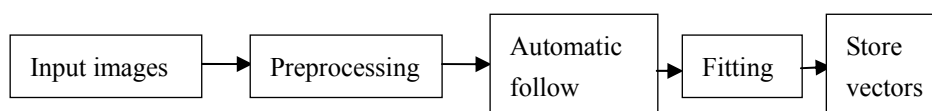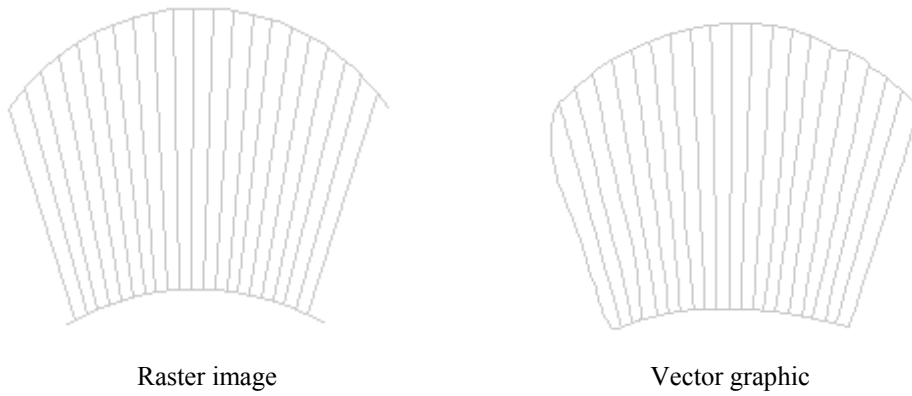
Input images	→	Preprocessing	→	Automatic follow	→	Fitting	→	Store vectors

Figure 1. Whole Process of Vectorzation

Raster image   Vector graphic

Figure 2. The Contrast Between Raster Image and Vector Graphic

Modern Applied Science

9 771913 184002   0 6 >